Novel sensors technologies applied to force spectroscopy in molecular biology

Laura Gonzalez Claramonte

Novel sensors technologies applied to force spectroscopy in molecular biology

---

Laura Gonzalez Claramonte

Barcelona, September 2014

DOCTORAL THESIS

UNIVERSITAT DE BARCELONA
Facultat de Física
Departament d'Electrònica

Novel sensors technologies applied to force spectroscopy in molecular biology

---

Doctoral program:

Biomedicine

Research Line:

Biomedical Engineering

Supervisors:

Dr. Manel Puig-Vidal and **Dr. Jorge Otero Díaz**

Author:

Laura Gonzalez Claramonte

Abstract

Force plays an essential role in all fields of biology. Measurement of these forces with high precision provides information about the structure, dynamics, intra and intermolecular interactions, and the mechanical properties of the biomolecules and, in general, about molecular basis of diverse biological phenomena. The main objective accomplished in this work of thesis is the development of sensors technologies applied to force spectroscopy measurements and the demonstration of its possibilities in real molecular studies. Scanning probe microscopy (SPM) is a fast growing technology that has been the source for the development of an immense variety of applications to investigate materials and molecules at nanoscale. As another technology, SPM is constantly improving through different advances in instrumentation level and the emergence of new applications. From the analysis of the main limitations of quartz tuning fork (QTF) based nanosensors on one side, and the conventional force spectroscopy with cantilever tips on the other side, the main considerations have been determined for the technological developments on force microscopy applications.

One of the main limitations of tuning fork probes is that they are usually custom-made because no commercial probes suitable for a wide range of experiments are available. The custom-made devices show considerable variation in dynamic response, poor lateral resolution and the characterization of the sensors remains unclear for force quantification. A new controller is developed to ensure the same dynamic response of different sensors in order to maintain the conditions in which the measurements are conducted. Also, a new method to improve lateral resolution of the QTF probes when working in liquid is proposed in this thesis based on attaching a standard AFM tip to the end of the fiber probe which has been previously sharpened. A method to calculate the spring constant of the QTF based sensors from easily measurable parameters is presented. The method is based on a finite element analysis (FEA) model which includes the electrical part and can be used to calculate the spring constant of a QTF accurately for quantitative measurements. Results obtained in real biological experiments are promising and show the possibilities of the shear force microscopy improvements developed in this work of thesis. In a first experiment, a self-assembled monolayer (SAM) of micropatterned antibodies is imaged with three different techniques and in a second experiment, molecular interaction measurements are performed between biotin-streptavidin complex.

The main problem for comparing steered molecular dynamics (SMD) simulation results with experimental data is that SMD simulations were restricted to nanosecond timescales. A high-speed force spectroscopy methodology has been developed to achieve rates comparable to SMD simulations. The validation of the technique is performed with titin unfolding measurements allowing the direct comparison of experimental and simulated forces.

Contents

1 Introduction

1.1 Studying biomolecules at the nanoscale

Biological physics research is becoming increasingly quantitative, and this fact is producing fruitful collaborations between biologists and mathematicians, physics or engineers to develop new technologies to explore biological mechanisms. For example, to measure forces in biological systems, model molecular dynamics or develop high-resolution microscopy. To understand the most of the biological processes is necessary to study the phenomena involved at the minimal biological unit, a single biomolecule. Due to molecular heterogeneity, if we study a property as a mean average of a bulk ensemble, in most of the cases, we cannot obtain a general representation of this property in a given single molecule [1]. Single-molecule techniques can provide new information, for example, as a probability distribution of the values for the property of the studied system. This is complemented by powerful visualization methods which help to the understanding of the experiments. Technological developments in experimental single-molecule biophysics have been of great importance and it is a field of continuing growth expanding its applications since the lasts twenty years. Those techniques can use electrons, photons or force to measure or manipulate and can provide, for example, information about the position of a biomolecule at a certain time or measure the forces exerted by the molecule (see Figure 1). Among all these techniques, we can also do differentiation in techniques that allow to manipulate and techniques to detect individual molecules in real time. In the first group, the most common techniques are: atomic force microscopy (AFM), optical tweezers (OT), magnetic tweezers (MT) and biomembrane force probe (BFP). In the second group, we also have AFM and primarily optical techniques based on single-molecule fluorescence. There are also several combinations among them to obtain enhanced precision [2].

Single-molecule fluorescence is based on the detection of light emitted by fluorophores after being excited that have been attached to the molecule under quest. Detection of single molecules is possible by exciting a very small volume with light and observing the emitted signal. Typical volumes are on the order of the femtoliter (a water drop of diameter on the order of a micron). They are very useful to study the presence of biomolecules and the spatial resolution is, in general, limited by the Rayleigh criteria (200 nm). A powerful technique to detect conformational changes is fluorescence resonance energy transfer (FRET) by means of describing energy transfer between a donor and an acceptor attached to specific binding sites on the molecule with around 10 nm resolution [3]. Other measurements using total internal reflection fluorescence (TIRF) allow to determine the orientation of individual molecules with tens of millisecond resolution [4]. The

evolution of TIRF microscopy yields fluorescence imaging with one nanometer accuracy (FIONA) [5]. The method was famously used to examine the step lengths of myosin molecules moving along actin filaments in vitro. The drawback in most cases of fluorescence techniques is the photobleaching and the chemistry involved to attach the fluorophores to the biomolecules.

There are of course many other techniques, for instance to study the biomolecules structure and composition such as nuclear magnetic resonance (NMR), diffraction techniques as X-ray spectroscopy or electron microscopies (TEM/SEM). In these techniques, in some way, the sample cannot be in physiological conditions either because the environment is air or vacuum, the measurement source is invasive or because the sample needs some preparation such as the adding of a contrast agent [6].

From all of these techniques for single-biomolecule studies, AFM is the one that allow imaging and force measurements in physiological conditions without a special treatment of the sample. I would say that, nowadays, the most widespread and commercially available single-molecule technique in biophysics labs is the AFM. It allows one to take images of individual molecules adsorbed to surfaces in their native environment. At the same time with the AFM it is possible to immobilize molecules one at a time by attaching one end of the molecule to the AFM tip, the other being immobilized on the surface. By moving the tip relative to the substrate it is then possible to pull the molecule away from the surface and exert mechanical force.

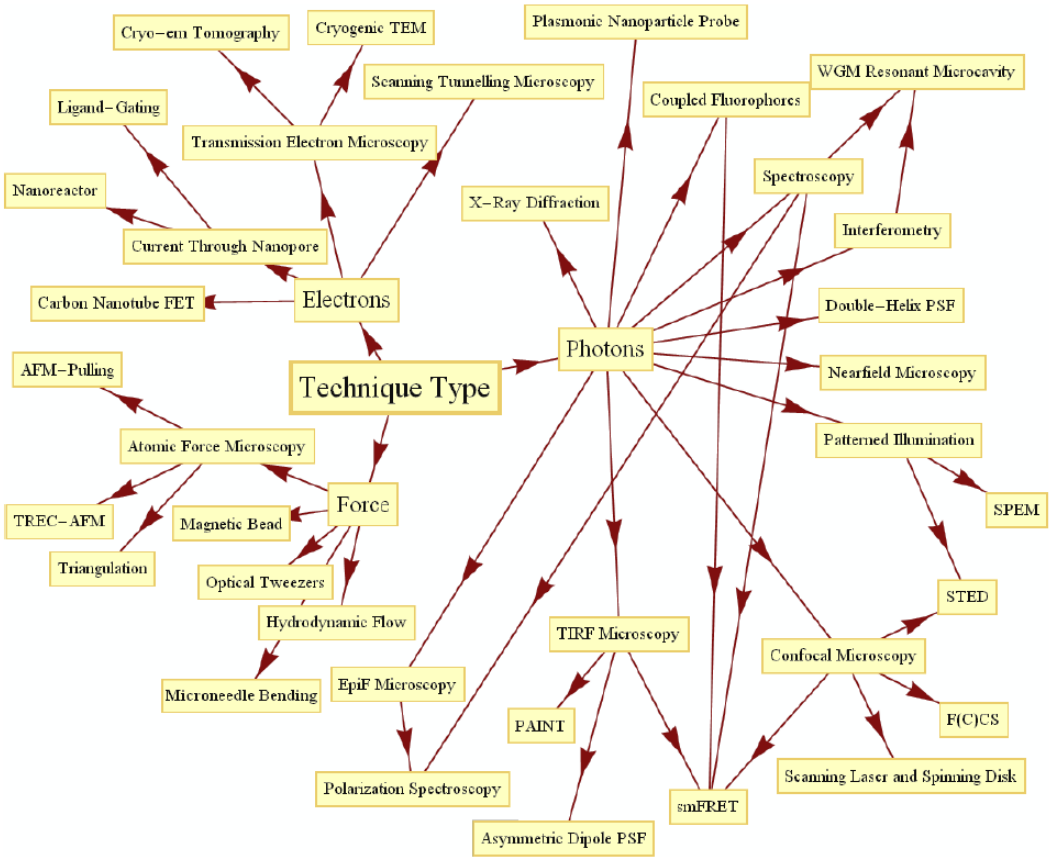

Figure 1. Scheme of the type of the single-molecule techniques [7]

Immobilization techniques of biomolecules to the AFM tip and to the substrate are very important because they have a direct effect on the measurement. In recent years, there has been a great interest in development of strategies to modify chemically the AFM tips and to functionalize the surface and these tips

[8-9]. One interesting method to immobilize biomolecules on the surface is to create a patterned self-assembled monolayer (SAM), molecules which are able to assemble themselves in the same orientation under certain conditions. These patterns can be formed by micro-contact printing technique [10] or dip-pen nanolithography [11].

1.1.1 Measuring forces at molecular level

Force plays an essential role in all fields of biology. This is valid spanning molecular to tissue scales, macroscopic bodies and systems (eg, mechanical action such as can be observed during muscle contraction) and also, and perhaps above all at the microscopic level as force is involved in events as cell adhesion [12], molecular interactions [13], DNA mechanics [14], motor protein movement [15], and protein folding and stabilization [16-19]. The forces experienced and generated

by biomolecules are multiple in nature and can range from subpiconewton extend to several nanonewton (Table 1) [20].

Type of Force	Example	Rupture Force (pN)
Breaking of a covalent bond	C-C	≡1600
Breaking of a noncovalent bond	Biotin/streptavidin	≡160
Breaking of a weak bond	Hydrogen bond	≡4
Langevin force	on E-coli	0.01 (1s)
Stretching dsDNA	to 50% relative extension	0.1
Developped by a molecular motor	Kinesin walking on microtubule	5 (max)
Electrostatic/ Van der Waals		1-1000
Magnetic		$<<10^{-6}$

Table 1. Examples of forces at molecular level and their approximate magnitude.

Measurement of these forces with high precision provides information about the structure, dynamics, intra and intermolecular interactions, and the mechanical properties of the biomolecules and, in general, about molecular basis of diverse biological phenomena [21-26]. Different techniques have been developed to address this task, particularly at the single molecule level. Each of these techniques can be used for different ranges of forces (Figure 2). However, the way in which the force is measured is different among these methods. The atomic force microscopy (AFM) uses a silicon probe mounted on a soft cantilever spring to measure the force between the probe tip with a radius of ~10–50 nm and a second surface. Force bends the cantilever and this deflection is detected with a laser beam [27] (Figure 2). Optical tweezers (OT) measures the displacement of a small bead trapped in a highly focused laser beam and biomembrane force probe (BFP) measures the displacement of a vesicle (or a membrane of cell, functionalized bead, etc.) held by suction in a micro-pipette. In this case, the soft spring of the sensor is the tension in the vesicle and can be controlled by the suction pipette that sets the hydrostatic pressure difference across its membrane [28]. OT uses the restoring force generated by the photonic gradient of the laser that traps the bead [29-30].

Another single molecule method is magnetic tweezers (MT) [31]. A magnetic tweezers apparatus consists of magnetic micro-particles, which can be manipulated with the help of an external magnetic field. The position of the magnetic particles is

then determined by a microscopic objective with a camera. As a constant force technique, MT measure the time-dependence of length changes of the sample. The surface force apparatus (SFA) [32] measures the force as a function of the separation distance between materials bond to two crossed cylinders and senses the distance between the surfaces using optical interferometry. However, the probed regions are large (1–5 μm^2) and typically reflect a large number of molecular interactions, making it well suited for determining surface or adhesion energies [33].

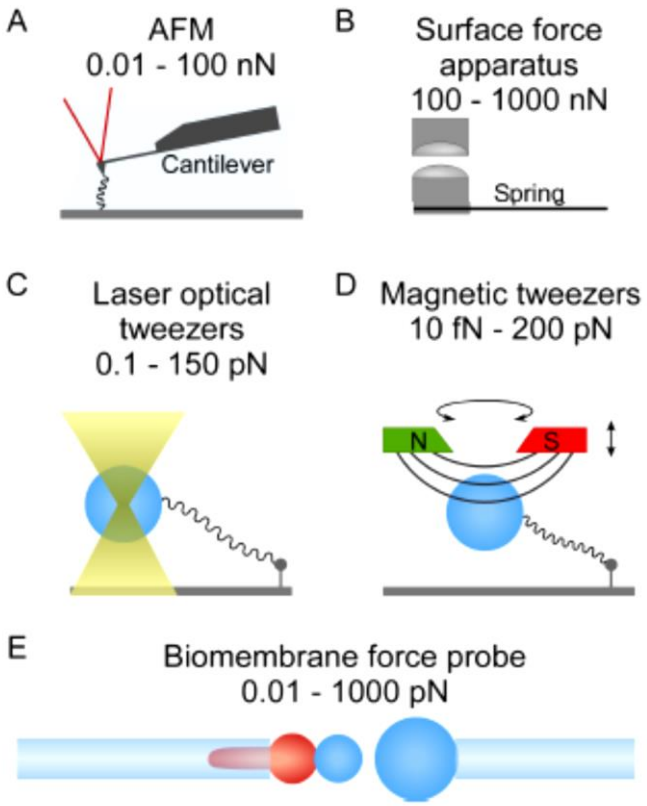

Figure 2. Force probes used to directly measure protein interaction forces. (A) The AFM, showing the probe tip attached to the cantilever force transducer. (B) The SFA, showing the two crossed cylinders and the force-transducing spring. (C) OT, in which the bead is held in the optical trap. (D) MT with a magnetic bead in the magnetic field of a strong magnet. (E) The BFP, consisting of a membrane capsule aspirated into a pipette used as a spring with adjustable stiffness. [34]

Steered molecular dynamics (SMD) simulations, or force probe simulations, apply forces to a protein in order to manipulate its structure by pulling it along desired degrees of freedom. These experiments can be used to reveal structural changes in a protein at the atomic level. SMD is often used to simulate events such as mechanical unfolding or stretching [35] or unbinding force between ligand-receptor pairs [36].

1.2 Atomic force microscopy

In 1986, Binnig, Quate, and Gerber introduced the atomic force microscope (AFM) as an innovative method to image both conducting and non-conducting surfaces [37]. The AFM belongs to the family of scanning probe microscopes (SPM), which all use a sharp tip to probe the sample surface. However, each SPM technique relies on a different measurable quantity like tunneling currents in the scanning tunneling microscope (STM) [38], potential offset between sample and tip in the Kelvin probe microscope (KPM) [39], magnetic forces in the magnetic force microscope (MFM) [40], or light in the scanning near field microscope (SNOM) [41].

There are two main working modes in scanning probe microscopy. The imaging mode measures a property of the sample (usually the topography) in function of the X and Y position. In the spectroscopy mode, the local properties at one point of the sample are measured in function of another parameter different from the XY position. The mechanism to obtain an image is to maintain constant the interaction between the probe and the sample surface (the near-field force, the tunneling current, etc.). While scanning the sample in X and Y direction, the Z position is adjusted by a feedback loop to keep constant the measured interaction. The reconstruction of these Z corrections in function of the X and Y position of the piezo scanner is then a three-dimensional representation of the scanned sample surface. The AFM technique is based on the measurement of the interaction force between a nanometric radius tip and the sample surface. The tip is usually at the end of a microfabricated cantilever which bends when a force occurs. The reflection of a laser on a photo detector is used to measure the deflection of the cantilever (Figure 3). There are some methods for imaging in AFM. Contact mode or “static mode” where the tip is dragged across the sample measuring the deflection of the cantilever. The method most extended is to make the interaction intermittent. It is what is known as “dynamic mode”: the probe is oscillated and the interaction between the tip and the sample modulates the amplitude (AM-AFM, also known as “tapping mode”), the phase (PM-AFM) or the frequency (FM-AFM) of the cantilever oscillation. In the “non-contact” mode, the tip-sample interaction is by means of long-range forces.

Another major application of AFM (besides imaging) is force spectroscopy, especially in life sciences, which consists on the direct measurement of the tip-sample interaction forces as a function of the gap between the tip and sample (the result of this measurement is called a force-distance curve [42]). For this method, the AFM tip is extended towards and retracted from the surface as the deflection of the cantilever is monitored as a function of piezoelectric displacement. These measurements have been used to measure the local nanomechanical properties of

the sample quantitatively: elasticity [43], viscoelasticity [44], adhesion [45], single molecule stretching and rupture forces [46], etc.

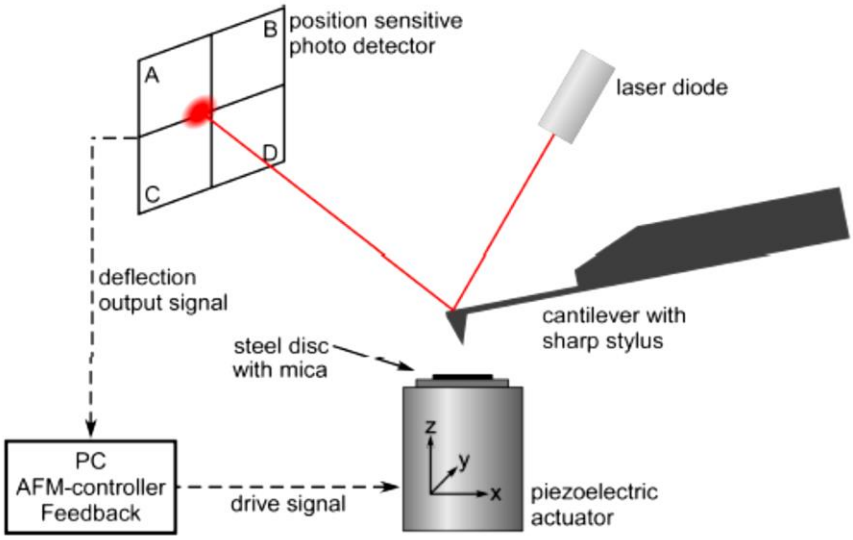

Figure 3. Scheme of a typical AFM setup. The sample is mounted on top of the piezoelectric actuator, which allows sub-nanometer positioning. For AFM imaging, the sample is raster-scanned below a sharp tip mounted at the end a soft cantilever. For force spectroscopy, the sample is repeatedly approached and retracted from the cantilever tip. Vertical cantilever deflection results in a change of the position of the laser spot on the photo detector.

Atomic force microscopy has become a highly valuable research tool in biology and medicine due to its special characteristics: (i) AFM can image the surface morphology in 3D with nanometric accuracy in the X and Y axis and with sub-nm resolution in Z, (ii) samples don't need any special treatment and they can be studied under their physiological conditions (in liquid). Moreover, (iii) the interaction between the probe and the sample can be maintained so gentle that it doesn't damage the biological samples. And as mentioned before, (iv) multiple properties of the sample can be measured apart from the morphology: mechanical and electrical properties, molecular interactions, unbinding forces, etc. For instance, *Scheuring et Al.* investigated in [47] how the composition and architecture of photosynthetic membranes of a bacterium change in response to light (Figure 4A) or morphology of living bacteria can be seen in image Figure 4B.

First studies in molecular biology with AFM were the topographies of membrane proteins with molecular resolution in 1991. The AFM tip was used to dissect the top-layer of the double layered gap junction assembly [48]. Since then, studies in molecules like DNA and proteins [49] (and DNA protein interaction [50]) have been performed by imaging with the AFM. With the development of the high-resolution high-speed AFM [51], fast dynamic processes, like protein motion, can be studied [52]. In the study of interaction forces, the most challenging application is protein unfolding, where the measurement of the rupture forces of the different structures of the molecule can be measured [53].

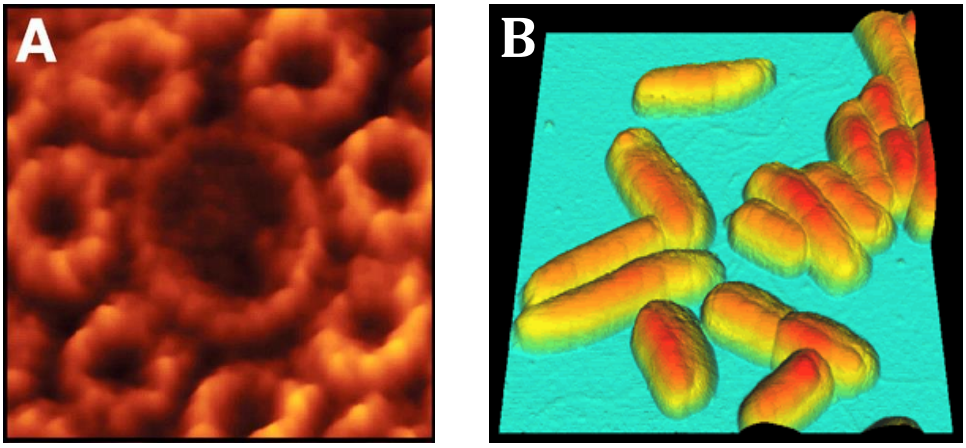

Figure 4. (A) Structure of photosynthetic complexes in high-light– and low-light–adapted chromatophores of *Rsp. Photometricum* (scan field: 23 nm; Z-range: 2 nm) [47]. 3D topography of living *Escherichia coli* bacteria (scan field: 9µm x 9µm; Z-range: 781 nm) (from www.jpk.com image gallery).

1.2.1 Force spectroscopy

In AFM based force spectroscopy, two major kinds of measurements can be performed depending on the parameter that is constant: velocity or force.

Constant Velocity Force Spectroscopy

A typical force curve measurement is shown in Figure 5: In region (1) AFM tip is not in contact with surface; (2) Very close to the surface the cantilever can be suddenly attracted by the sample due to adhesion forces ("jump–to–contact" [54]). (3) Tip is being pushed into de surface and cantilever is bent upwards in direct proportion to the z-piezo height. The cantilever is withdrawn after a defined setpoint of deflection is reached (4) and cantilever is more and more unbent moving upwards (5). In (6) usually the tip adheres to sample surface bending the cantilever in opposite direction until the tip "jumps–off–contact" that the tip loses the contact and cantilever deflection comes back to the initial position. The linear region in (3) is related to the viscoelastic properties of the sample and we can obtain the stiffness of the system. The elastic deformations of the sample in the contact curves can be related to its Young's modulus after applying a model [55] to determine the contact area. The adhesion can be evaluated from the measurement in (6) [55].

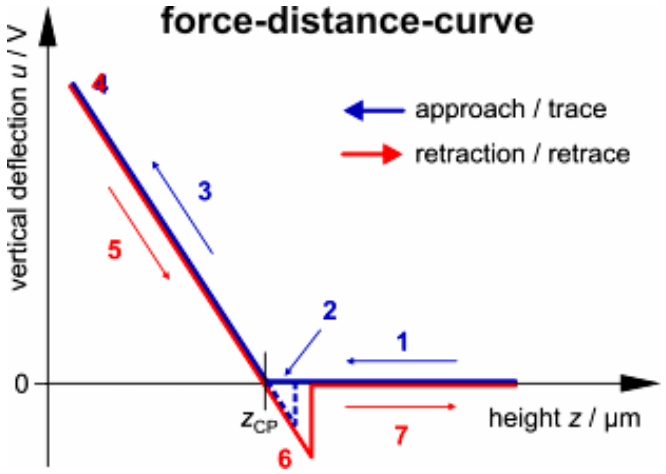

Figure 5. Different zones in a typical contact force versus Z displacement curve.

Constant Force Spectroscopy

In contrast to the constant velocity approach, where the cantilever deflection is a function of time, the constant force or "force clamp" aims to keep the cantilever deflection and hence, a constant strain at the molecule over time [56-58]. As a result of the rapid relaxation of the molecule, the Z actuator quickly moves in a nonlinear manner to restore the tension in the molecule. Consequently, the information is obtained from the time-dependent piezo position. Each step in the Z motion versus time diagram reflects an unfolding event and is associated with a step size characteristic. This approach allows the direct measurement of the force-dependent life-times of proteins and their domains.

Single Molecule Force Spectroscopy (SMFS)

In single molecule force spectroscopy with AFM, the cantilever is used as a tool that can pick up single molecules anchored to the sample surface by approaching the surface to the cantilever and allowing it to rest while in physical contact. Primary experiments were into studying receptor/ligand interactions as biotin-avidin [13], complementary strands of DNA [59] or antibody-antigen pairs [60]. The biotin/(strept)avidin ligand/receptor pair has been used as a model system because of its unusually high affinity and the availability of structural data. Also, the AFM has proven particularly useful in studying intramolecular interactions, as for example stretching of the DNA double helix or unfolding/refolding process of multi-domain protein molecules. Plotting the force as a function of tip-sample separation yields a F-D trace containing information about structural transitions of the molecule when stretched. The first AFM-based SMFS unfolding and refolding experiments were performed in the 1997 revealing saw-tooth patterns [18] on the sarcomeric protein of striated muscle, the titin.

Combinations of AFM experiments with steered molecular dynamics (SMD) simulations enriched atomic-level descriptions [35, 61] of receptor-ligand binding

[13, 63] and forced protein unfolding [18]. However, a velocity difference of about six orders of magnitude prevented direct comparison of SMD with FS. Indeed, resulting forces from simulations are higher than experimental values in force spectroscopy measurements. In the case of the Titin I91 concatemers simulations resulted in unfolding forces of ~1 nN, nearly an order of magnitude greater than experimental values [64-65]. Improved computational abilities have allowed simulations that unfolded I91 at 2800 mm/s (still faster than experiment by ~2.5 orders of magnitude), reporting forces of ~500 pN [66].

Although SMFS has a lot of potential applications for chemistry and biology at the nanoscale, there are still points to improve in this technique [67].

- The temporal resolution still limits the application of rapid SMFS to study biological processes. The temporal resolution of SMFS is determined by the resonant frequency of the piezoelectric positioner and the cantilever. Currently, the temporal resolution in SMFS is in millisecond scale, which is slower than many biological processes and is far from the μs-timescale of the steered molecular simulations (SMD). For force-clamp technique, the temporal resolution improvement would be a key point to extent their applications.
- The resolution of the force is restricted by the thermal motion of the cantilever. In principle, the smaller the cantilever, the lower is the thermal noise. With modern manufacturing technique, the resolution of the force cantilever can be as low as 1-2 pN.
- The cantilever drift limits the slow processes by SMFS. The laser used to detect cantilever deflection heats the solution locally in the fluid chamber. Excessive heat causes the movement of the fluid and changes the refractive index, which is the key factor representing the thermal drift of cantilever.
- The chemical-bonding of the molecules to the cantilever or to the surface is limited and the success rate for stretching individual molecules is very low. Moreover, it cannot always guarantee single molecule events as multiple molecules can be collected simultaneously.

1.3 High Speed Atomic force microscopy

Most commercially available AFMs are built to use 50-500 μm long cantilevers, and consequently bio-imaging with nanometer resolution is usually achieved within a timescale of one to several minutes, thus limiting AFM imaging to structural applications of stable samples. Fortunately, speed limitations of the AFM were overcome with smaller cantilevers but with a spring constant smooth enough (k~100pN/nm and 6 μm long with f = 1 MHz in liquid). High resolution scanning of biological samples at video rate, called high-speed atomic force microscopy (HS-AFM), in physiological conditions is now possible [68]. It has been developed since 1993 and it was fully completed in 2008 [69].

After different technical developments, piezo scanner stability, optimization of the optical detection system and fast feedback response [70-71], video-speed AFM of molecular dynamics was possible [72]. For example, Myosin-V walking on actin filaments was imaged in [73] and direct imaging of single molecule diffusion on and in membranes in [74-75].

Imaging rate is, at present, higher than ten frames per second and the spatial resolution is comparable to the conventional AFM [72]. Recording a high-resolution AFM topography using contact mode AFM typically takes ~90-100 s, while high-speed AFM can reach imaging rates of > 10 images/s. Recently, it is also possible to study dynamic events in live cells. In [76], a hybrid system is developed where an optical microscope is integrated in HS-AFM. The new setup was used to study the diffusion and interaction of AQP0 on intact eye lens cells.

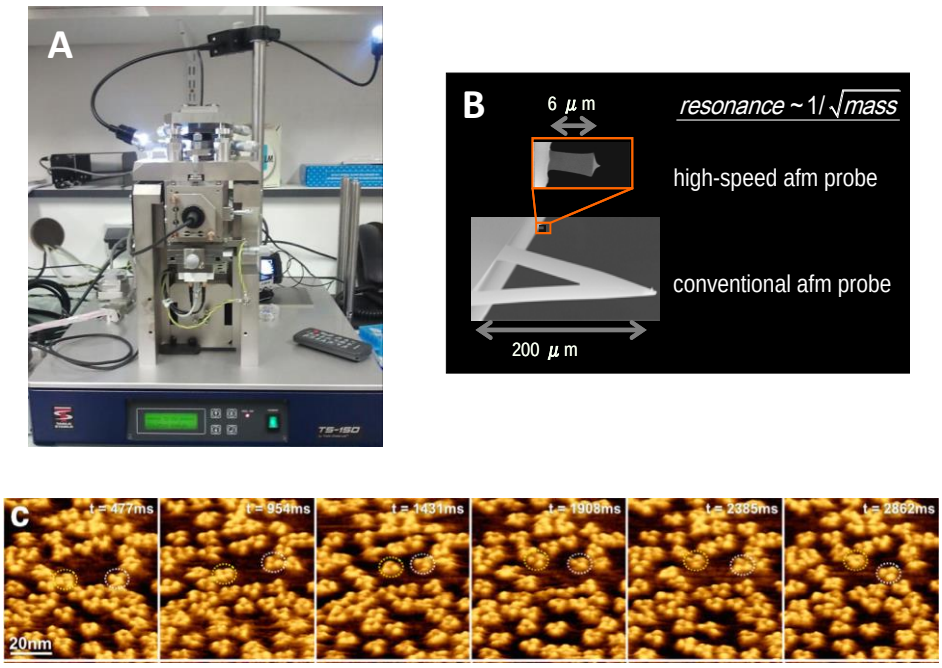

Figure 6 (a) High Speed AFM commercial equipment. (b) High-speed atomic force microscopy cantilever. (c) Lateral and rotational diffusion dynamics analysis of OmpF [74].

1.4 Quartz tuning fork sensors

1.4.1 Basics

Quartz tuning fork based sensors have several advantages with respect to silicon cantilevers such as high rigidity of the prongs (which prevents the tip jumps to contact at very small tip-sample distances), high quality factor Q (10-100 times greater than the cantilevers), piezoelectric deflection reading of the arms and the possibility to measure in ultra-high vacuum, low temperatures and high magnetic fields. These features have made possible to achieve atomic resolution images [77-78] and high sensitivity in the measurement of forces at the atomic scale [79-80].

The first implementation of quartz tuning forks in scanning probe microscopy was in a Scanning Near-field Acoustic Microscopy (SNAM) experiment by Günther et al. and dates back to 1988 [81]. The growing use of tuning forks in different branches of SPM was initiated by the need to suppress light from laser-based detection and to ease experimental setups. Karrai and Grober [82] for example expanded its use to Scanning Near-field Optical Microscopy (SNOM) in 1995. Since then, they have been widely used to study and manipulate matter at the nanoscale [77, 82-84].

The detection of deflection of the prongs is performed exploiting native piezoelectric effect of quartz, producing an electric polarization proportional to the strain of the prongs which loads the electrodes. By oscillating the prongs in the resonance, it produces an electric current of the order of 1 nA per nanometer of the arms oscillation, which may be detectable with similar power amplifiers employees in STM microscopes. Therefore, an optical assembly is not needed to detect the deflection.

In general, quartz tuning forks have been used in two different geometries to be implemented as sensors in SPM. In the first, both arms are allowed to freely oscillate parallel to the sample surface known as shear mode (tuning fork sensor geometry, Figure 7A). In the second, the probe oscillates in perpendicular direction to the surface (perpendicular mode, Figure 7B). Usually in the latter configuration, the upper arm is fixed firmly to a massive support [85], becoming the tuning fork in a quartz cantilever (*qPlus* sensor). The *qPlus* sensors have two main advantages: its dynamics is similar to the cantilevers used in AFM and effective spring constant k_{eff} is lower than the sensor with tuning fork geometry. However, QTF sensors in shear mode have an order of magnitude quality factor Q much larger and produce at least double of the current piezoelectric than *qPlus* sensors for a given vibration amplitude [86].

While the use of sensors based on *qPlus* configuration has matured enough, it remains difficult to obtain quantitative tip-sample interaction forces in shear mode. The reason is that the formalism developed for cantilever dynamics is not strictly

valid for sensors with tuning fork geometry in shear mode [87]. Although the beam theory can be applied in *qPlus* sensors [85] type, since the dynamics is like that of a conventional cantilever, there are applications where tuning fork sensor geometry may be more appropriate.

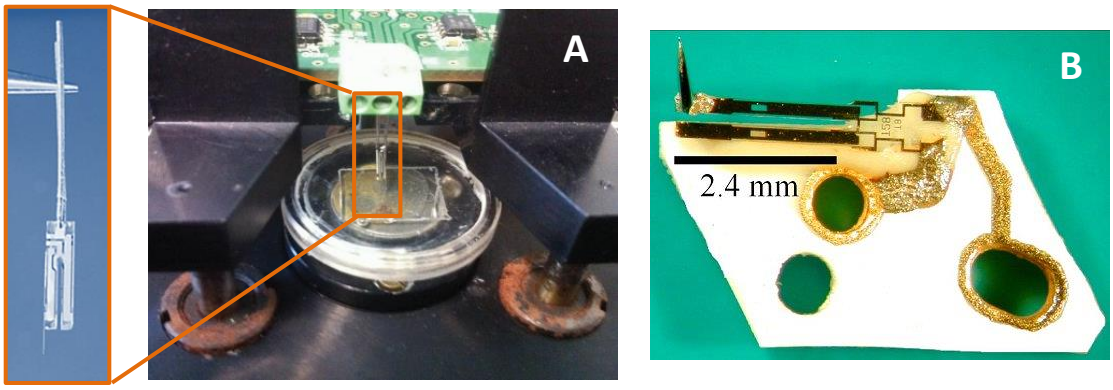

Figure 7. The two most common configurations for the QTF. (A) Shear mode, where the device is electrically oscillated parallel to the sample surface and the current through the two prongs is measured. (B) where the device is used to oscillate perpendicular to the sample surface, and the upper arm is fixed to a support [88].

The QTF can be either electrically driven by a voltage applied between the electrodes or mechanically excited by an external dithering piezo actuator. If the latter configuration is used, the coupling between the dither and the sensor is not easy to quantify and the existence of mechanical losses causes uncertainties. For the mechanically driven, the device should be calibrated to relate the measured voltage with the amplitude of oscillation. For the electrically driven device (with a signal of amplitude *Vrms* at frequency f), the amplitude of oscillation A can be evaluated from the current *Irms* by using the model in [89]:

$$A = \sqrt{\frac{V\ I\ Q}{2\pi f_0\ k_{eff}}} \qquad (1)$$

The most direct benefit of using QTFs is their high quality factor when operating in liquid. In ionic liquids measurements is a key parameter to obtain good results [90]. The high static spring constant allows very low amplitudes of oscillation, which together with the high Q provides a high sensitivity in the detection of the frequency shift and interaction forces. There have been reported in [79] and [80] that *fN* forces can be measured using these sensors. Advantages in the potential applications are wide due to the fact that there is no need to use a laser and a photodiode to measure the interaction. It can be easily integrated with optical techniques and it opens a wide range of applications in biomedical research. The tip is mm long, so the sample access is much better than with standard cantilevers; with QTF, experiments can be performed in Petri dishes, well-plates and other array-like sample preparations. One application of interest in the field of microfluidics is to perform measurements on an

enclosed physiological environment with a liquid cell where the buffer can be pumped. Commercial liquid cells for AFM are relatively large in terms of the required liquid volume in microfluidics, besides it is difficult to obtain large concentrations of the studied biomolecules in many cases [91]. Long tip and laser-free detection also ease the integration of more than one sensor in the measurement setup to conduct complex experiments with more than one probe [92].

The optical detection system with the laser used to measure the deflection of the cantilever in a conventional AFM allows good performances but has critical disadvantages for some specific applications. For example, for *in situ* measurement in a vacuum chamber, cryogenic environment measurement, dark environment measurement, or inside an enclosed chip, the optical deflection technique cannot be employed. Specifically, there are many weak points of the optical deflection technique; (i) taking large space, (ii) inconvenience of optical alignment, (iii) vulnerability to external noise, (iv) unavoidable optical exposure, and (v) high dissipative power. Heat dissipation of the laser diode produces elongation and bending of the cantilever causing thermal drift. Furthermore, optical interferences are usually observed in liquid medium with conventional optical sensing. Also, alignment of the laser beam can be a complicated task in liquid medium. Ultimately, the integration of QTF sensors in microanalysis systems and lab-on-a-chip devices could solve some of the problems associated with mass detection using microfabricated cantilevers [93].

But one of the main drawbacks of QTF sensors is that there are no commercial devices suitable for working in liquid media. Therefore, these nanotools are usually custom-made and because of the manufacturing process it is very difficult to obtain repeatable probes with an exact response. Other disadvantage of QTF in front of cantilevers is that, tip radiuses of the probes are not so smaller than commercial AFM tips and lateral resolution is worse. Another unsolved issue is the quantification of the interaction forces when working in shear mode because there is no a clear method to obtain the effective spring constant K_{eff}. Relative mechanical measurements have already done in polymers and bacteria biofilms [94] but it is difficult to obtain quantitative values of forces implicated during mechanical characterization. Even so, some scientific teams have implemented first experiments to show the ability of QTF as biomolecular recognition nanosensor. The self-sensing probes can be functionalized to recognize specific molecules in the sample surface [95-96].

1.4.2 Operation

The tuning forks are miniature quartz crystals resonators used as a time base in electronics and watch industries. To develop a fork-based miniaturized force sensor for STM / AFM microscope, a sharp tip is attached at the end of one of his arms. When a gradient of forces is acting on the tip, it causes a change in the resonant frequency of the sensor, so it can be used as a sensor for dynamic AFM microscopy. Unlike the cantilevers, quartz tuning forks are very stiff (spring constant arms k = 10^3 - 10^4 Nm^{-1}) which allows a highly reduced tip-sample distance without the tip jumps to contact, even for oscillation amplitudes very small [97-98].

The tuning forks are commercially available through companies that sell electronic components and its price round 0.1 - 1 € per unit. The QTF are hermetically enclosed in a capsule exiting the two electrodes, which are used to excite the oscillation of the tuning fork and measuring the piezoelectric current. Although there are many manufacturers and models, the size and type of housing is fairly standardized. In our experiments we used QTFs with a resonance frequency of 32,768 Hz (AB38T model, AbraconCorp., USA). As a first step, the metallic cover of the resonator was removed and a chemically sharpened SiO_2 fiber was attached to one of the prongs of the QTF. To taper the probes, a 125 μm optical fiber was dipped into 40% HF solution with a layer of iso-octane (C_8H_{18}) on top to protect against the acid vapors, as proposed in [99]. The process is self-terminating and lasted around 90 min. Once the etching had stopped, the fibers were rinsed with ethanol and water and mounted onto the resonator with cyanoacrylate glue, with a length of 3-4 mm protruding from the fork. This is the minimum length necessary to work with the liquid cell while maintaining the QTF resonating in air. The longer the fiber, the lower of the Q obtained due to the extra mass and unbalancement of the sensor. Anyway, more important for the drop of the Q is the immersion depth of the fiber end in the liquid [100]. The tip radiuses were between 100 and 150 nm.

This work is centered in shear mode operation and electrically excited because we considered that the two prongs freely oscillating quartz tuning fork is the most suitable configuration in front of perpendicular mode, to be embedded in a compact biosensor and for the measurements quantification. Therefore, a specific circuitry is implemented to drive the tuning fork and measure the current using a transimpedance amplifier (TIA). The choice for the TIA was an OPA656 from Texas Instruments, with a 10^6 V/A gain and 1 MHz bandwidth.

1.4.3 QTF applications in biology

The use of QTF to work with biological samples has not been extensively reported if compared with studies reported using conventional AFM cantilevers. Nevertheless, in the last few years some works have reported the use of QTF in imaging cells [101], bacteria [94] or biomolecules [102] (see figure 8). Qualitative molecular recognition has been performed between avidin and lysozyme antibody in [96] in shear mode. Also, relative mechanical measurements are performed in [94] on *Pseudomonas aeruginosa* during early stages of biofilm formation.

Besides, there are few works on quantitative molecular interaction forces with such a probe in solution. In [95], the specific interaction between a ligand and its receptor is studied with the QTF sensors quantifying the force gradient curves. Small non-linear jumps in the phase curve are identified as unbinding events between the ligand-receptor pair.

As the resonance frequency of the QTF depends on the mass adsorbed on its prongs, it can be used as mass sensor. In [93], QTF are used as mass sensors to evaluate *Pseudomonas aeruginosa* biofilm growth and in [103] two antibiotics are studied on the bacterial biofilm.

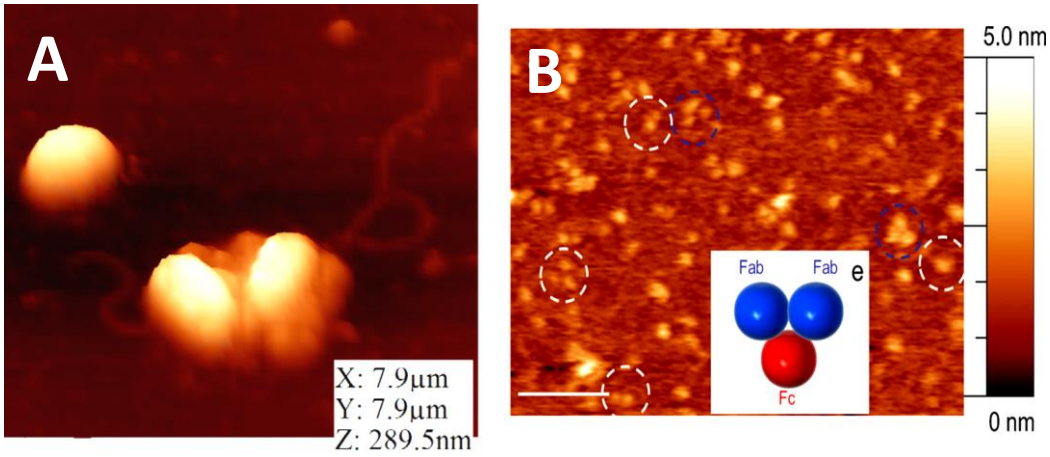

Figure 8. (A) 3D topography of *Pseudomonas aeruginosa* bacteria over gold surface in air [94]. (B) Topography image of IgG antibodies adsorbed onto mica surface [102].

2 Objectives

The main objectives of this thesis is the development of *novel sensors technologies applied to force spectroscopy in molecular biology* and its validation in real molecular studies.

- More specifically, the thesis has been focused on developing technology for: (i) Shear force microscopy using quartz tuning fork based sensors as self-sensing probes where they are an alternative to standard cantilevers to overcome the limitations of the optical detection system in a conventional AFM instrument. (ii) High speed force spectroscopy methodology to achieve rates comparable to SMD simulations for a direct comparison of experimental and simulated forces.
- Once the technology is developed, different experiments in molecular biology will be performed aiming to show its possibilities.

To accomplish the first objective, it has been divided into different subobjectives as problems that should be solved:

- One of the main limitations of tuning fork probes is that they are usually handmade because no commercial probes suitable for a wide range of experiments are available. The handmade devices show considerable variation in dynamic response, thereby hindering the repeatability of experiments. A new controller is needed to ensure the same dynamic response of different sensors in order to maintain the conditions in which the measurements are conducted.
- As mentioned before, QTF-based sensors are usually custom-built in the laboratory by manually attaching a sharpened fiber to one of the prongs of the QTF. The probe tips are generally made of silicon fiber that is tapered using chemical etching techniques or mechanically drawn using a commercial micropipette puller obtaining a tip radius of 100-150 nm. This value is about 10 times higher than the commercial AFM tips, therefore, a method to reduce the tip radius of the probes is required to achieve a comparable lateral resolution than AFM tips and the sensor should be operable in shear mode in a liquid environment.
- Characterization of the QTF-based sensors for quantitative measurements remains unclear. Analytical and numerical models currently existing in the literature lack of the coupling between the electrical and the mechanical aspects of the sensors. It is necessary to study the sensor dynamics to better understand and quantify different parameters of the sensors. The sensor's spring constant and the oscillation amplitude are required parameters to evaluate the tip-sample forces; however, there is certain controversy within

the research community as to how to arrive at a value for the static spring constant of the device when working in shear mode. It is indispensable to find a method to find these indispensable parameters for a sensor calibration and forces quantification.

- The main problem for comparing SMD results with experimental data is that SMD simulations were restricted to nanosecond timescales (due to the high computational demand of all-atomistic simulations). A high speed force spectroscopy methodology will be developed to achieve rates comparable to SMD simulations for a direct comparison of experimental and simulated forces.

Once the technology is developed, different biological experiments will be carried out with the objective to demonstrate the possibilities of the developed technologies in real applications:

- Different imaging techniques of biomolecules will be tested trying to find the optimal one applied to the QTF based nanosensors.
- Molecular interaction experiments will be carried out to show the ability of the QTF probes to perform specific interaction measurements between receptor-ligand pairs in liquid medium.
- Unfolding measurements of titin will be performed at high speeds to be compared with simulation results.

3 Results

3.1 Technological development for shear force microscopy

3.1.1 Associated Publication 1

Electronic driver with amplitude and quality factor control to adjust quartz tuning fork sensors response for atomic force microscopy

By

Laura González, Jorge Otero, Gonzalo Cabezas and Manel Puig-Vidal

SIC-BIO, Bioelectronics and Nanobioengineering Group, Department of Electronics, University of Barcelona, Marti i Franques, 1, 08028, Barcelona, Spain

Published in

Sensors and Actuators A: Physical *184 (2012) 112– 118*

Sensors and Actuators A 184 (2012) 112–118

Contents lists available at SciVerse ScienceDirect

Sensors and Actuators A: Physical

journal homepage: www.elsevier.com/locate/sna

Electronic driver with amplitude and quality factor control to adjust the response of quartz tuning fork sensors in atomic force microscopy applications

Laura González, Jorge Otero, Gonzalo Cabezas, Manel Puig-Vidal*

SIC-BIO, Bioelectronics and Nanobioengineering Group, Department of Electronics, University of Barcelona, Marti i Franques, 1, 08028, Barcelona, Spain

ARTICLE INFO

Article history:
Received 20 January 2012
Received in revised form 19 June 2012
Accepted 19 June 2012
Available online 4 July 2012

Keywords:
Atomic force microscopy
Quartz tuning fork
Q control
Self-sensing probe

ABSTRACT

Quartz tuning fork-based sensors are self-sensing probes that are gaining popularity in atomic force microscopy. They do not need a laser-photodiode system and they have a higher quality factor in liquid than standard cantilevers. However, the main limitation of tuning fork probes is that they are usually handmade because no commercial probes suitable for a wide range of experiments are available. The handmade devices show considerable variation in dynamic response, thereby hindering the repeatability of experiments. To overcome this problem, here we develop an electronic driver to simultaneously control the quality factor (Q) and the oscillation amplitude (A) of the device. The driver provides clear advantages over classical Q-control modules where the amplitude of oscillation is modified when the Q factor is changed. Direct measurements on a commercial interferometer showed that the effective Q factor can be adjusted to experimental requirements while maintaining the mechanical amplitude of oscillation constant. Experimental amplitude vs. distance curves confirm that our driver achieves an equivalent dynamic response from distinct handmade sensors (with varying mechanical characteristics) by means of electronic adjustment. The driver is a simple but effective method to ensure the same measurement conditions with a range of quartz tuning fork probes and also the reliability and repeatability of experiments.

1. Introduction

Atomic force microscopy (AFM) is widely used to image sample surfaces with high accuracy [1,2]. However, despite the wide application of this technique in air, the imaging of soft biological samples in liquid presents several difficulties. Imaging biological samples, such as biomolecules, requires the maintenance of a constant, very small interaction force between the tip and the sample surface. Commercial AFM sensors present a very low quality factor (Q) when samples are immersed in liquid and they are very difficult to integrate into multiprobe systems [3]. In contrast, quartz tuning fork (QTF)-based sensors have the capacity to image the topography of samples with sub-nm resolution [4]. QTFs are self-sensing probes, so they are suitable for use in a multiprobe station [5] working with biological samples [6]. QTF sensors are resonators based on the piezoelectric properties of quartz. Several attempts have been made to study QTFs for their use in scanning probe microscopy [7]. These devices present a very stable resonance frequency and a very narrow band. As they present a higher Q (1000–5000) than standard cantilevers, QTFs show high performance in experiments performed in a liquid environment. For instance, differences of 110 nm have been reported in cytospin membrane topography [8] when the cell is in air or immersed in liquid, red blood cell morphology has been accurately measured [9], and recognition events between avidin/biotin and lysozyme/anti-lysozyme have been detected in the phase image at a high signal-to-noise ratio [10].

One of the main drawbacks of QTF sensors is that there are no commercial devices suitable for working in liquid media. Thus these nanotools are custom-made and because of the manufacturing process it is very difficult to obtain repeatable probes with a similar response. Given that the lack of repeatability is usually the main source of error in quantitative measurements, it is common to use more than one QTF sensor in the same study because the tip can become contaminated, damaged or even broken. When performing an experiment, it is crucial to ensure the same dynamic response of the sensor in order to maintain the conditions in which the measurements are conducted.

To overcome the differences between sensors, here we develop a module to control the quality factor (Q) and vibration amplitude (A). The quality factor is controlled analogically and the amplitude vibration digitally (with an algorithm). The control module is integrated with the QTF and drives the interface circuitry, which was designed to be transparent to commercial atomic force microscopes. All the experiments presented in this study were performed on a commercial Cervantes atomic force microscope (Nanotec

* Corresponding author. Tel.: +34 934039163; fax: +34 934021148.
E-mail address: manel.puig@ub.edu (M. Puig-Vidal).

0924-4247/$ – see front matter © 2012 Elsevier B.V. All rights reserved.
http://dx.doi.org/10.1016/j.sna.2012.06.016

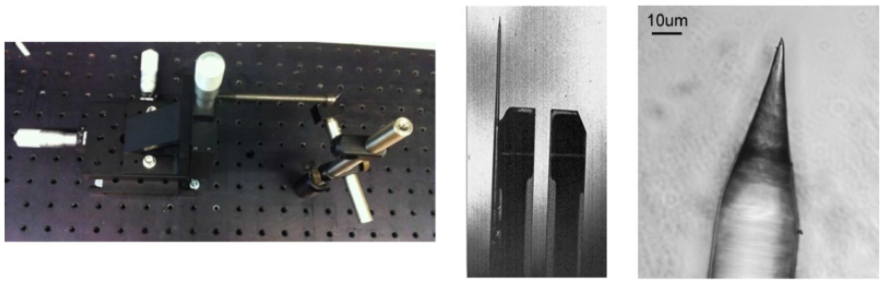

Fig. 1. (a) Mechanical equipment for the assembly and gluing of the sharpened fiber tip to tuning fork. (b) Optical image of the chemically sharpened fiber mounted on a quartz tuning fork resonator. The tines are $L = 3.6$ mm long, $W = 0.6$ mm wide and $T = 0.3$ mm thick. (c) Optical images of one of the QTF fiber tips used in the experiments.

Electrónica S.L.) [11] without any change in the hardware or software of the microscope. The module allows control of the Q and A parameters independently in order to achieve the same desired response in different handmade QTF-based sensors [12].

In amplitude modulation imaging, sensor response is characterized by the reduction of the vibration amplitude (A/A_0) in function of the tip–sample distance, Z, where A represents the present oscillation amplitude and A_0 the free amplitude of the QTF. Thus the dynamic response can be measured by moving the tip close to the surface of a non-deformable substrate. Generally speaking, commercially available Q-controllers [13] do not control the free amplitude of oscillation. In FM mode, they often integrate a second feedback to maintain the oscillation amplitude constant during the measurement; however, in order to change the free amplitude, the operator has to change the driving voltage manually. As a result, if the driving voltage is kept constant, the amplitude of the excitation voltage applied to the fork at the resonance frequency is higher when Q is increased and lower when this parameter is decreased. Accordingly, the mechanical (A) varies in function of Q [14,15].

In the literature there is some controversy regarding the suitability of the Q-control module to modify sensor parameters. Some authors do not report a true improvement in image acquisition by changing the effective Q electronically [16]. However, Q-control systems are studied mostly because they notably enhance imaging of soft biological sample topography as a result of the reduction of tip–sample interaction [17]. Moreover, a similar Q-control system can be applied to cantilever-based AFM, rather than to standardize sensor response, to change the Q controlling A. Increasing effective Q in phase modulation also leads to greater force sensitivity [18]. This phenomenon was studied in liquids [19], where it was found that Q-controlled A modulation enhanced image quality. An example of improved imaging can be found in [20] where the measured DNA heights were found to be higher as a result of the force exerted over the sample being lower when Q-control is active.

To ensure the reliability of the implemented driver operation and to validate our electrical measurements from the current through the fork, A was calibrated by an interferometer that directly measured mechanical oscillation. In this regard, the oscillation amplitude of a QTF was measured for two Q factors but the output voltage was regulated in resonance frequency. Having validated the performance of the first module, we adjusted two handmade QTF-based sensors with distinct mechanical behavior to achieve the same dynamic response. The method presented here allows the operator to obtain the same dynamic response from handmade QTF-based nanosensors, thereby ensuring the repeatability of the experiments.

2. Materials and methods

2.1. Quartz tuning fork-based nanosensors

For a configuration where one prong of the QTF is clamped, the resonance frequency (f_0) of the device depends on the spring constant (k) and effective mass (m) of the tuning fork (see Eq. (1)) [21]. The spring constant depends on physical and geometrical properties as shown in Eq. (2) where E is the quartz Young's modulus, W is the width, T is the thickness and L is the length. Thus when a force is applied to the QTF, there will be a resonance frequency shift that depends on the force gradient. Nevertheless, the coupling between the two prongs has to be incorporated in the models when both prongs oscillate freely [22,23].

$$f_0 = \frac{1}{2\pi}\sqrt{\frac{k}{m}} \tag{1}$$

$$k = \frac{E}{4}\frac{WT^3}{L^3} \tag{2}$$

Commercial QTFs were encased in a vacuum and their $f_0 = 2^{15}$ (32,768 Hz) and $Q = 40{,}000$–$50{,}000$. To use the QTFs as sensors for AFM, first we removed the protective metallic capsules from the forks. A sharpened fiber was then glued to the end of one of their prongs. The 125-μm SiO_2 fibers were sharpened using the meniscus etching technique [24]. The fibers were immersed in a 40% HF solution with a protective isooctane (C_8H_{18}) layer, which produced a repeatable tip radius of about 200 nm (see Fig. 1c). The etched fiber was glued to the QTF by a mechanical apparatus 3 μm long in each 3 directions (Fig. 1a). All the probes were 8 mm long, half of this length was glued while the other half with the sharpened end stood out from the tine. All the sensors were built in the same way and had a similar mass load in one prong. The Q decreased as a result of the mounting process and it was strongly dependent on fiber length. In general, a fiber length of 4 mm was enough to work with the end inside the liquid cell. The QTF continued to resonate in air, obtaining a high Q value of around 2000. Consequently, this was the length chosen to build the QTF-based sensors.

The QTFs were electrically driven to their resonance frequency and their A was calculated by measuring the current through the sensor. The electronic driving circuit was based on a transimpedance amplifier (TIA) and lock-in amplifier modules. The mechanical vibration amplitude was calculated using the expression given by Eq. (3) [25], where V_{rms} is the excitation voltage, I_{rms}

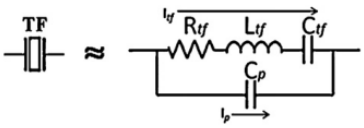

Fig. 2. Butterworth–Van Dyke equivalent circuit for the tuning fork.

is the measured current through the QTF, k is the spring constant, f_0 is the free resonance frequency, and Q is the quality factor.

$$A_0 = \sqrt{\frac{QV_{rms}I_{rms}}{k2\pi f_0}} \tag{3}$$

All the experiments were performed in amplitude modulation detection. Interaction forces between the tip and the sample surface were evidenced as a shift in resonance frequency. As the device was driven at a constant frequency, there was a change in the oscillation amplitude of the device [26].

2.2. Electronics

The mechanical behavior of QTF devices can be modeled by an electrical equivalent circuit (Butterworth–Van Dyke model) [27] based on a serial LRC resonator with a parallel parasitic capacitance, as shown in Fig. 2. The capacitance C_{tf} and inductance L_{tf} model the potential and kinetic energy storage, respectively, the resistor R_{tf} the dissipation and the parallel capacitance C_p all the parasitic capacitors related to contacts, cables, etc.

As current losses are produced by the parasitic capacitance of the QTF [28], we added a module to compensate this effect. Currents through the fork (using the Butterworth–Van Dyke model) and a parasitic capacitor with a simple driving circuit are shown in Eqs. (4) and (5). This asymmetry limits the signal-to-noise ratio (SNR) as shown in Eq. (6), where w is frequency and V_{drive} is the driving voltage to the QTF prongs. To maximize SNR, parasitic current Ip was nulled near the resonance frequency of the device by implementing a compensating circuit. The same capacitance current but shifted 180° in phase, the value of which can be adjusted with a variable capacitor [28], was added to the current flowing through the device. Thus, only the current passing through the QTF was amplified by the TIA and it was translated into voltage to measure the extent of oscillation with a lock-in amplifier.

$$I_{tf} = \frac{V_{drive}}{R_{tf} + (1/jwC_{tf}) + jwL_{tf}} \tag{4}$$

$$I_p = V_{drive} \cdot jwC_p \tag{5}$$

$$\mathrm{SNR} = 20 \cdot \log\left(\frac{I_{tf}}{I_p}\right) = 20 \cdot \log\left(\frac{1}{C_p \cdot (L_{tfw^2} + R_{tf}jw + (1/C_{tf}))}\right) \tag{6}$$

Once the effect of the parasitic capacitor is minimized near to the resonance frequency, Q and A in resonance are the critical parameters that contribute to the dynamic response of the sensor. These parameters are related to the QTF behavior and the handmade production process. The behavior can vary greatly between sensors. In order to implement a proper and reliable QTF-based sensor, a precise and independent control of these two parameters is required. We developed an optimized and fully custom-designed electronic module for this purpose.

Several approaches have been used to tune the Q of the QTF device. In [29,30], the current through the QTF is measured by a TIA, the feedback signal is amplified with a certain gain (in-phase to increase the Q and counter-phase to decrease the Q) and is added to the original driving voltage of the QTF. Our Q-control module was based on the amplitude and phase feedback of the output voltage through the TIA. The circuit in Fig. 3a shows the electronic driver used with the Q control. After the parasitic capacitor had been compensated, the current was fed back to increase/decrease the effective Q value. With the parasitic capacitance compensated and Q value selected, the oscillation amplitude was adjusted to the resonance frequency using an iterative algorithm that changes the excitation voltage entering the QTF, according to the output voltage required (see Fig. 3b). To achieve the same dynamic response in the devices, the driving voltage was selected in function of the output amplitude desired. Thus if the Q value was changed was detected, it was necessary to recalculate a new driving voltage to obtain the desired oscillation amplitude, which corresponds with a certain current I_{rms} flowing through the tuning fork. In this way, these two parameters were controlled independently.

The Q value of the sensors differed depending on the fabrication process. Q factors between 1000 and 5000 were obtained.

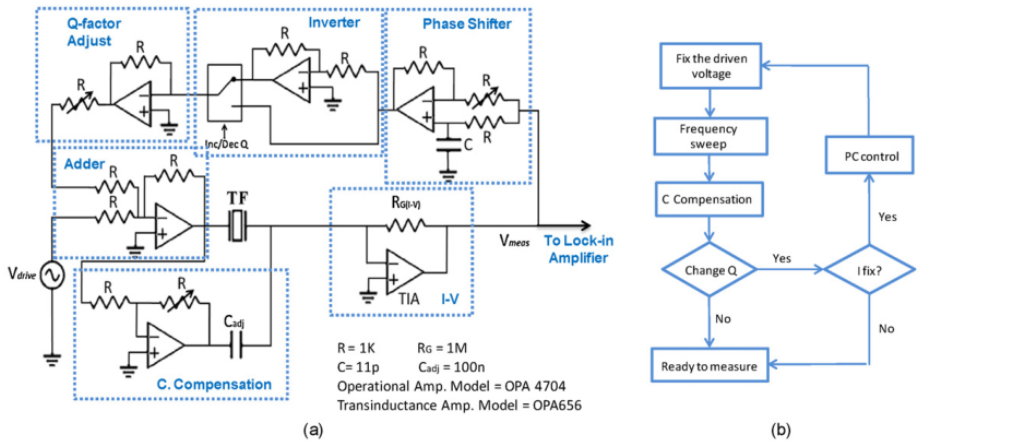

Fig. 3. (a) Electrical circuit implemented with subcircuit to compensate the parasitic capacitor and a module to control the Q value. (b) Flow diagram of the A adjustment algorithm.

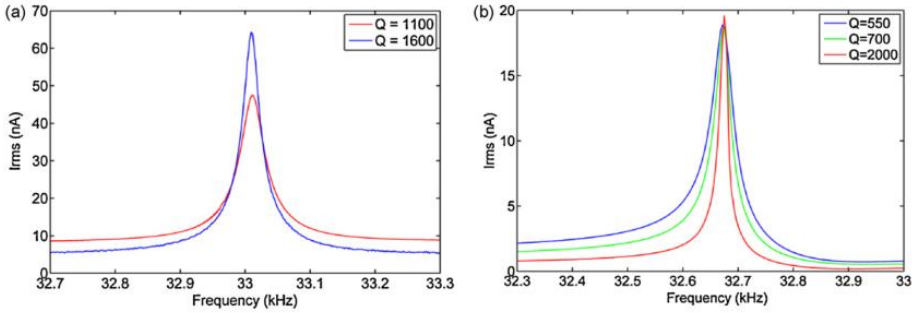

Fig. 4. (a) Frequency responses of a QTF driven at 50 mV for $Q = 1100$ and $Q = 1600$ using a classical Q-control system where A is not adjusted when the Q-factor is modified. (b) Frequency responses of a QTF driven at 20 mV before and after using the novel Q-control module where A is maintained constant.

The Q-control module is able to change the Q values in a limited range: in our case, for a QTF which has a resonant frequency of 32.592 Hz and Q value of 2400 when the tip was glued, Q factors from 500 to 10,600 were obtained by adjusting amplifier to maximum gain and phase shifter from 180° to 0°, respectively. This range of Q values was wide enough to match different sensors with initial different parameters (Q and A) to obtain the same mechanical behavior. Using classical Q-control modules amplitude oscillation A changes according with the selected Q value, higher A value when Q increases and lower when Q decreases (Fig. 4a). Our implemented electronic driver, with the developed novel Q-control method, was able to change the quality factor of the device while maintaining constant the oscillation amplitude as indicated in Fig. 4b. The variability in the output measured with the lock in amplifier was of

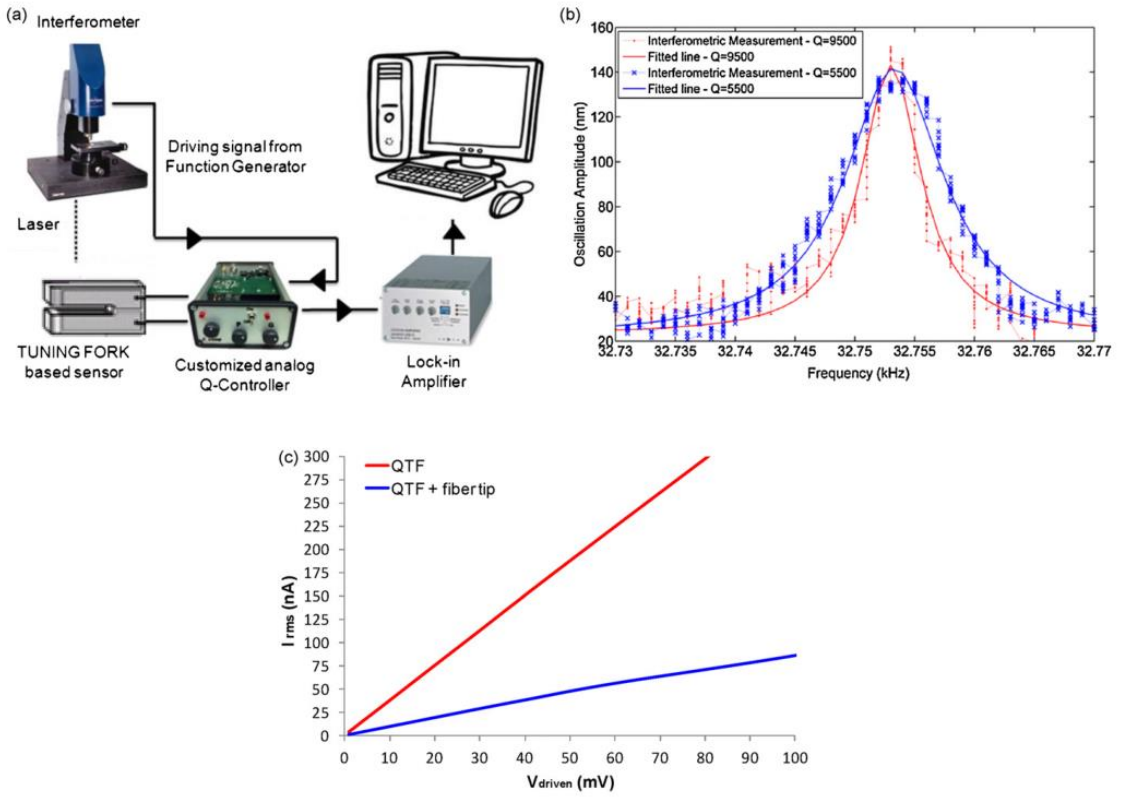

Fig. 5. (a) Schematic measurement set-up of the system required for obtaining QTF voltage output and mechanical vibration by an interferometer. The interferometric vibrometer equipment used was a Zoom Surf 3D from Fogale Nanotech, the lock-in amplifier was from Anfatech and the iterative algorithm software for controlling oscillation amplitude was written in LabView code. (b) Oscillation amplitude (measured with the interferometer) of a QTF nanotool for excitation amplitude of 40 mV when changing the quality factor from 9500 to 5500. (c) Piezocurrent measured in the resonance frequency of a QTF with and without a fiber tip for a range of driving voltages.

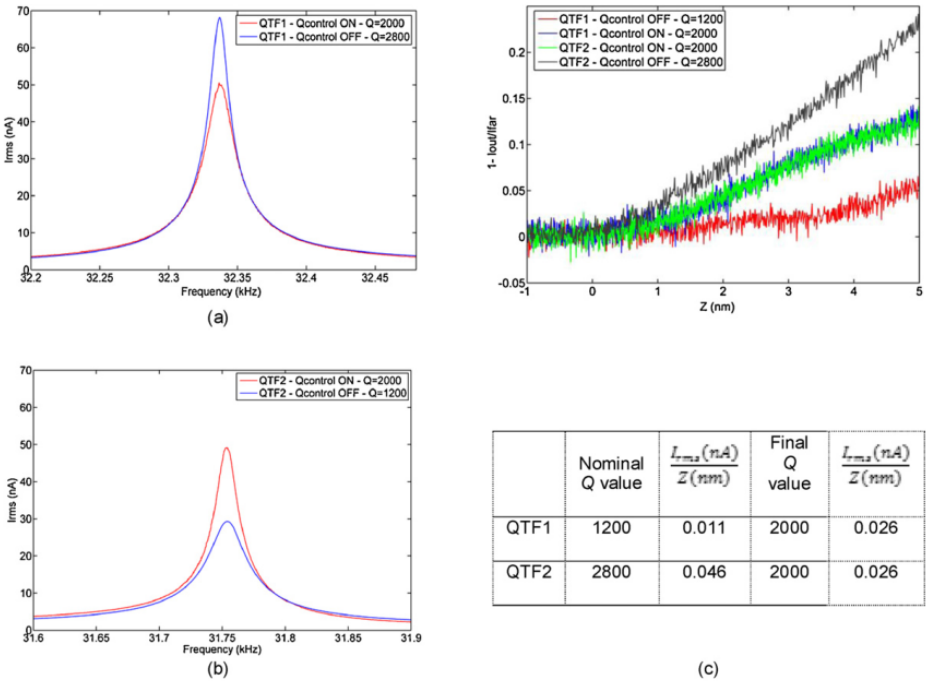

	Nominal Q value	$\frac{I_{rms}(nA)}{Z(nm)}$	Final Q value	$\frac{I_{rms}(nA)}{Z(nm)}$
QTF1	1200	0.011	2000	0.026
QTF2	2800	0.046	2000	0.026

Fig. 6. (a) Frequency responses of QTF1. The blue line is the initial resonance curve before using the *Q*-control module presenting a nominal *Q* value = 2800 and the red line is the resonance curve when *Q* factor wais decreased to 2000 using the *Q*-control system and driving voltage is adjusted by software to have I_{rms} = 50 nA. (b) Frequency responses of QTF2. Blue line is the initial resonance curve before using the *Q*-control module presenting a nominal *Q* value = 1200 and the red line is the resonance curve when *Q* is increased to 2000 using the *Q*-control system and driving voltage is adjusted by software to have I_{rms} = 50 nA. (c) The tip–sample distance relationship of amplitude for two QTFs with different initial characteristics and adjusted by the *Q*-control module to have an identical response. I_{out} (nA) is the measured output current through the QTF and I_{far} (nA) is the output current when the tip is far from the sample in resonance frequency.

19.04 ± 0.49 mV, then the error in the amplitude control was below 2.5%.

3. Results

3.1. Interferometer based measurements

In this experiment, we checked that modification of the *Q* factor value without changing the *A* value was not an electronic artifact and that the mechanical oscillation at the resonance frequency was maintained constant. The *A* of the QTF was calculated from measuring the current passing through the device, following the expression in Eq. (3); however, this is an indirect measurement. When changing the amplitude and phase of the driving signal, it was necessary to confirm that *A* could still be calculated from the measurement of the current passing through the nanotool. The *A* parameter was directly measured using an interferometric vibrometer (ZoomSurf 3D from Fogale Nanotech [31]) to confirm that the true oscillation amplitude had not changed when we obtained the same current measurement.

The motion of the *A* was detected using the stroboscopic mode, which is the most suitable approach for dynamic measurements. The QTF was illuminated with a beam of coherent light that was split into two by a grating mirror. The path difference between the two beams was then related to a phase difference and the *Z* movement of the QTF was calculated with nm accuracy in a range of $\lambda/2$ [32].

The experimental setup is shown in Fig. 5a. Measurements were performed on a QTF whose output current was kept constant and *Q* value was changed with the *Q*-control module. Interferometric measurements were fitted with a Lorentzian function, a characteristic resonance curve for quartz resonators [33]. Fig. 5b shows the mechanical oscillation amplitude frequency response of the QTF sensor without a fiber tip, measured with the interferometer. The QTF used showed an original *Q* value of 9500 when it was biased at 40 mV. When using our electronic module, the *Q* value was decreased to 5500 while keeping *A* constant. Both measurements showed the same mechanical oscillation amplitude, in spite of changing the effective *Q* value electronically (see Fig. 5b). Interferometric measurements were performed on a QTF without a fiber tip because in the measurement setup described it was only possible to measure the oscillation of one prong. The assumption of symmetrical movement of the two prongs was valid only with a fiberless sensor. Since the relationship between measurements of output current I_{rms} of the QTF with and without a fiber tip was proportional, interferometric measurements of oscillation amplitude were also assumed to be proportional. The piezocurrent measured at resonance frequency for a range of driving voltages is shown in Fig. 5c for a QTF with and without a tip. The relationship between driving voltage and current measurement was linear to 100 mV, the range we tested and used for this work. Exactly, oscillation amplitude is linearly proportional to the driving amplitude until at least 100 mV, which is the range usually used. Higher excitation amplitudes are not practical in real applications because high mechanical

oscillation amplitudes increase dissipation and interaction forces between the probe and the sample surface.

3.2. Experimental dynamic response measurement

Sensor behavior depends mainly on Q and A_0 parameters. By adjusting these two parameters, the QTF sensor response can be modified. As the electrical impedance of the device does not change, if the same current through the QTF is measured at the resonance frequency after modifying its Q electronically, it means the QTF driving voltage V_{rms} has not changed in resonance frequency (confirmed from interferometric measurements that the mechanical oscillation remained the same).

According to expression of Eq. (3), for two nanosensors with a certain value of oscillation amplitude A in resonance, we measure the same I_{rms} and considering K and f_0 constant parameters. If these devices present different nominal Q values, then V_{rms} in resonance should be properly adjusted in each case to maintain the same A value when the Q-control loop is switched on. The two nanosensors, which presented initial different parameters, were modified to exhibit the same response by adjusting the Q and A_0 values. Each QTF presented a different nominal Q (2800 for QTF1 and 1200 for QTF2). These Q factors were modified using the Q-control module by changing them in both cases to the final desired value of 2000. The output current I_{rms} in resonance frequency was adjusted to 50 nA, setting the appropriate input voltage V_{rms} for each QTF once the Q-control loop was activated. The resulting frequency responses for QTF1 and QTF2 are presented in Fig. 6a and b, respectively.

The dynamic response of a QTF sensor was characterized by performing approach curves toward a gold substrate. The QTF was driven at resonance frequency and A_0 was constant when the tip was far from the sample. When the interaction force between the probe tip and the sample substrate appeared, A was reduced and the sensor response I_{rms} (nA) vs. Z (nm) was measured.

Amplitude vs. tip–sample distance curves were performed measuring amplitude (equivalent to I_{rms}) dependence when approaching the QTF tip to the gold surface. Each nanosensor was characterized for two Q factors, the nominal and the final desired values. When the two QTFs were adjusted to have the same A_0 and Q, the response was the same (note green and blue lines in Fig. 6c). The devices presented the same slope in the characteristic curve, thus indicating that we obtained two QTF nanosensors with the identical dynamic behavior.

4. Conclusions

Here we develop a Q and A control module to match the response of QTF-based nanosensors for AFM applications. Our results show that by electronically controlling the Q factor and A in the nanotool, the response of the device can be modified to the requirements of the experiments. First, by interferometric measurements, we have shown that the effective Q of the QTF can be altered without changing the mechanical vibration amplitude. Thus, the effective Q factor can be increased or decreased independently of the output current, thus maintaining the peak of resonance constant. This result confirms a theoretical concept that has sometimes appeared confusing in previous studies and confirms that we have not introduced an artificial electronic trick in the measurements. In a second step, we adjusted two hand-built nanosensors to obtain an identical dynamic response. These results validate our electronic driver as a highly useful tool for working in AFM as it allows repeatable measurement setup conditions throughout the experiment.

The novel driver described here allows adjustment of the characteristic response (mV/nm) without changing the experimental setup. This feature is an advantage over standard AFM systems, where the cantilever must be physically replaced to change the response or sensitivity of the measurement sensor. In addition, using our driver, the dynamic response of the QTF sensor can be chosen to meet sample requirements, for instance, higher Qs for imaging soft biological samples [34] or lower ones for harder samples.

As the probes are handmade, it is crucial to maintain identical sensor characteristics while performing the same experiment. Even when an accurate micrometric setup was used for QTF sensor production, the frequency response obtained for each sensor differed. QTF symmetry in frequency response was broken when the fiber was attached and Q was reduced significantly as a result of the mass added to one of the prongs. Moreover, as the QTF became imbalanced, the oscillation amplitude of the two prongs differed and the effective spring constant was increased [7]. Here the implemented driver adjusted the electrical parameters Q and A to counteract the effect of the imbalance. Since the tip mass loads were very similar between the sensors, we succeeded in standardizing their dynamic response, although the variation in effective spring constant was not controlled. Nevertheless, the main contribution of this study is that electronic adjustment of Q and the current through the QTF achieves an equivalent response of sensors and thus allows comparable results.

Our results show that the novel controller allows the operator to adjust the variable capacitor to compensate the parasitic capacitance of the device and to tune the Q factor smoothly and adjust it independently of A. In short, this is a simple and effective method for overcoming the main drawback of handmade QTF sensors in AFM applications. Moreover, our electronic module can be easily integrated into commercial microscopes and reliably used in AFM systems.

Acknowledgments

This work was supported in part by the Spanish *Ministerio de Educación* through project TEC2009-10114 and grants BES-2010-031186 and AP2006-01079, and also by the regional Catalan authorities through project VALTEC09-2-0058.

References

[1] G. Binnig, C.F. Quate, C. Gerber, Atomic force microscopy, Physical Review Letters 56 (1986) 930.
[2] J. Zhao, et al., Metrological atomic force microscope with self-sensing measuring head, Sensors and Actuators A 167 (2) (2011) 267–272.
[3] W. Yashiro, I. Shiraki, K. Miki, A probe-positioning method with two-dimensional calibration pattern for micro-multi-point probes, Review of Scientific Instruments 74 (2003) 2722.
[4] E. Wutscher, F.J. Giessibl, Atomic force microscopy at ambient and liquid conditions with stiff sensors and small amplitudes, Review of Scientific Instruments 82 (2011) 093703.
[5] J. Otero, M. Puig-Vidal, L. Ribas-Xirgo., Multirobot control system design for nanomanipulation applications, International Journal of Factory Automation, Robotics and Soft Computing 1 (2008) 53–59.
[6] J. Otero, L. González, G. Cabezas, M. Puig-Vidal, Multi-tool platform for morphology and nanomechanical characterization of biological samples with coordinated self-sensing probes, IEEE/ASME Transactions on Mechatronics PP (99) (2012) 1–9.
[7] A. Castellanos-Gomez, A.N. Agraït, G. Rubio-Bollinger, Dynamics of quartz tuning fork force sensors used in scanning probe microscopy, Nanotechnology 20 (Issue 21) (2009) 215502.
[8] W.H.J. Rensen, N.F. van Hulst, Imaging soft samples in liquid with tuning fork based shear force microscopy, Applied Physics Letters 77 (2000) 10.
[9] S. Kwon, S. Jeong, Y. Kang, Topography and near-field image measurement of soft biological samples in liquid by using a tuning fork based bent optical-fiber sensor, Review of Scientific Instruments 82 (2011) 043707.
[10] M. Hofer, et al., Molecular recognition imaging using tuning fork-based transverse dynamic force microscopy, Ultramicroscopy 110 (2010) 605–611.
[11] Cervantes AFM system Technical Specifications. http://www.nanotec.es/products/cervantes.php, January 2012.
[12] J. Otero, M. Puig-Vidal, G., Cabezas, L. Gonzalez, Microscopy device with a resonant fork and a control unit for a nanosensor based on a resonant fork, Patent ES 201031135, 23 July 2010.

[13] Q-control Module from NanoAnalytics. http://www.nanoanalytics.de/en/hardwareproducts/q-control/index.php.
[14] J. Jahng, M. Lee, H. Noh, Y. Seo, W. Jhe, Active Q control in tuning-fork-based atomic force microscopy, Applied Physics Letters 91 (2007) 023103.
[15] G. Ctistis, Controlling the quality factor of a tuning-fork resonance between 9 K and 300 K for scanning-probe microscopy, Journal of Physics D: Applied Physics 44 (2011) 375502.
[16] R.W. Stark, G. Schitter, A. Stemmer, Tuning the interaction forces in tapping mode atomic force microscopy, Physical Review B 68 (2003) 085401.
[17] A.D.L. Humphris, A.N. Round, M.J. Miles, Enhanced imaging of DNA via active quality factor control, Surface Science 491 (3) (2001) 468–472.
[18] N. Kobayashi, et al., High force sensitivity in Q-controlled phase-modulation atomic force microscopy, Applied Physics Letters 97 (2010) 011906.
[19] H. Hölscher, U.D. Schwarz, Q-controlled amplitude modulation atomic force microscopy in liquids: an analysis, Applied Physics Letters 89 (2006) 073117.
[20] D. Ebeling, et al., Imaging of biomaterials in liquids: a comparison between conventional and Q-controlled amplitude modulation ('tapping mode') atomic force microscopy, Nanotechnology 17 (2006) S221–S226.
[21] G. Simon, M. Heyde, H. Rust, Recipes for cantilever parameter determination in dynamic force spectroscopy: spring constant and amplitude, Nanotechnology 18 (2007) 255503.
[22] B.P. Ng, et al., An improved dynamic model of tuning fork probe for scanning probe microscopy, Journal of Microscopy 234 (Pt 2) (2009) 191–195.
[23] A. Castellanos-Gomez, A.N. Agraït, G. Rubio-Bollinger, Force-gradient-induced mechanical dissipation of quartz tuning fork force sensors used in atomic force microscopy, Ultramicroscopy 111 (2011) 186–190.
[24] S. Mononobe, Near-field optical fiber probes and the imaging applications, in: Progress in Nano-Electro-Optics III, Springer, Berlin, 2005.
[25] J. Liu, A. Callegari, M. Stark, M. Chergui, A simple and accurate method for calibrating the oscillation amplitude of tuning-fork based AFM sensors, Ultramicroscopy 109 (2008) 81–84.
[26] P. Sandoz, J. Friedt, E. Carry, Vibration amplitude of a tip-loaded quartz tuning fork during shear force microscopy scanning, in, Review of Scientific Instruments 79 (2008) 086102.
[27] F.J. Giessibl, High-speed force sensor for force microscopy and profilometry utilizing a quartz tuning fork, Applied Physics Letters 73 (1998) 3956–3958.
[28] Y. Quin, R. Reifenberger, Calibrating a tuning fork for use as a scanning probe microscope force sensor, Review of Scientific Instruments 78 (2007) 063704.
[29] G. Ctistis, Controlling the quality factor of a tuning-fork resonance between 9 and 300 K for scanning-probe microscopy, Journal of Physics D: Applied Physics 44 (2011) 375502.
[30] V.T. Tung, S.A. Chzhik, T.X. Hoai, Parameters of tip–sample interactions in shear mode using a quartz tuning fork AFM with controllable Q-factor, Journal of Engineering Physics and Thermophysics (2009) 140–148.
[31] Interferometric Vibrometer Technical Specifications. http://www.fogale.fr/optical_profilers/pages/laserdoppler, January 2012.
[32] R. Leach, L. Brown, R. Blunt, M. Conroy, Guide for the Measurement of Smooth Surface Topography using Coherence Scanning Interferometry, National Physical Laboratory Good Practice Guide, num. 18, 2008.
[33] K. Karraï, R.D. Grober, Piezo-electric tuning fork tip–sample distance control for near field optical microscopes, Ultramicroscopy 61 (1995) 197–205.
[34] M. Antognozzi, et al., Increasing shear force microscopy scanning rate using active quality factor control, Applied Physics Letters 82 (2003) 2761.

Biographies

Laura González received the degree in electrical engineering from the Polytechnic University of Catalonia, Barcelona, Spain, in 2008. She received the M.Sc. degree in biomedical engineering from the University of Barcelona (UB), Barcelona, Spain, in 2010, where she is currently working toward the Ph.D. degree in the Microrobotics and Nanocharacterization Laboratory in the Electronics Department of the Physics Faculty. Her research interests include scanning probe techniques and developing self-sensing probes and their associated interface electronics for molecular and cellular biological studies.

Jorge Otero received the degree in computer science from the Polytechnic University of Catalonia, Barcelona, Spain, in 2003, and the M.Sc. degree in electronics engineering, in 2006, and the M.Sc. degree in biomedical engineering and the Ph.D. degree in biomedicine in 2008 and 2011, respectively, all from the University of Barcelona (UB), Barcelona, Spain. Since 2005, he has been with the UB for the EU projects I-SWARM and CELLPROM, and since 2006, he has been a Researcher in the physics faculty granted by the Spanish Ministerio de Educación y Ciencia in the Spanish University Professor Formation program. He is currently a Postdoctoral Researcher and Part-time Professor at the same institution. His research interests include collaboration between ultrahigh-resolution robots and novel microscopy techniques for studies in molecular and cell biology.

Gonzalo Cabezas received the degree in electronic engineering in 2006 and the M.Sc. degree in electronics in 2011 from the University of Barcelona, Barcelona, Spain. Before finishing his studies, he joined the Fundació Bosch i Gimpera and the Electronic Department at the University of Barcelona, where he engaged in the developing of biomedical devices for bioimpedance measurements in blood cell detection. In 2009, he joined the Nanotechnology Platform in the Institute for Bioengineering of Catalonia (IBEC). Since 2011, he has been with the SIC-BIO group at the University of Barcelona. His research is focused on electronic development and improvement of an atomic force microscope station based on tuning fork resonators.

Manel Puig-Vidal (M'xx) was born in Igualada, Spain, in 1965. He received the M.Sc. degree in physics from Barcelona University, Barcelona, Spain, in 1988, and the Ph.D. degree in microelectronics from the University Paul Sabatier, Toulouse, France, in 1993. From 1989 to 1993, he was a Research Fellow in the Laboratoire d'Automatique et d'Analyse des Systèmes (LAAS), Toulouse, France, working in Latch-up Free Smart-Power technology for automotive applications. In 1993, he was appointed as an Assistant Professor of electronics at the University of Barcelona working in the field of power electronics. Since 1995, he has been a Professor Titular at the University of Barcelona, teaching courses on power electronics and control systems. He is the Head of the Bioelectronics Research Group associated with the Institute of Bioengineering of Catalunya (IBEC), Barcelona, Spain. Since 1995, he has been participating in different European projects in the field of microrobotics for biomedical applications. His research interests include bioelectronic systems design, portable electronics for in vitro diagnosis medical devices, microrobotics, and AFM nanobiocharacterization for biomedical applications.

3.1.2 Associated Manuscript 1

Improving the lateral resolution of quartz tuning fork-based sensors in liquid by integrating commercial AFM tips into the fiber end

By

Laura González[a], David Martínez-Martín[b,1], Jorge Otero[a], Pedro J. de Pablo[b], Manel Puig-Vidal[a] and Julio Gómez-Herrero[b]

[a]SIC-BIO, Bioelectronics and Nanobioengineering Group, Departament d'Electrònica, Universitat de Barcelona, Marti i Franques 1, 08028 Barcelona, Spain.

[b]Departamento de Física de la Materia Condensada, C-3, Universidad Autónoma de Madrid, Cantoblanco, 28049 Madrid, Spain.

[1]Current address: ETH Zurich, Biosystems Science and Engineering, CH-4057 Basel, Switzerland.

submitted for peer-review to

Sensors and Actuators A: Physical.

Improving the lateral resolution of quartz tuning fork-based sensors in liquid by integrating commercial AFM tips into the fiber end

L. González[a], D. Martínez-Martín[b,1], J. Otero[a], P. J. de Pablo[b], M. Puig-Vidal[a], J. Gómez-Herrero[b]

[a]SIC-BIO, Bioelectronics and Nanobioengineering Group, Departament d'Electrònica, Universitat de Barcelona, Marti i Franques 1, 08028 Barcelona, Spain.

[b]Departamento de Física de la Materia Condensada, C-3, Universidad Autónoma de Madrid, Cantoblanco, 28049 Madrid, Spain.

[1]Current address: ETH Zurich, Biosystems Science and Engineering, CH-4057 Basel, Switzerland.

Abstract

The use of quartz tuning fork sensors as probes for scanning probe microscopy is growing in popularity. Working in shear mode, some methods achieve a lateral resolution comparable with that obtained with standard cantilevered probes, but only in experiments conducted in air or vacuum. Here, we report a method to produce and use commercial AFM tips in electrically driven quartz tuning fork sensors operating in shear mode in a liquid environment. The process is based on attaching a standard AFM tip to the end of a fiber probe which has previously been sharpened. Only the end of the probe is immersed in the buffer solution during imaging. The lateral resolution achieved is about 6 times higher than that of the micro etched fiber on its own.

Keywords: Atomic force microscopy; Scanning probe microscopy; Quartz tuning fork; Self-sensing probe; Shear force microscopy; Nanotip

Introduction

In recent years, atomic force microscopy (AFM) based on a quartz tuning fork (QTF) has become increasingly popular, especially due to the self-sensing detection it affords without the need for an optical feedback system. Furthermore, QTF-based sensors present low internal dissipation, high quality factors (*Q*) and high static spring constants (*K*); features that make these nanosensors very attractive for use in liquid environments to study biomaterials and biological samples [1][2]. Such properties allow stable low oscillation amplitudes to be achieved and thereby make it possible to work in a non-contact regime, avoiding the drawback of the tip to jump to contact at small tip–sample distances [3].

There are two common QTF configurations, depending on which spatial direction the oscillation is in: parallel (shear mode) or perpendicular (tapping mode) to the sample surface. To work in liquid in shear mode, only the fiber end of the QTF sensor is immersed in the liquid; as illustrated in Figure 1.

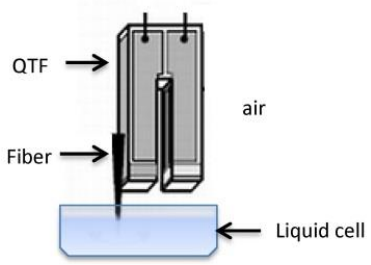

Fig. 1 Schematic of the QTF configuration working in shear mode in a liquid environment.

QTF-based sensors are usually custom-built in the laboratory by manually attaching a sharpened fiber to one of the prongs of the QTF. The probe tips are generally made of silicon fiber that is tapered using chemical etching techniques or mechanically drawn using a commercial micropipette puller [4][5] to obtain a tip radius of 100-150 nm. The conventional etching method (Turner method) [6] consists of immersing the optical fiber in hydrofluoric acid with a layer of an organic solvent over it. At the interface between the two layers the meniscus height decreases and this is where the taper forms. This process has been refined to optimize probe properties such as surface roughness, cone angle and especially the tip geometry and radius. New techniques have also been appeared: tube-etching [7], selective etching [8] and dynamic meniscus etching [9].

Different setups and additional production steps have been devised to achieve a similar tip radius to that of commercial AFM tips; although it remains unclear how effective they are at imaging in liquid media in shear force mode. Some of the different techniques employed to reduce the radius in QTF probes are: etching different materials [10][11], incorporating microfabrication processes [12][13], integrating non-commercial tips made of different materials such as diamond [14] or attaching commercial AFM tips [15][16].

Different materials have been used as chemically or electrochemically sharpened probes for QTF sensors and they have been employed in different scanning probe microscopy (SPM) setups, such as near-field scanning optical microscopes (NSOM) and scanning tunneling microscope (STM)-AFM hybrid systems: nickel in [17], polymethylmethacrylate (PMMA) in [10] and carbon fiber tips in [11]. Recently, Jung and co-workers [18] proposed a method to produce polymer tips on the cross-section of optical fibers, capable of achieving a 45 nm radius tip. Other strategies based on different microfabrication processes have been devised to integrate a sharp tip into the resonator for use in tapping mode: lithography in [12], anisotropic wet etching and a focused ion beam (FIB) in [13] and the commercially available Akiyama probe [19][20].

Attaching commercial AFM tips at the end of one of the prongs of a QTF has led to the same apex radius as standard AFM tips. For tapping mode, [21] attaches silicon AFM tips to image biological samples and [15] shows atomic resolution and magnetic contrast. However, the application of these nanosensors is limited to air conditions. For shear mode, a cantilever segment is glued to the QTF for noncontact mode in air in [16][22] or for shear-mode magnetic force microscopy in [23].

However, studies in liquid environments require the immersion of the attached AFM tip in buffer solution, in both tapping and shear mode. If a larger amount of buffer is used, the surface tension readily elevates the meniscus, thereby covering the electrodes and causing a short-circuit. Thus the external electrodes of the QTF preclude its utilization in aqueous solutions unless the whole sensor is

coated with an electrophoretic paint [24]; but as the whole sensor is immersed in liquid, the Q factor decreases and sensitivity does too. This problem can be overcome by using such a small volume of buffer that it only just covers the surface of interest; although the drop of liquid evaporates rapidly. One way to resolve that problem is to use a liquid with a much lower evaporation rate than that of water-based buffers [25]; but then the sample will not be under physiological conditions.

In this work we present a feasible technique to improve the lateral resolution of a QTF in shear mode in a liquid medium, for studies of biological samples. Our method is based on attaching a standard AFM tip to the end of a fiber that has previously been sharpened chemically. As the QTF can be maintained oscillating in air while the tip is immersed in the buffer, our approach overcomes the main limitation of previous work in liquid environments.

Material and Methods

In our experiments we used QTFs with a resonance frequency of 32,768 Hz (AB38T model, AbraconCorp., USA). As a first step, the metallic cover of the resonator was removed and a chemically sharpened SiO_2 fiber was attached to one of the prongs of the QTF. To taper the probes, a 125 µm optical fiber (ref: SM600 single mode fiber from Thorlabs, Germany) was dipped into 40% HF solution with a layer of iso-octane (C_8H_{18}) on top to protect against the acid vapors, as proposed in [26]. The process is self-terminating and lasted around 90 min. Once the etching had stopped, the fibers were rinsed with ethanol and water and mounted onto the resonator with cyanoacrylate glue, with a length of 3-4 mm protruding from the fork. This is the minimum length necessary to work with the liquid cell while maintaining the QTF resonating in air. The tip radiuses were between 100 and 200 nm, but for our purpose this was not critical since we intended to reduce the fiber diameter until just enough surface remained to maintain contact between the AFM tip and the probe.

Once the fiber was mounted onto the QTF, the sensor was placed in a micropositioner with a magnetic base incorporating 3 DOF of movement (from SUSS Microtec, Germany). The cantilever chip was attached with silver paint to a 100 Ohm resistor 30 W 5%, with the cantilever protruding from the resistor. Figure 2 is a schematic representation of the setup for the tip attachment procedure. The cantilever and QTF probe were aligned under an optical microscope with a 20X objective. The fiber was placed at the very end of the cantilever on the opposite side from the tip (see Fig. 3A). The tips used in this work were commercial chips (CONT model, NanoWorld, Switzerland). The AFM probes were from made of Si without any coating, with 450 µm cantilevers and a nominal spring constant of 0.2 N/m. The tips were 10 µm high and presented a nominal radius of 10 nm.

We used *nural 26* glue (Henkel Ibérica S.A., Spain), as it has strong adhesive properties (100 kg/cm^2 after six hours), to attach the AFM tip to the fiber. We were able to accelerate the hardening by increasing the temperature to approximately 70°C. We needed rapid drying because the longer it takes; the more easily the fiber becomes misaligned from the AFM tip. Thus, the resistor terminals where DC polarized and the heat of the resistor dissipated accelerating the drying process. A temperature of 85°C was reached in the resistor at 15 volts. As the amount of glue needed was very small, the hardening took around 90 minutes.

After attaching the fiber to the cantilever, we removed the cantilever from the glued tip using a tungsten probe (model 17680 from Cascade Microtech GmbH, Germany) placed in another micropositioner. We also removed the leftover segment of the cantilever. The resistor to which the

AFM chip was connected was then grounded and the STM probe connected to a DC voltage. The STM probe was moved close to the cantilever just below the tip, a voltage of 15 - 20 volts was supplied to create a short-circuit and the cantilever was broken off at the point of contact, as illustrated in Figure 3B. The most critical step was the last one: placing the tungsten tip in the correct position, close enough to the cantilever to break it but without damaging the tip. Even so, the process was successful around 80% of the time.

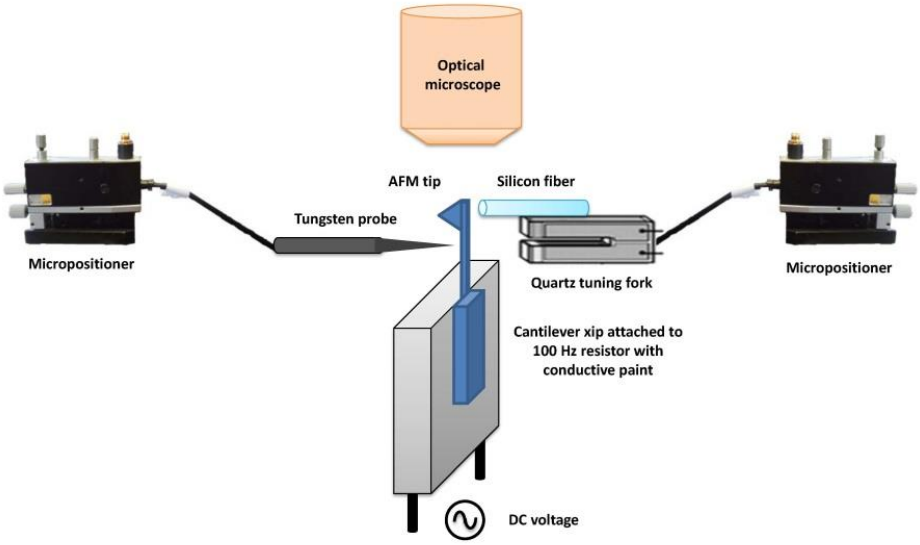

Fig. 2 Schematic of the setup for the tip attachment procedure showing the resistor where the cantilever is glued with silver paint and the two micrometer manipulators: one for the tungsten tip and one for the QTF sensor with the fiber previously sharpened. The fiber end and cantilever tip are aligned under an optical microscope (x10 Carl Zeiss lens). The objects in the figure are not to scale.

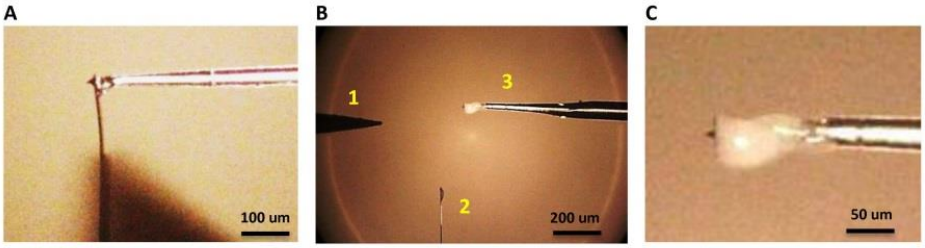

Fig. 3 (A) AFM cantilever tip glued to a silicon fiber previously sharpened by chemical etching. (B) A tungsten tip (1) is employed to break the leftover segment of the cantilever (2) when the glue is dry. (C) Magnification of image B showing the AFM tip attached to the fiber probe (3).

The sensor was mounted on an adapted STM head integrated into a commercial AFM microscope (Nanotec Electrónica, Spain). A fully custom-made electronics module was used to drive the QTF electrically [27] to its resonance frequency. A transimpedance amplifier (TIA) (model OPA656, Texas Instruments, USA) converted the current through the QTF into voltage with a 10^6 V/A gain. The current losses due to parasitic capacitance related to the contacts and cables were compensated with a subcircuit with the same capacitance but 180° phase shifted [28]. A driving signal was applied to drive the QTF at its resonance frequency using an integrated generator in the lock-in amplifier. The final resonance frequency after adding the extra mass of the fiber and AFM tip was shifted to 32,720 Hz and the resulting Q factor was 2,647.

Results and Discussion

Measurements on calibration grid

To evaluate the lateral resolution, a silicon test structure with a pyramidal calibration pattern was scanned (model TGG01, Mikromasch, Estonia). The image was registered in amplitude modulation where the input of the main feedback is the amplitude of the QTF current signal, while the variable phase is also recorded. We employed a low voltage-driven amplitude (3 mV) to minimize the amplitude of oscillation of the probe and reduce the effective tip radius. A vibration amplitude of ~1 nm was derived as reported in [29]. The set point of the feedback was set to 83% of the maximum free amplitude at the resonance frequency: A_{set}/A_{free} = 0.83.

The calibration grating is characterized by the small curvature of the edges (less than 10 nm) and it has a pitch of 3 um and a height of 1.8 um. The fiber probe with the AFM tip at the end was immersed in the buffer solution where the sample was also submerged (see Fig. 4A). Figure 4 B and C are images of the topography and profile, respectively, of the grating taken in shear force mode with an AFM tip mounted on a QTF fiber probe in buffer solution using a liquid cell. The measurement buffer was PBS with a pH of 7.4. As shown in Figure 4D, the scanning area was 7 um x 7 um and the line scan speed was 0.28 line/s.

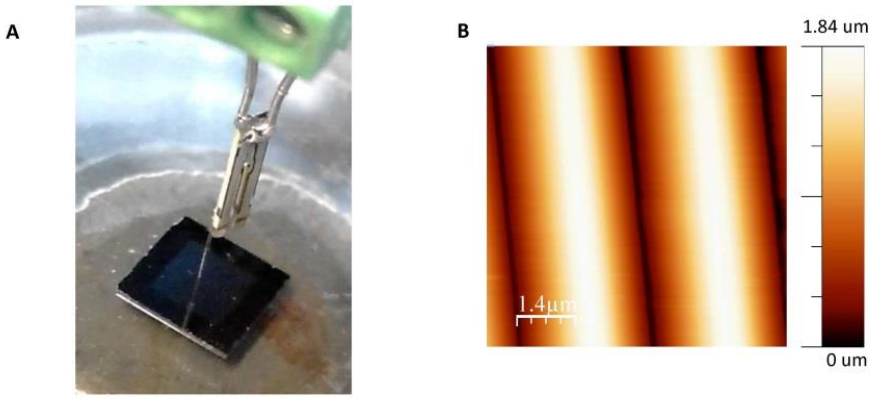

5

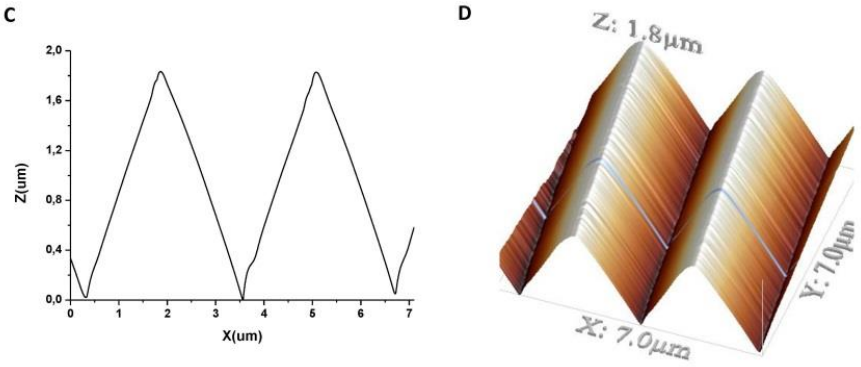

Fig. 4 (A) Measurement set-up. The QTF probe is immersed in buffer solution to access the sample using a liquid cell. (B) Shear force image of the TGG01 3 um pyramidal calibration grating. Image size is 7 um x 7 um. The topographic profile of 1024 p. and the same image rendered in 3D are shown in (C) and (D) respectively.

The resulting shape of the edges of the pyramids in the image is the dilation geometry of the tip and the pattern [30] and it is difficult to quantify the tip radius exactly, as the two geometries are unknown. Since the performance of the tip is related to the sharpness and acuteness of the line profile [31], we imaged the same structure in a buffer solution with a QTF-based sensor with a fiber probe, and with an AFM cantilever tip to compare the topographic profiles. The results are shown in Figure 5, where the topographic profile of the previous image taken with the AFM tip attached to a QTF (blue line) is superimposed over the profiles obtained with the other two sensors: QTF with a fiber probe chemically tapered (black line) and a commercial AFM cantilever tip in tapping mode (green line). In general terms, the profile obtained from the image taken with the QTF with a fiber probe is of poor quality, and it is clearly distorted by the irregular shape of the fiber. The improvement in lateral resolution of the tip apex through adding a commercial AFM tip to the fiber probe (blue, Fig. 5) is approximately 6-fold, compared to that of the naked fiber (black, Fig. 5). In contrast, similar image quality was obtained with the AFM tip attached to the QTF and with the commercial tip, as expected. Both are capable of handling large variations in sample height and show well-defined edges. Qualitatively, the AFM cantilever tip represents the triangular shape of the pattern slightly better with smoother slopes. This could be due to the effect of the lateral oscillation of the tip when working in shear mode with the QTF. Even though the driving amplitude is very small (3 mV) to minimize the lateral oscillation and it is damped by the viscosity of the buffer, lateral resolution could be affected by an extremely low increase of the effective tip radius. Nevertheless, we cannot appreciate any significant difference between the two profiles amplified in Figure 5B.

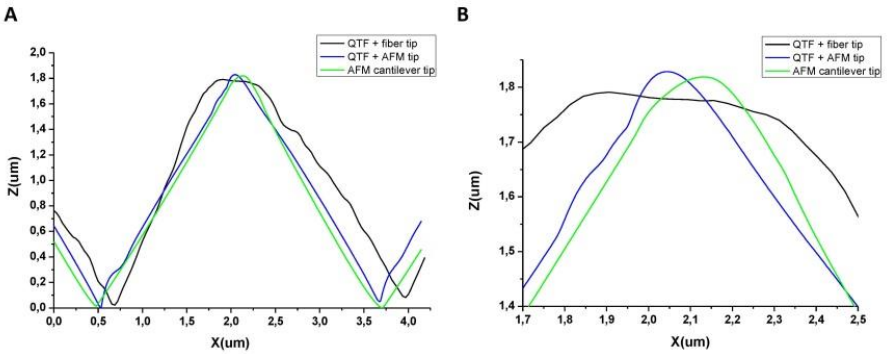

Fig. 5 (A) Direct comparison of the topographic profiles of one of the features of the imaged calibration pattern with: QTF with fiber, QTF with AFM tip and with AFM cantilever tip. (B) Magnified image of the edge of the pyramidal structure. Notice that about 6 blue peaks fit within the black naked fiber profile.

Measurements on soft samples

Once the resolution is determined with a calibration grid, a soft sample is imaged in liquid in order to check the feasibility of the developed technique. The sample had bacteria *Escherichia Coli* in stationary phase. In this approach the sterile loop was used to scrap a small quantity of bacteria from the agar plate into 10ml of LB, which was left at 37ºC at 250 rpm for 15 hours (overnight culture). 600 µl were transferred into a micro-centrifuge tube and centrifuged at 3000 rpm for 3 min. The pellet was re-suspended in 600 µl in milli-q water diluted 1/20. From the aliquot prepared, 40µl were pipette onto the freshly cleaved HOPG substrate. Then, the sample was left to dry for 1 hour to improve the fixation to the substrate and then rehydrated with milli-q to be placed in the fluid cell and imaged with the tuning fork sensor.

The image was also taken in amplitude modulation applying low driven voltage to minimize the oscillation amplitude. The set point of the feedback was set in this case to 87% of the maximum free amplitude at the resonance frequency. As shown in Figure 6, the scanning area was 4.8 um x 4.8 um and the line scan speed was 0.5 line/s. Compared, with the silicon test structure, in this case the tip-sample interaction must be gentler avoiding sample damage while scanning.

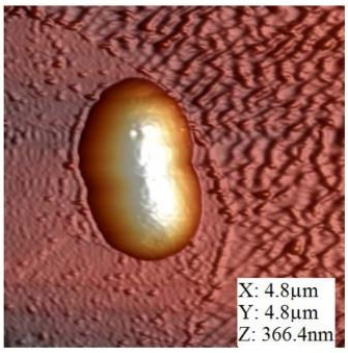

Fig. 6 Shear force image of a single *E. Coli* bacteria. Image size is 4.8 um x 4.8 um.

Conclusions

Here we report the first feasible technique to obtain a QTF-based sensor with the same tip radius as commercial AFM tips, to work in shear mode in liquid environments. Previous works have demonstrated that the attachment of commercially available AFM tips increases lateral resolution. Nonetheless, in previous research the AFM tips were directly attached to the end of one of the prongs of the tuning fork. Therefore, to use the QTF sensor to take measurements in liquid environments at least part of the prong needed to be immersed in the buffer solution (damping the oscillation of the QTF and therefore reducing its quality factor). Moreover, if the liquid is conductive, the electrodes of the nanosensors might be short-circuited. The work presented here (attaching the AFM tip to the end of the silicon fiber tip) resolves these issues. The method for preparing and joining the AFM tips to the QTF is easy and reliable. We notably improve the tip apex of the probe compared to the chemically sharpened fiber, achieving the same performance as that of a commercial AFM tip. A comparable topographic image of a specific patterned structure and a soft sample are successfully obtained in a buffer solution. We show that with our sensors it is possible to acquire high resolution images in liquid media, necessary to study biomaterials or biological samples under physiological conditions. This process overcomes one of the limitations present in shear force microscopy using QTF-based nanosensors to work in liquid media as the lateral resolution is equivalent to that achieved with a commercial AFM tip.

Acknowledgments

This work was supported by the Spanish Ministerio de Educación under project TEC2009-10114 and grant BES-2010-031186.

References

[1] J. Otero, L. González, M. Puig-Vidal, Nanocharacterization of Soft Biological Samples in Shear Mode with Quartz Tuning Fork Probes, Sensors 12(4) (2012) 4803-4819.

[2] L. González, J. Otero, J.P. Agusil, J. Samitier, J. Adan, F. Mitjans, M. Puig-Vidal, Micropattern of Antibodies Imaged by Shear Force Microscopy: Comparison between Classical and Jumping Modes, Ultramicroscopy 136 (2014) 176-184.

[3] F.J. Giessibl, Atomic resolution on Si (111)-(7×7) by noncontact atomic force microscopy with a force sensor based on a quartz tuning fork, Appl. Phys. Lett. 76 (2000) 1470.

[4] P. Hoffmann, B. Dutoit, R. Salath, P. Salath, Comparison of mechanically drawn and protection layer chemically etched optical fiber tips, Ultramicroscopy 61 (1995) 165-170.

[5] Y.K. Cheong, K.S. Lim, W.H. Lim, W.Y. Chong, R. Zakaria, H. Ahmad, Fabrication of tapered fibre tip using mechanical polishing method, Rev. Sci. Instrum. 82 (2011) 086115.

[6] D.R. Turner, Etch procedure for optical fibers, U.S. Patent No. 4,469,554 (1984).

[7] R. Stockle, C. Fokas, V. Deckert, R. Zenobi, B. Sick, B. Hecht, U.P.Wild, High-quality near-field optical probes by tube etching, Appl. Phys. Lett. 75 (1999) 160–2.

[8] B.A.F. Puygranier, P. Dawson, Chemical etching of optical fibre tips – experiment and model, Ultramicroscopy 85 (2000) 235-248.

[9] L.H. Haber, R.D. Schaller, J.C. Johnson, R.J. Saykally, Shape control of near-field probes using dynamic meniscus etching, Journal of Microscopy, Vol. 214 (2004) 27–35.

[10] H. Chibani, K. Dukenbayev, M. Mensi, S.K. Sekatskii, G. Dietler, Near-field scanning optical microscopy using polymethylmethacrylate optical fiber probes, Ultramicroscopy, Vol. 110, Issue 3 (2010) 211-215.

[11] A. Castellanos-Gomez, N. Agraït and G. Rubio-Bollinger, Carbon fibre tips for scanning probe microscopy based on quartz tuning fork force sensors, Nanotechnology 21 (2010) 145702 (9pp).

[12] T. Akiyama , U. Staufer, N.F. de Rooij, L. Howald, L. Scandella, Lithographically defined polymer tips for quartz tuning fork based scanning force microscopes, Microelectronic Engineering 58–58 (2001) 769–773.

[13] H. Hida, M. Shikida, K. Fukuzawa, S. Murakami, Ke. Sato, K. Asaumi, Y. Iriye, Ka. Sato, Fabrication of a quartz tuning-fork probe with a sharp tip for AFM systems, Sensors and Actuators A 148 (2008) 311–318.

[14] J.W.G. Tyrrell, D.V. Sokolov, H.U. Danzebrink, Development of a scanning probe microscope compact sensor head featuring a diamond probe mounted on a quartz tuning fork, Meas. Sci. Technol. 14 (2003) 2139–2143.

[15] S. Rozhok and V. Chandrasekhar, Application of commercially available cantilevers in tuning fork Scanning Probe Microscopy (SPM) Studies, Solid State Communications 121 (2002) 683-686.

[16] M. Labardi and M. Allegrini, Noncontact friction force microscopy based on quartz tuning fork sensors, Appl. Phys. Lett. 89 (2006) 174104.

[17] J.P. Ndobo-Epoy, E. Lesniewska, J.P. Guicquero, Shear force microscopy with a nanoscale resolution, Ultramicroscopy 103 (2005) 229–236.

[18] B.J. Jung, H.J. Kong, Y.H. Cho, K.S. Lee, C.H. Park, D.Y. Yang, K.S. Lee, Fabrication of sharp-needled conical polymer tip on the cross-section of optical fiber via two-photon polymerization for tuning-fork-based atomic force microscopy, Optics Communications 286 (2013) 197–203.

[19] T. Akiyama, U. Staufer, N.F. de Rooij, Self-sensing and self-actuating probe based on quartz tuning fork combined with microfabricated cantilever for dynamic mode atomic force microscopy, Applied Surface Science 210 (2003) 18–21.

[20] T. Akiyama, N.F. de Rooij, U. Staufer, M. Detterbeck, D. Braendlin, S. Waldmeier, M. Scheidiger, Implementation and characterization of a quartz tuning fork based probe consisted of discrete resonators for dynamic mode atomic force microscopy, Rev. Sci. Instrum. 81(2010) 063706.

[21] G.M. King and G. Nunes, Attractive-mode force microscope for investigations of biomolecules under ambient conditions, Rev. Sci. Instrum., Vol. 72, No. 11 (2001).

[22] H. Göttlich, R.W. Stark, J.D. Pedarnig, W.M. Heckl, Noncontact scanning force microscopy based on a modified tuning fork sensor, Rev. Sci. Instrum., Vol. 71, No. 8, (2000).

[23] K. Kim, Y. Seo, H. Jang, S. Chang, M.H. Hong, W. Jhe, Shear-mode magnetic force microscopy with a quartz tuning fork in ambient conditions, Nanotechnology 17 (2006) S201–S204.

[24] J. Polesel et Al., Force Spectroscopy by Dynamic Atomic Force Microscopy on Bovine Serum Albumin proteins changing the tip hydrophobicity, with piezoelectric tuning fork self-sensing

scanning probe, Sensors and Actuators B 161 (2012) 775– 783.

[25] E. Wutscher and F.J. Giessibl, Atomic force microscopy at ambient and liquid conditions with stiff sensors and small amplitudes, Rev. Sci. Instrum. 82 (2011) 093703.

[26] S. Mononobe, Near-field optical fiber probes and the imaging applications: Progress in Nano-Electro-Optics III, Springer, Berlin, 2005.

[27] L. González, J. Otero, G. Cabezas, M. Puig-Vidal, Electronic driver with amplitude and quality factor control to adjust the response of quartz tuning fork sensors in atomic force microscopy applications , Sensors and Actuators A 184 (2012) 112– 118.

[28] Y. Quin, R. Reifenberger, Calibrating a tuning fork for use as a scanning probe microscope force sensor, Review of Scientific Instruments 78 (2007) 063704.

[29] J. Liu, A. Callegari, M. Stark, M. Chergui, A simple and accurate method for calibrating the oscillation amplitude of tuning-fork based AFM sensors, Ultramicroscopy 109 (2008) 81–84.

[30] J.S. Villarrubia, Algorithms for scanned probe microscope image simulation, surface reconstruction, and tip estimation, J. Res. Natl. Inst. Stand. Technol. 102 (1997) 425.

[31] U. Hubner, W. Morgenroth, H.G. Meyer, T. Sulzbach, B. Brendel, W. Mirande, Downwards to metrology in nanoscale: determination of the AFM tip shape with well-known sharp-edged calibration structures, Appl. Phys. A 76 (2003) 913.

3.1.3 Associated Publication 2

Finite element analysis of electrically excited quartz tuning fork devices

By

Roger Oria, Jorge Otero, Laura González, Luis Botaya, Manuel Carmona and Manel Puig-Vidal*

Department of Electronics, University of Barcelona, Marti i Franques, 1, 08028, Barcelona, Spain

** Current address : Institute for Bioengineering of Catalonia, 08028 Barcelona, Spain.*

Published in

***Sensors** 13 (2013) 7156 – 7169*

Sensors **2013**, *13*, 7156-7169; doi:10.3390/s130607156

OPEN ACCESS

sensors

ISSN 1424-8220

www.mdpi.com/journal/sensors

Article

Finite Element Analysis of Electrically Excited Quartz Tuning Fork Devices

Roger Oria, Jorge Otero, Laura González, Luis Botaya, Manuel Carmona and Manel Puig-Vidal *

Department of Electronics, University of Barcelona, Marti Franques, 1, 08028 Barcelona, Spain; E-Mails: roria@el.ub.es (R.O.); jotero@el.ub.es (J.O.); lgonzalez@el.ub.es (L.G.); lbotaya@el.ub.es (L.B.); mcarmona@el.ub.es (M.C.)

* Author to whom correspondence should be addressed; E-Mail: manel.puig@ub.edu; Tel.: +34-93-403-9161; Fax: +34-93-402-1148.

Received: 1 March 2013; in revised form: 22 May 2013 / Accepted: 28 May 2013 / Published: 30 May 2013

Abstract: Quartz Tuning Fork (QTF)-based Scanning Probe Microscopy (SPM) is an important field of research. A suitable model for the QTF is important to obtain quantitative measurements with these devices. Analytical models have the limitation of being based on the double cantilever configuration. In this paper, we present an electromechanical finite element model of the QTF electrically excited with two free prongs. The model goes beyond the state-of-the-art of numerical simulations currently found in the literature for this QTF configuration. We present the first numerical analysis of both the electrical and mechanical behavior of QTF devices. Experimental measurements obtained with 10 units of the same model of QTF validate the finite element model with a good agreement.

Keywords: quartz tuning fork; finite element modeling; piezoelectric sensors

1. Introduction

In the past several decades, Atomic Force Microscopy (AFM) has been employed to measure the nano-scale properties of both soft [1–3] and non-coated [4,5] samples due to the high resolution of the technique. The ability to image, measure, and manipulate matter at the nano-and even atomic scale [6], is the defining attribute which has led to AFM being considered such a valuable and successful tool in nanotechnology. AFM techniques are based on the measurement of the interaction forces between a

nanometer-sized tip and the sample surface [7]. Commercial AFM nanosensors are based on the fabrication of microcantilevers with a very sharp tip [8,9]. However, commercial AFMs are limited in their functionality within certain scenarios. High stiffness of the cantilever is required in order to achieve small oscillation amplitudes and to prevent noisy measurements [6], which is not always accomplished. Additionally, the quality factor is often diminished when AFMs are immersed in liquid environments, and they are quite difficult to implement in multi-probe configurations [10].

As an alternative to classical AFM nanosensors, the use of Quartz Tuning Forks (QTFs) has been proposed. QTFs are piezoelectric devices that are commonly known for their application in customer electronics. In 1989, QTFs started to be used in microscopy [11–14]. One great advantage is the ability to combine the functions of a sensor and actuator, thus reducing the overall instrument complexity. In addition, QTF offers a stable and a very narrow band [15]. Moreover, higher quality factors (Q) are attributed to QTFs, as opposed to standard cantilevers, which make them suitable for applications in a liquid environment. Different analytical models of QTFs have been developed in the literature [16–21], but the dynamics response of the electrical and mechanical coupling of these devices remains unclear. All of these models are based on the cantilever configuration for mechanical excitation, except in the case described in [19], where an electrical circuit is introduced as a means to drive the QTF to the resonance frequency leading to compensation between the electrical energy and the mechanical energy of the QTF.

Finite Element Analysis (FEA) has been widely used in sensor analysis and design [22–24] as an alternative to the analytical models. So far, only a few studies have been found [18,25–29] with respect to QTFs. In [18,26] a modal analysis and calculation of the static capacitance for an optimum design is reported. In [25] the modal analysis of the sensor is reported. In study [28], the oscillator behavior of the QTF probe for different angles of the attached tip is studied for different vibrational modes. In [27,29] experimental data and numerical simulations are reported to compare and quantify the spring constant of the QTF. The main limitation of these models is that they do not consider the electromechanical coupling for the dynamic response of the device. In order to obtain accurate results, the complete system must be analyzed carefully; otherwise, uncertainties such as material properties, dimensions of the sensor—especially separation between the prongs and the base contribution of the QTF—and the electrode definition, which can introduce shifts in parasitic contribution, will likely lead to erroneous results.

We present herein a 3D finite-element model of the QTF, which models the coupling between the mechanical and the electrical behavior of the device by implementing the electric part, composed of a: voltage source, electrodes, and compensation circuit. In the first section, the mechanical model is presented. In the second section, the electromechanical model highlights the importance of accurately defining the geometry of the two electrodes. Finally, experimental measurements, which validate our finite element model, are shown.

2. Sensor Principles and Modeling

2.1. Theory

The tuning fork is a bimorph cantilever based on the piezoelectric properties of the quartz. The sensor consists of two prongs attached to a base, which normally is clamped to a holder. Each of the prongs is coated with a thin layer of a conductor material, which permits the resonator to be driven

either electrically or mechanically. In the former case, a potential difference between the electrodes is applied, whereas in the second one a dither is attached to one of the prongs of the QTF. Given the type of driver employed, either the electrical current through the device—for electrical excitation—or the generated piezoelectric voltage—for mechanical excitation—are related to the fork's vibration amplitude.

In microscopy applications, the QTF is driven to its resonance frequency by either mechanical or electrical excitation. There are two main vibrational modes for the same mechanical deformation: in-phase and anti-phase modes. For electrical excitation, the generated current can just be measured in the anti-phase mode because the current is only generated in the system when both prongs are vibrating in opposite directions.

In order to properly characterize the QTF dynamics, analytical models have been proposed in the literature [16–21]. Models from [16,19] have succeeded compared to the others by establishing a now well-known formulation for the calculation of those parameters, which are not straightforward to obtain. The main two parameters that these models propose are the spring constant (K) and the amplitude of oscillation (A) of the sensor. The spring constant of the sensor can be expressed as [19]:

$$K = 0.2575\frac{TW^3E}{L^3} \quad (1)$$

where T, W and L correspond to the dimensions of the thickness, width, and length of the prongs of the QTF, respectively; and E is the Young's modulus of the quartz.

It is worthwhile to mention that the calculation of the spring constant has led to great controversies and discrepancies in the research community due to the lack of a generalized model. Although the cantilever-based model for studying the dynamics of QTF is the most accepted model, a two-coupled oscillator model has been utilized in [17,20,21]. The coupled-oscillator model discusses the necessity to link the dynamics of the two prongs of the QTF. In [20,21] it is reported that the calculation of the spring constant using the cantilever model underestimates its true value. In contrast, [27] it shows that the cantilever model overestimates the spring constant value. Moreover, in studies [27,28] the contribution of the QTF base in the calculation of the spring constant is discussed. The differences seen in the literature [13,21,27], can play a crucial role if quantitative measurements are needed.

In the case of electrical excitation, the amplitude of oscillation can be calculated by using the following [19]:

$$A = \sqrt{\frac{V_{rms}I_{rms}Q}{K2\pi f_o}} \quad (2)$$

where V_{rms} is the amplitude of the excitation signal, I_{rms} the measured current, and the quality factor, defined as:

$$Q = \frac{f_o}{\Delta f} \quad (3)$$

where f_0 is the resonance frequency and Δf is the bandwidth of the QTF when the amplitude decays 3 dB.

2.2. Model of the Mechanical Structure Using Finite Element Model

In this work, a finite element model (FEM) of the QTF is proposed. In order to make an accurate 3D model, dimensions of the QTF are set in accordance to measurements carried out in an optical microscope (B-353MET model, Euro-Microscopes). In contrast to commercial AFM sensors where cantilevers present a rotation with respect to the X coordinate, the tuning fork model rotates with respect to the Z coordinate; thus, the width (*W*) and the thickness (*T*) are defined in a opposite ways compared to AFM cantilevers, as seen in Figure 1.

Figure 1. (**a**) Dimensions and geometry of QTF (in μm) (**b** and **c**) Vibrational modes for in-phase and anti-phase mode of QTF. Bar colors indicate arbitrary units of the displacements along the X coordinate.

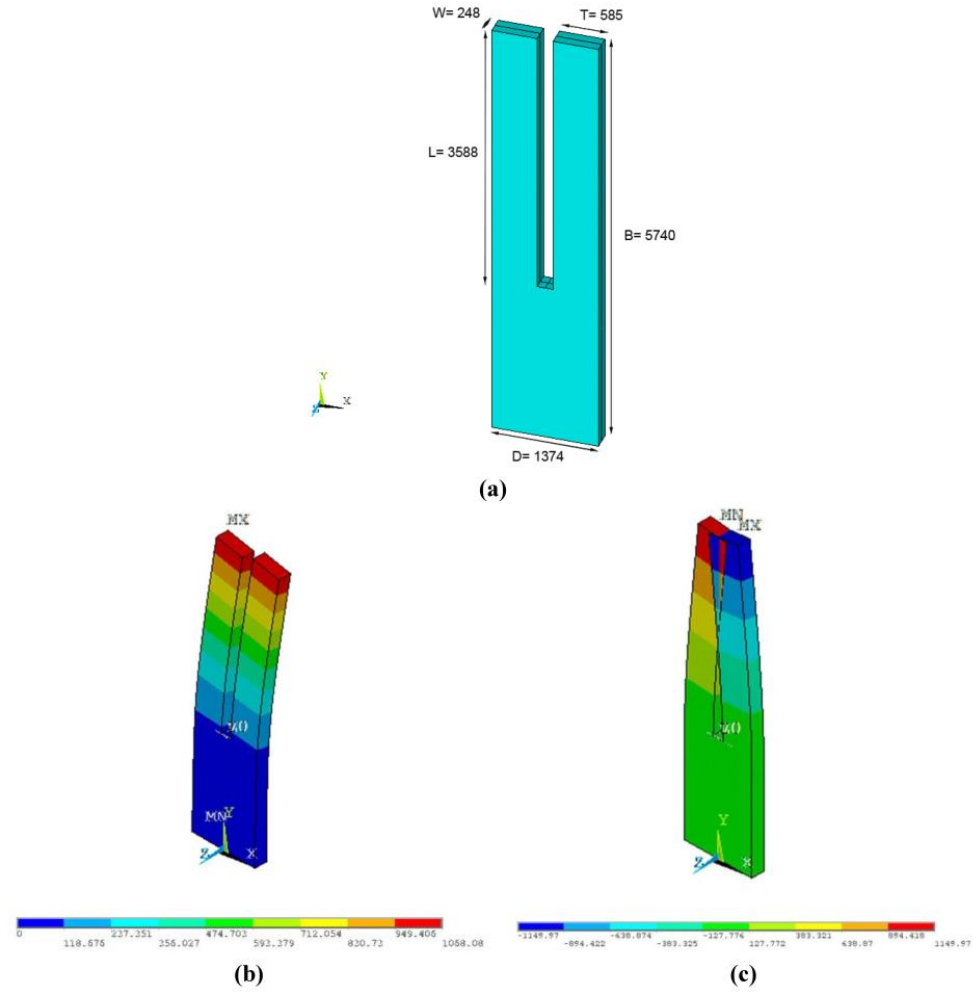

As it was previously stated, the QTF is based on piezoelectric phenomena. Therefore, linear piezoelectricity equations of elasticity have to be defined and coupled to the electrostatic charge by means of piezoelectric constants [30]:

$$\begin{bmatrix}\epsilon_p\\ D_i\end{bmatrix} = \begin{bmatrix}S_{pq}^E & d_{pk}\\ d_{iq} & \epsilon_{ik}^\sigma\end{bmatrix}\begin{bmatrix}\sigma_q\\ E_k\end{bmatrix} \quad (4)$$

$$\begin{bmatrix}\sigma_p\\ D_i\end{bmatrix} = \begin{bmatrix}Y_{pq}^E & e_{pq}\\ e_{iq} & \epsilon_{ik}^\epsilon\end{bmatrix}\begin{bmatrix}\epsilon_q\\ E_k\end{bmatrix} \quad (5)$$

$\{\sigma_p\}$ =Stress vector

$\{D_i\}$ = Electric flux density vector

$\{E_K\}$ = Elastic strain vector

$\{\epsilon_q\}$ = Electric field intensity vector

$[Y_{pq}^E]$ = Elasticity matrix

$[e_{pk}]$ = Piezoelectric stress matrix

$[\epsilon_{ik}^\epsilon]$ = Dielectric matrix

The different physical properties of quartz have been widely studied [31,32]. However, elastic, piezoelectric, and the dielectric permittivity matrices differ slightly among the various reported results. In the present work, properties from [32] have been chosen because more sophisticated measurement techniques—based on resonance ultrasound spectroscopy—are used to determine the values. The piezoelectric coefficients can be seen as follows:

$$[Y_{pq}^E] = \begin{bmatrix} 86.76 & 6.86 & 11.85 & -18.02 & 0 & 0\\ 6.86 & 86.76 & 11.85 & -18.02 & 0 & 0\\ 11.85 & 11.85 & 105.46 & 0 & 0 & 0\\ -18.02 & 18.02 & 0 & 58.14 & 0 & 0\\ 0 & 0 & 0 & 0 & 58.14 & -18.02\\ 0 & 0 & 0 & 0 & 18.02 & 39.95 \end{bmatrix} GPa$$

The piezoelectric constant matrix, which permits the structural and electrical behavior of the material to be coupled, is defined as follows:

$$[e_{pk}] = \begin{bmatrix} -0.151 & 0 & 0\\ 0.151 & 0 & 0\\ 0 & 0 & 0\\ 0.061 & 0 & 0\\ 0 & -0.061 & 0\\ 0 & 0.151 & 0 \end{bmatrix} \frac{C}{m^2}$$

The piezoelectric behavior of the material is accomplished by using the element type SOLID226 in ANSYS.

The model is defined in uMKS units according to ANSYS nomenclature. The model is composed of 12,384 hexahedral elements with a size of 60 μm, which is translated into 59,340 nodes. In addition, the bottom of the base is constrained to emulate the clamped structure of the real device.

2.3. Electrodes Definition and Parasitic Capacitance Compensation

For the implementation of the electrical part and to couple it with the mechanical behavior of the QTF, the loaded and the grounded electrodes needed to be defined. In addition, the electrodes also define the way in which the deformation occurs when an electric field is applied, and hence the type of acoustic wave generated [33].

As shown in Figure 2(a,b), the electrodes are placed in this particular alignment to obtain and optimize the maximum charge transfer. The electrodes were defined on the surface nodes of the tuning fork according to optical microscope measurements, thus simulating the thin layer of the conductor material. The surface nodes of each electrode of the QTF are coupled together, which sets the same amount of voltage for each node.

Figure 2. (**a** and **b**) Electrodes of the QTF are according to the optical microscope measurements. (**c**) The electrodes in ANSYS are defined at the bottom and top face of the QTF symmetrically. Dimensions are in μm.

(**a**)

(**b**)

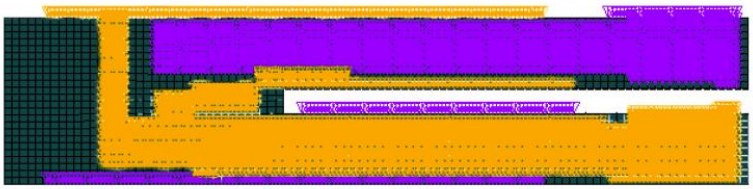

(**c**)

Therefore, two groups of nodes are created. Each electrode is defined by 2,317 elements that are translated into 6,390 nodes. An independent voltage source links one node from each of the two groups together implemented by using the element CIRCU94. One group is defined as the loaded electrode such that a symmetric sinusoidal voltage wave is supplied to it, while the other electrode is grounded.

The electrical part of the QTF is modeled by an equivalent circuit (Butterworth-Van Dyke model) based on a serial RLC circuit with a parallel capacitor [34]. The resistor models the dissipation, the capacitor and the inductor model the potential and the kinetic energy storage, and the parallel capacitor models all the parasitic contributions due to contacts, cables, *etc.* (Figure 3(a)).

Figure 3. (**a**) Equivalent circuit of the QTF (Butterworth-Van Dyke model) (**b**) Electric circuit composed of power supply and inductor. The power supply permits the QTF to be driven electrically, and the inductor allows compensating for the parasitic capacitance.

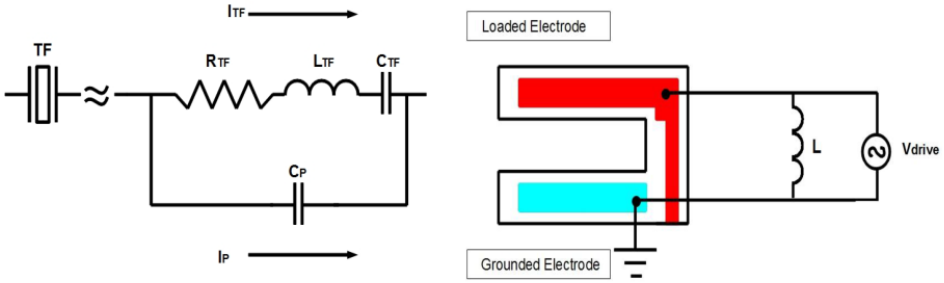

(**a**) (**b**)

One of the main problems is that the current flowing through the QTF becomes dominant away from the resonance frequency due to parasitic capacitance; this phenomenon is responsible for asymmetries and shifts in the frequency response. Thus, it is required to compensate for the parasitic current. In the proposed model, an inductor element with CIRCU94 is implemented within ANSYS for this very reason, whereas a means to compensate in the experimental setup will be explained later. Therefore, the voltage source and the inductor determine the final excitation circuit.

Parasitic capacitance can be obtained by doing harmonic simulation over a broad frequency range by interpreting the contribution of this capacitance as the slope of a linear fit dependent on the frequency response. Using Equation (8), the value of the inductor is modeled from the real part of the impedance equal to the parasitic capacitance:

$$X_c = X_L \tag{6}$$

$$\frac{1}{2\pi f C} = 2\pi f L \tag{7}$$

$$L = \frac{1}{(2\pi f)^2 C} \tag{8}$$

In order to perform the harmonic simulation, one more input parameter is needed: the quality factor of the QTF. The quality factor is defined in numerical simulations through the damping ratio (ξ) of the device:

$$\xi = \frac{1}{2Q} \quad (9)$$

For our model, the inductance was calculated to be 26.5 H by using Equation (8).

Parasitic contribution in the finite element model is only due to the electrodes rather than contacts, cables, *etc.* Therefore, the model is expected to have less parasitic capacitance than in the experimental setup. However, one must keep in mind that this compensation plays an important role in the experimental configuration of the QTF probe.

Concerning the way in which the measurements are taken, the device is electrically driven, and the amplitude of oscillation is obtained by measuring the current through the QTF. An AC voltage source at the resonant frequency of the fork is applied, and the current is measured by a transimpedance amplifier (TIA) with a gain $R_G = 10^6$ (V/A).

In the experimental setup, a capacitor-compensated circuit was implemented to drive the QTF [35]. This type of compensation circuit was chosen because of the high magnitude of inductor, which would make it infeasible to implement practically. In that circuit (Figure 4), the parasitic current is compensated with a sub-circuit with the same capacitance by using a tunable variable capacitor, but with 180° phase.

Figure 4. Implemented circuit for parasitic capacitor compensation.

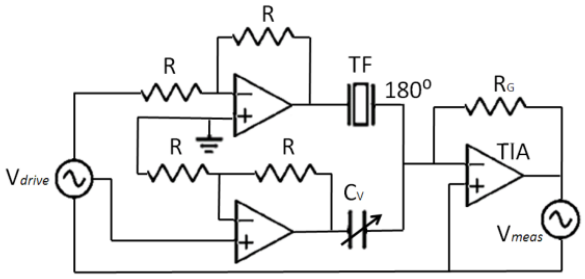

As a consequence, only the current through the nanosensor is amplified by the TIA, and it is translated into voltage to measure the extent of oscillation with a lock-in amplifier [15].

3. Results and Discussion

The first objective in validating our model was to obtain the resonance frequency of the QTF, for both the in-phase and anti-phase vibrational modes.

For the in-phase mode, when both prongs are vibrating in the same direction, our model demonstrates a resonance frequency of 27,433 Hz. However, we have not verified this value experimentally due to the small readout signal that is not distinguishable from the intrinsic noise of the equipment. Nevertheless, in study [21] the in-phase mode shows significant agreement with our model.

Regarding the anti-phase mode, when both prongs are vibrating in the opposite direction, the resonance frequency is completely observed and well correlated with the nominal value of 32,768 Hz provided by the manufacturer [36]. Table 1 summarizes the different vibrational modes seen below:

Table 1. Resonance frequency for the in-phase and anti-phase vibrational modes.

	In-Phase Mode [Hz]	Anti-Phase Mode [Hz]
Castellanos *et al.* [21]	27,800	32,766
Experimental Results	-	32,768
FEM Results	27,433	32,768
Manufacturer [36]	-	32,768

In order to validate the dynamics response of the model proposed, ten QTFs of the same model and manufacturer (*Abracon* AB38T) were electrically driven from 10 mV up to 100 mV. The quality factor and the current through the devices were measured. In Table 2 the quality factor of the ten devices, and the respective damping ratios, which are used in the simulations are shown. Q factors of the sensors were calculated by applying a pseudo-Lorentzian fit [15] to the experimental current *versus* frequency curve [16].

Table 2. Quality factor of the ten QTF. Q values were experimentally measured, and implemented in FEM through the damping ratio.

QTF	Quality Factor (Q)	Damping Ratio (ξ)
QTF1	104542	4.78e-06
QTF2	112800	4.43e-06
QTF3	113077	4.42e-06
QTF4	102144	4.89e-06
QTF5	110724	4.51e-06
QTF6	109778	4.55e-06
QTF7	101471	4.92e-06
QTF8	135054	3.70e-06
QTF9	107489	4.65e-06
QTF10	120019	4.16e-06

The first step to validate the model was to compare experimental and simulation data for one tuning fork with several V_{drive}. As shown in Figure 5, the amplitude of the current is proportional to the V_{drive} as expected. The agreement of the model for all ten devices is between the 91% and 98%.

In order to properly validate the proposed model, several QTFs have to be characterized. Comparison of the ten different QTFs was performed between measured and simulation data for a single V_{drive}.

The amplitude of oscillation can be experimentally obtained by interferometric techniques [15,37], which are difficult to practically carry out, or theoretically obtained from Equation (1). This parameter is necessary to fully understanding the electromechanical behavior of the QTF; our model presents a straightforward approach.

As shown in Figure 6, simulation data indicates a linear relationship, which may be attributed to the fact that harmonic simulations in ANSYS resolve the time-dependent equations of motion for linear structures undergoing steady-state vibration. However, this confirms the actual electromechanical behavior of the QTF, which had been previously identified by examining the electrical current peaks through the QTF for the chosen range of V_{drive}. Therefore, it can be assured that the QTF behaves linearly between 10 mV and 100 mV, which is well captured by the proposed model.

Figure 5. (**a**) Amplitude of the current for two QTFs for V_{drive} 30 mV and 50 mV, respectively. (**b**) Current peaks at the resonance frequency and relative error between experimental and numerical data.

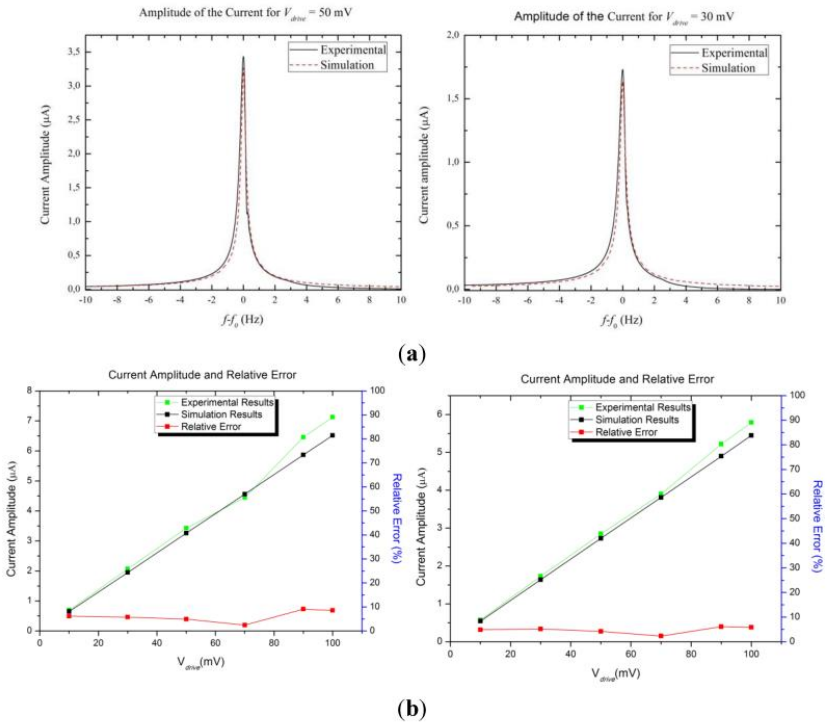

Figure 6. Results of the amplitude of oscillation of the ten QTFs from the finite element model.

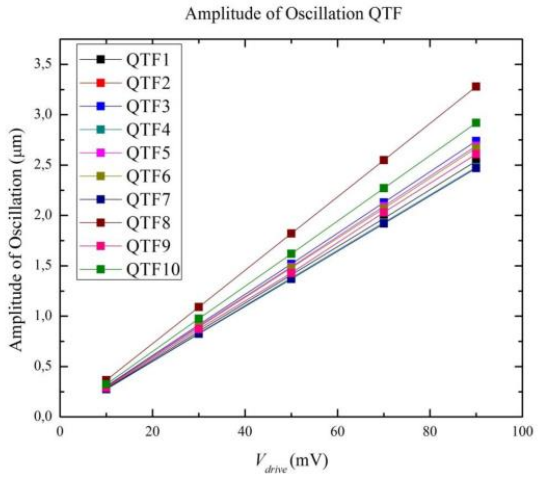

Finally the validation of the QTF as a sensor was done by small-mass loading one of the prongs of the device in the finite element model and measuring the shift in the resonant frequency produced by the added mass. A small cube of solid material with a known mass was coupled to the left prong of the QTF, in a similar way that the experiments conducted in [21] and [38]. Results are shown in Figure 7. The sensitivity of the device as mass sensor was 57 ng/Hz, which was in good agreement with results reported for the experimental measurements in [38]. For high added masses, the model shows a non-linear behavior, as shown in the experiments in [21].

Figure 7. Results of the frequency shift produced by the added mass from the finite element model.

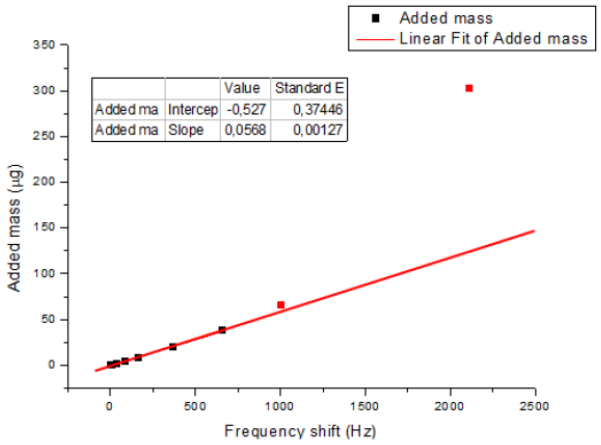

4. Conclusions

A new model of quartz tuning fork with two free prongs and electrically excited is presented based on finite element analysis developed in ANSYS by incorporating the electrical part: excitation, compensation circuit and the electrodes. The model has been validated by measuring ten separate quartz tuning forks at different driving amplitudes—from 10 mV to 100 mV—which exhibit a strong agreement between 91% and 98%. The remaining error can be attributed to small geometric differences between the electrodes of the model and the electrodes from the actual quartz tuning fork. In addition, the parasitic capacitance cannot always be completely compensated in the experimental measurements.

Finally, the model proposed herein allows from the comparison between experimental and simulation data, which is complicated to achieve from other models in the literature. These analytical models are normally developed for mechanically excited quartz tuning forks implying that the dither driving energy must be determined. However, this is no easy task due to the appearance of mechanical losses and the coupling between the sensor and dither, which are difficult to quantify. Our developed model also overcomes the difficulty of measuring certain parameters, such as the amplitude of oscillation and the sensitivity. With the results obtained, the model could be used to calculate the effective spring constant of the device as deeply discussed in [21].

Acknowledgments

This work was supported in part by the Spanish Ministerio de Educación under project TEC2009-10114 and also by the regional Catalan authorities under project VALTEC09-2-0058.

Conflict of Interest

The authors declare no conflict of interest.

References

1. Radmacher, M.; Fritz, M.; Hansma, P.K. Imaging soft samples with the atomic force microscope: gelatin in water and propanol. *Biophys. J.* **1995**, *69*, 264–270.
2. Sokolov, I.; Ong, Q.K.; Shodiev, H.; Chechik, N.; James, D.; Oliver, M. AFM study of forces between silica, silicon nitride and polyurethane pads. *J. Coll. Inter. Sci.* **2006**, *300*, 475–481.
3. Müller, D.J.; Dufrêne, Y.F. Quartz tuning fork atomic force microscopy: A nanoscopic window on the cell surface. *Trends Cell Biol.* **2011**, *21*, 461–469.
4. Rico, F.; Roca-Cusachs, P.; Gavara, N.; Farré, R.; Rotger, M.; Navajas, D. Probing mechanical properties of living cells by atomic force microscopy with blunted pyramidal cantilever tips. *Phys. Rev. E* **2005**, *72*, 1914–1924.
5. Gavara, N.; Chadwick, R.S. Determination of the elastic moduli of thin samples and adherent cells using conical atomic force microscope tips. *Nat. Nanotech.* **2012**, *7*, 733–736.
6. Giessibl, F.J.; Bielefeldt, H.; Hembacher, S.; Mannhart, J. Imaging of atomic orbitals with the atomic force microscope. experiments and simulations. *Annal. Der. Phys.* **2001**, *10*, 887–910.
7. Binnig, G.; Quate, C.F.; Gerber, C. Atomic force microscope. *Phys. Rev. Lett.* **1986**, *56*, 930–933.
8. Albrecht, T.R.; Akamine, S.; Carver, T.E.; Quate, C.F. Microfabrication of cantilever styli for the atomic force microscope. *J. Vacu. Sci. Technol. A Vacu. Surf. Films* **1990**, *8*, 3386–3396.
9. Akamine, S.; Barrett, R.C.; Quate, C.F. Improved atomic force microscope images using microcantilevers with sharp tips. *Appl. Phys. Lett.* **1990**, *57*, 316–318.
10. Otero, J.; González, L.; Cabezas, G.; Puig-Vidal, M. Multitool platform for morphology and nanomechanical characterization of biological samples with coordinated self-sensing probes. *IEEE/ASME Trans. Mechatron.* **2013**, *18*, 1152–1160.
11. Günther, P.; Fischer, U.C.; Dransfeld, K. Scanning near-field acoustic microscopy. *Appl. Phys. B* **1989**, *48*, 89–92.
12. Shang, G.Y.; Qiao, W.H.; Lei, F.H.; Angiboust, J.F.; Troyon, M.; Manfait, M. Development of a shear force scanning near-field fluorescence microscope for biological applications. *Ultramicroscopy* **2005**, *105*, 324–329.
13. Hofer, M.; Adamsmaier, S.; van Zanten, T.S.; Chtcheglova, L.A.; Manzo, C.; Duman, M.; Mayer, B.; Ebner, A.; Moertelmaier, M.; Kada, G.; *et al.* Molecular Recognition imaging using tuning fork-based transverse dynamic force microscopy. *Ultramicroscopy* **2010**, *110*, 605–611.
14. Otero, J.; Gonzalez, L.; Puig-Vidal, M. Nanocharacterization of soft biological samples in shear mode with quartz tuning fork probes. *Sensors* **2012**, *12*, 4803–4819.

15. González, L.; Otero, J.; Cabezas, G.; Puig-Vidal, M. Electronic driver with amplitude and quality factor control to adjust the response of quartz tuning fork sensors in atomic force microscopy applications. *Sens. Actuators A Phys.* **2012**, *184*, 112–118.
16. Karrai, K.; Grober, R.D. Piezoelectric tip-sample distance control for near-field optical microscopes. *Appl. Phys. Lett.* **1995**, *66*, 1842–1844.
17. Naber, A. The tuning fork as sensor for dynamic force distance control in scanning near-field optical microscopy. *J. Micros.* **1999**, *194*, 307–310.
18. Lee, S.K.; Moon, Y.H.; Yoon, J.H.; Chung, H.S. Analytical and finite element method design of quartz tuning fork resonators and experimental test of samples manufactured using photolithography I - significant design parameters affecting static capacitance c(0). *Vacuum* **2004**, *75*, 57–69.
19. Liu, J.; Callegari, A.; Stark, M.; Chergui, M. A simple and accurate method for calibrating the oscillation amplitude of tuning-fork based AFM sensors. *Ultramicroscopy* **2008**, *109*, 81–84.
20. NG, B.P.; Zhang, Y.; Kok, S.W.; Soh, Y.C. An improved dynamic model of tuning fork probe for scanning probe microscopy. *J. Micros. Oxford* **2009**, *234*, 191–195.
21. Castellanos-Gomez, A.; Agraït, N.; Rubio, G. Dynamics of quartz tuning fork force sensors used in scanning probe microscopy. *Nanotechnology* **2009**, *20*, 5502–5518.
22. Mohammed, A.A.S.; Moussa, W.A.; Lou, E. High-performance piezoresistive MEMS strain sensor with low thermal sensitivity. *Sensors* **2011**, *11*, 1819–1846.
23. Ansari, M.Z.; Cho, C. Deflection, frequency, and stress characteristics of rectangular, triangular, and step profile microcantilevers for biosensors. *Sensors* **2009**, *9*, 6046–6057.
24. Ma, C.-C.; Huang, Y.-H.; Pan, S.-Y. Investigation of the transient behavior of a cantilever beam using PVDF sensors. *Sensors* **2012**, *12*, 2088–2117.
25. Wang, Y.; Sun, Y.N.; Qin, B.K. Finite element simulation of the vibratory characteristics for quartz tuning fork gyroscope. *J. Beijing Inst. Technol.* **2002**, *11*, 155–158.
26. Xu, J.; Bo, Y. Finite Element Method Design and Fabrication of Thermo-Sensitive Quartz Tuning Fork Resonators as Temperature Sensor. In Proceedings of the 2006 1st IEEE International Conference on Nano/Micro Engineered and Molecular Systems, Zhuhai, China, 18–21 January 2006; pp. 1228–1233.
27. Simon, G.H.; Heyde, M.; Rust, H.P. Recipes for cantilever parameter determination in dynamic force spectroscopy: Spring constant and amplitude. *Nanotechnology* **2007**, *18*, 5503–5515.
28. Higuchi, S.; Kuramochi, H.; Kubo, O.; Masuda, S.; Shingaya, Y.; Aono, M. Angled long tip to tuning fork probes for atomic force microscopy in various environments. *Rev. Sci. Instrum.* **2011**, *82*, 3701–3706.
29. Vörden, D.V.; Lange, M.; Schmuck, M.; Schmidt, N.; Möller, R. Spring constant of a tuning-fork sensor for dynamic for microscopy. *Beilst. J. Nanotechnol.* **2012**, *3*, 809–816.
30. Takács, G.; Rohal'-Ilkiv, B. *Model Predictive Vibration Control*, 1st ed.; Springer: London, UK, 2012; p. 87.
31. Bechmann, R. Elastic and piezoelectric constants of alpha-quartz. *Phys. Rev.* **1958**, *110*, 1060–1061.
32. Ogi, H.; Nakamura, N.; Sato, K.; Hirao, M.; Uda, S. Elastic, anelastic, and piezoelectric coefficients of alpha-quartz determined by resonance ultrasound spectroscopy. *J. Appl. Phys.* **2006**, *100*, 3511–3517.

33. Friedt, J.M; Carry, E. Introduction to the quartz tuning fork. *Amer. J. Phys.* **2007**, *75*, 415–422.
34. Giessibl, F.J. High-speed force sensor for force microscopy and profilometry utilizing a quartz tuning fork. *Appl. Phys. Lett.* **1998**, *73*, 3956–3958.
35. Qin, Y.; Reifenberger, R. Calibrating a tuning fork for use as a scanning probe microscope force sensor. *Rev. Sci. Instrum.* **2007**, *78*, 3704–3711.
36. Datasheet Tuning Fork Abracon. Available online: http://www.abracon.com/Resonators/AB38T.pdf (accessed on 23 February 2013).
37. Sandoz, P.; Friedt, J.M.; Carry, E. Vibration amplitude of a tip-loaded quartz tuning fork during shear force microscopy scanning. *Rev. Sci. Instrum.* **2008**, *79*, 6102–6105.
38. Waszczuk, K.; Gula, G.; Swiatkowsky, M.; Olszewski, J.; Herwich, W.; Drulis-Kawa, Z.; Gutowicz, J.; Gotszalk, T. Evaluation of Pseudomonas aeruginosa biofilm formation using tuning fork mass sensors. *Sens. Actuators B Chem.* **2012**, *170*, 7–12.

3.1.4 Associated Manuscript 2

Determination of the static spring constant of electrically-driven quartz tuning forks with two freely oscillating prongs

By

Laura González, Roger Oria, Luis Botaya, Manel Puig-Vidal and Jorge Otero*

SIC-BIO, Bioelectronics and Nanobioengineering Group, Departament d'Electrònica, Universitat de Barcelona, Marti i Franques 1, 08028 Barcelona, Spain.

** Current address : Institute for Bioengineering of Catalonia, 08028 Barcelona, Spain.*

submitted for peer-review to

Nanotechnology.

Determination of the Static Spring Constant of Electrically-Driven Quartz Tuning Forks with two Freely Oscillating Prongs

Laura González, Roger Oria, Luis Botaya, Manel Puig-Vidal, Jorge Otero*

SIC-BIO, Bioelectronics and Nanobioengineering Group, Departament d'Electrònica, Universitat de Barcelona, Marti i Franques 1, 08028 Barcelona, Spain.

* Current address : Institute for Bioengineering of Catalonia, 08028 Barcelona, Spain.

Abstract

Quartz tuning forks (QTFs) have become popular in nanotechnology applications, especially as sensors for scanning probe microscopy. The sensor's spring constant and the oscillation amplitude are required parameters to evaluate the tip-sample forces; however, there is certain controversy within the research community as to how to arrive at a value for the static spring constant of the device when working in shear mode. Here, we present two different methods based on finite element simulations, to determine the value of the spring constant of the sensors: the Amplitude and Cleveland methods. The results obtained using these methods are compared to those using the geometrical method, and show that the latter overestimates the spring constant of the device.

Keywords: Spring constant; Scanning probe microscopy; Quartz tuning fork; Self-sensing probe; Shear force microscopy.

1. Introduction

Quartz tuning forks (QTFs) are commercially-available crystal oscillators based on the piezoelectric properties of quartz. Originally used for time measurements due to their very precise oscillation frequency, QTFs have become popular for use in scanning probe microscopy (SPM) since their first reported SPM use in 1989 [1]. To use QTFs as force sensors they are modified by attaching a tapered fiber to one of their prongs. They present certain benefits over the standard microfabricated cantilevers [2]: high stiffness (> 10^3 N/m), high quality factor (Q) (> 10^3 at ambient conditions), and the fact that they do not need optical detection systems. With QTFs it is possible to image a sample with a high resolution (even atomic [3-4]) and to measure very low interaction forces (femtonewton-range forces have been measured using these sensors in a vacuum environment [5-6]). The resolution descends to the range of hundreds of piconewtons in air and liquid environments [7]. Different research describes the behavior and working principles of QTFs in the measurement of the interaction forces between the tip and the sample. In [8-9], the basic operation of the QTF for shear and friction force detection is studied. The fundamental limits of force detection are discussed in [10] and the relationship between the frequency shift of the tuning fork and the force gradient acting on the tip is reported in [11].

There are two main QTF working configurations, depending on which spatial direction the fork oscillates in: parallel (shear mode, Figure 1(b)) or perpendicular (intermittent or tapping mode, Figure 1(a)) to the sample surface. For the former mode, the two prongs oscillate freely; but for the latter, the tipless prong is usually firmly fixed to a supported structure (Q-plus scheme) [12] whereby the QTF is converted into a quartz cantilever. In Q-plus configuration, the force gradient can be calculated easily from the frequency shift, as in standard cantilevers. However, the piezoelectric

current is at least a factor of 2 lower than that of a QTF for a given oscillation amplitude. Moreover, *Q* is about one order of magnitude lower and it is strongly dependent on the way the fixed prong is attached [13]. When the tip is attached to one of the two free prongs to work in shear mode, the extra added mass results in a loss of balance of the dynamics of the QTF that causes a reduction in *Q*. However, it is possible to rebalance the sensor to take advantage of a higher *Q*.

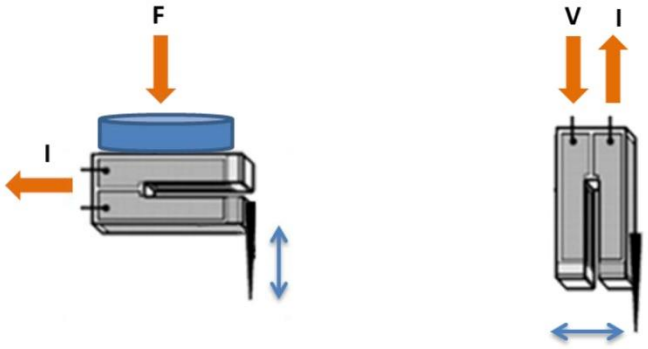

Figure 1. The two most common configurations for the QTF. Q-plus (a), where a dither piezo is used to oscillate the device perpendicular to the sample surface, and the piezovoltage generated is measured. Shear mode (b), where the device is electrically oscillated parallel to the sample surface and the current through the two prongs is measured.

Many researchers have reported different analytical models that describe QTF dynamics [8, 13-18] and different finite element analysis (FEA) models have been devised [19-21]. However, there are many discrepancies in the literature regarding calculation of the effective spring constant due to the lack of a generalized model. Furthermore, most of the models available have been established for the tapping configuration and mechanical excitation. The QTF can be either electrically driven by a voltage applied between the electrodes (while the current through the device is measured) or mechanically excited by an external dithering piezo actuator (in which case, the piezovoltage generated is measured). If the latter configuration is used, the coupling between the dither and the sensor is not easy to quantify and the existence of mechanical losses causes uncertainties. In recent work [21] we presented a new electromechanical model of the QTF with the two prongs free and electrically excited based on FEA. The electrical part (electrical driving, compensation circuit, electrodes and current measurement) is incorporated into the model and validated by comparing the simulation results with data measured experimentally. The finite element model designed allows certain important parameters to be determined which are hard to measure experimentally, such as the in-phase resonant frequency, the oscillation amplitude (*A*) and the sensitivity (*S*). All of these parameters are derived from data that is easily obtained in the experiments (*Q*, the anti-phase resonant frequency and the current through the device for a given excitation voltage).

To obtain a quantitative value for the interaction forces, it is necessary to know the effective spring constant (K_{eff}) of the QTF. In Q-plus configuration, the relationship between the force gradient acting between the tip and the sample surface, and the frequency shift produced is given directly by K_{eff}. As the sensor is turned into a conventional cantilever when one arm is fixed, the formula for a rectangular cross-sectioned cantilever can be applied to obtain the spring constant of the vibrating

prong [22]. When the two prongs are freely oscillating, as they are in the present work, the process of evaluating K_{eff} is not so straightforward since the coupling between the two arms affects the global dynamics of the QTF [19].

For microfabricated cantilevers there are well-known methods to evaluate the spring constant; but for QTF-based sensors there is no such standard calibration procedure. Some strategies used to calibrate the normal spring constant for cantilevers have been modified so that they can be applied to QTF devices. The most direct method is the measurement of the static deflection when a known force is applied. Nevertheless, for stiff sensors which have high spring constants (of the order of 10,000 Nm^{-1}) compared to standard cantilevers (0.01 – 100 Nm^{-1}), the method does not seem to be sufficiently accurate [23-25]. A version of the Cleveland method [26] for cantilevers is implemented for QTFs in [13, 19, 20]. An additional mass is attached to one of the arms of the QTF and the spring constant can then be determined from the resultant frequency shift. This method is not very user friendly since an experienced operator is needed and the sensor is potentially highly destructive [23]. The noise spectrum method is employed in [13, 20]. However, the measurement requires equipment with a very good signal-to-noise ratio (SNR) and good resolution in the range of interest. In [27-28] the electronic analogy approximation is utilized, but accurate calibration of the mechanical oscillation of the QTF sensor is required and that is not always easy since an interferometry set-up is needed [28-31]. The theoretical approach derived from beam theory is widely used [32-36], but it is not always suitable for the two free prongs configuration, as we mention above.

So, here we present a new method to quantify the effective spring constant from easily-measurable parameters in combination with the simulation results of the QTF finite element model [21]. The method is in agreement with the well-known Cleveland method modified for QTFs and corroborated via two different commercial devices: 32 kHz and 100 kHz.

2. Finite element model and analysis

A complete electromechanical model of the QTF with the two prongs free and electrically excited was devised and reported in [21]. Briefly, the excitation and the compensation circuits were incorporated into the model as the electrical part and this was coupled with the mechanical behavior of the QTF; the loaded and grounded electrodes were also incorporated into the model. The model was devised for a 32 kHz (QTF-32) decapsulated commercial QTF (AB38T model, AbraconCorp., USA) with a nominal resonance frequency of 32,768 Hz. A new model for a 100 kHz QTF (QTF-100) (CFV206 model, Citizen Finetech Miyota Co., Japan) is implemented in the present work, following the same procedure. The quartz structure and the electrode dimensions were measured using an optical microscope (B-353MET model, Euro-Microscopes, Spain). The material properties of the quartz (elastic, piezoelectric, and the dielectric permittivity matrices) were defined with the same values as for the 32 kHz model [34]. Figure 2 shows the two QTF models with the electrode configuration. The geometry of the electrodes is defined for the top and bottom parts symmetrically.

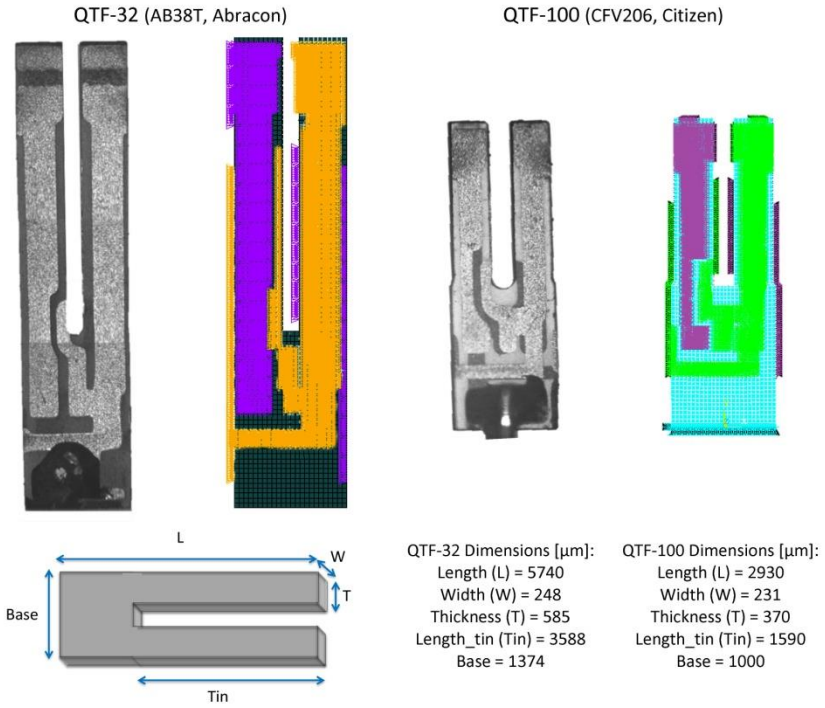

Figure 2. Electrode definitions and dimensions for the two different QTF models: 32 kHz (AB38T, Abracon) and 100 kHz (CFV206, Citizen).

The mechanical behavior of QTF devices can be modeled by an equivalent electrical circuit (Butterworth–Van Dyke model) [22] based on a serial LRC resonator with a parallel parasitic capacitance. The capacitance and inductance model the potential and kinetic energy, respectively; the resistor models dissipation and the parallel capacitance all the parasitic capacitors related to contacts, cables, etc.

Far from the resonance frequency, the current through the parasitic capacitor dominates, inducing asymmetries and shifts in the frequency response, and limiting the SNR. A shunt inductor element is added in ANSYS models to compensate the parasitic current and maximize the SNR. From a harmonic simulation over a broad frequency range, it is possible to obtain the contribution of the parasitic current as a slope at the base of the frequency response. Using Equation 1, the value of the inductor is modeled from the real part of the impedance which is equal to the parasitic capacitance. The calculated value of the shunt inductor for the 32 kHz model was 26.5 H and for the 100 kHz model it was 0.92 H.

$$L = \frac{1}{(2\pi f)^2 C} \qquad (1)$$

In the experiments, a fully custom-made electronic module was used to drive the QTF at its resonance frequency and the current through the device was measured using a transimpedance amplifier (TIA) [31]. The parasitic current was also balanced by introducing a compensating circuit

into the electronic driver. The compensation circuit was based on an adjustable capacitor instead of an inductor, as there were no coils available with the values required [28].

As the device was excited electrically, the sensor was driven with a voltage signal at its resonance frequency, and the current through the device was measured. The current is proportional to the mechanical amplitude of vibration of the QTF [13, 29, 30], which is a key parameter for the calibration of this kind of sensor. It can be obtained experimentally by optical methods [29, 37] (which in general require complicated experimental setups) or theoretically from equation 2 [17].

$$A = \sqrt{\frac{V\ I\ Q}{2\pi f_0\ k_{eff}}} \qquad (2)$$

Where A is the oscillation amplitude, V is the driving voltage, I the measured current, Q the quality factor, k_{eff} the effective spring constant of the device and f_0 the resonant frequency in the anti-phase mode. The expression is derived from the compensation of the loss of mechanical energy in each oscillation cycle with the electrical energy from the driving circuit.

There are two main vibrational modes of the QTF: in-phase and anti-phase modes. During the in-phase mode, the two prongs of the device oscillate in the same direction; whereas during the anti-phase mode they oscillate in opposite directions. Only the anti-phase mode can be detected electrically owing to the symmetrical electrode design. In in-phase mode, the electrical signals cancel out. Table 1 summarizes the resonance frequencies for the two vibrational modes for the two devices modeled: QTF-32 and QTF-100.

	QTF-32 [21]		QTF-100	
	In-Phase [Hz]	**Anti-Phase [Hz]**	**In-Phase [Hz]**	**Anti-Phase [Hz]**
FEM Simulations	27 433	32 768	81 280	99 999
Experimental		32 768		99 999.5
Manufacturer [38,39]		32 768		100 000

Table 1 Comparison of resonance frequencies from FEM simulation results and experimental measurements for the in-phase and anti-phase modes, for the QTF-32 and QTF-100.

The input parameters for the harmonic simulations were Q and the resonant frequency in the anti-phase mode (f_0). They were easily obtained experimentally by fitting the frequency response to a Lorentzian curve. Figure 3 shows the current amplitude plotted against frequency for a driving voltage of 10 mV for the two QTFs. There was 93.5% and 99.0% agreement between the simulated and experimental values of the curves for QTF-32 and QTF-100 respectively.

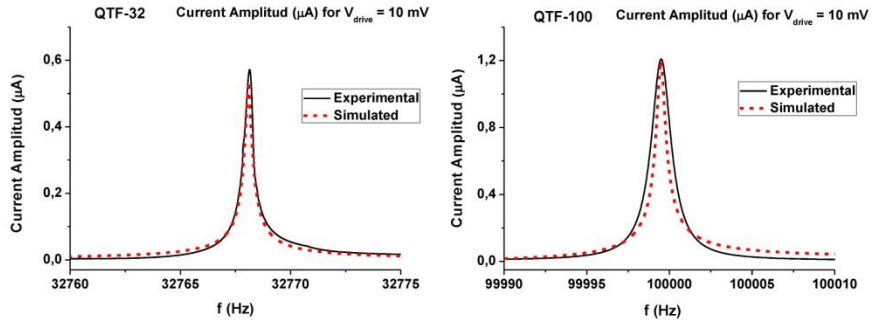

Figure 3. Piezoelectric current amplitude plotted against frequency for V_{drive} = 10 mV for two different QTFs with different resonance frequencies. The simulated and experimental peak values of the curves agree to within 93.5% and 99% for the QTF-32 and QTF-100 respectively.

Different devices with different *Q*s were measured and simulated for different driving voltages. Peak current values from simulations were compared with experimental measurements for five different devices of each type of QTF, as illustrated in Figure 4A. Figure 4B shows the oscillation amplitude of the models for the driving voltage range selected. Table 2 shows the computed and experimental results for a driving voltage of 10 mV.

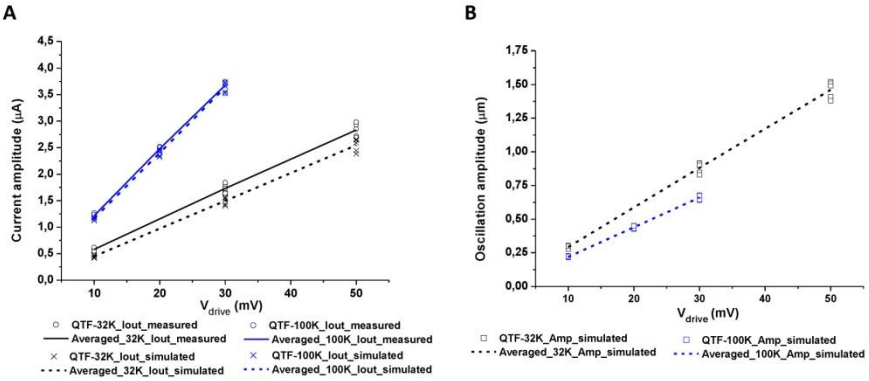

Figure 4. (a) Current peaks at the resonance frequency for five different devices of each type of tuning fork modeled (black lines for QTF-32; blue for QTF-100). Solid lines are the average tendency of the measured piezoelectric current and dashed lines the average of the current results from finite element models. (b) Oscillation amplitudes from simulations for both models.

	QTF-32				QTF-100			
	Q	I_{exp} **(nA)**	I_{sim} **(nA)**	A_{sim} **(nm)**	***Q***	I_{exp} **(nA)**	I_{sim} **(nA)**	A_{sim} **(nm)**
QTF1	104 542	572	505	282	202 612	1 247	1 200	213
QTF2	112 800	593	545	305	210 290	1 280	1 246	221
QTF3	113 077	574	546	305	204 300	1 280	1 210	215
QTF4	102 144	549	493	276	214 620	1 346	1 271	226
QTF5	110 724	618	535	299	213 492	1 313	1 264	225

Table 2 Comparison of experimental results for the current peak values for five QTFs of each type of device modeled, with simulations by FEM for a driving voltage of 10 mV. *Q* is measured and implemented as an input in the FEM simulations. The oscillation amplitude of each QTF obtained from the simulations is also shown in the fifth and ninth columns.

3. Effective spring constant

The effective spring constant was quantified by a new method from easily measurable parameters along with FEM simulations. The so-called "*Amplitude method*" is based on applying equation 2 to the experimental data and the mechanical oscillation obtained from the simulations in ANSYS. Below we present a simple procedure to calibrate the effective spring constant of the device which we validate with the Cleveland method and compare to the geometrical method.

3.1 Amplitude Method

From equation 3, it was possible to obtain the value of the effective spring constant, K_{eff}, once the other parameters were known. *Q*, the driving voltage (*V*), the piezoelectric current through the fork (*I*) and the resonance frequency (f_0) were all known parameters, or they were easily measurable experimentally for each device. The mechanical oscillation amplitude (A_0) was obtained after inputting the measured parameters (V, Q, f_0) into the FEM simulations. The two QTFs modeled (32 kHz and 100 kHz) were calibrated using this method. Five different devices of each type were measured at different driving voltages and their *Q* and f_0 were introduced as input parameters into FEM simulations. Hence, the oscillation amplitudes at the peak resonance were obtained for the different driving voltages. Figure 5 shows the results. The product $V * I * Q$ (V*A) is shown against $w * A^2$ (m^2rad/s), where the expected linear relationship can be seen. From a linear regression, the effective spring constant was calculated (grey line for QTF-100 and black line for QTF-32). From the data acquired, it was also possible to calibrate the piezoelectric coupling constant, α (µm/V), which is the ratio of the input voltage and the deflection of one prong of the QTF. In terms of the current, it can be written as: $\beta=\alpha * Z_{gain}$ (m/A), since the charge induced by the piezoelectric effect is proportional to the deflection; and the current is the parameter measured directly [10, 13, 19]. In addition, the relationship between the driving voltage and the oscillation amplitude was observed to be linear, in agreement with interferometric measurements reported in [29-31].

$$k_{eff} = \frac{V\ I\ Q}{A^2\ w_0} \qquad (3)$$

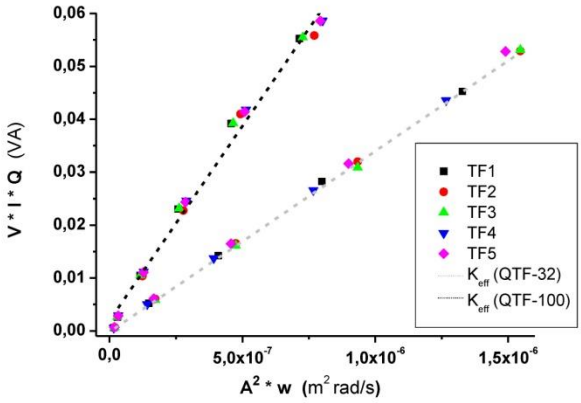

Figure 5. Representation of the two terms of the expression 3 with experimental data and the resulting oscillation amplitude from FEM models. Five different devices of each type of modeled tuning forks have been plotted and two regression lines (black line for QTF-32 and grey line for QTF-100) have been fitted to obtain the effective spring constant.

	QTF-32	QTF-100
K_{eff} [N/m]	34 167 ± 476	85 219 ± 1 260
α [µm/V]	0.46 ± 0.01	0.18 ± 0.01
β [m/A]	0.52 ± 0.01	0.20 ± 0.01

Table 3. A linear regression is applied to the data from Figure 5 and the effective spring constant (slope) is extracted. An estimation of the piezoelectric constants (α, β) is also obtained taking into account that the I-V gains (Z-gain) have been calibrated: 1,117,314 and 906,330 for QTF-32 and QTF-100 respectively.

3.2 Cleveland Method

A commonly accepted way to calculate the effective spring constant of microfabricated cantilevers is the Cleveland method. It is based on the measurement of the resonance frequency of the cantilever before and after adding a small mass at the end of the cantilever [26]. Using the coupled oscillator model, the method can be adapted to QTF sensors and the relationship between the change in the resonance frequency and the added mass can be obtained [13]. The anti-phase resonance frequency is measured while one prong is loaded with a small mass; since the relationship between the added mass and the inverse of the anti-phase frequency squared is linear when the added mass is much smaller than the effective mass of the prong:

$$\Delta m = \frac{K_{eff}}{(2\pi f)^2} - m_{eff} \qquad (4)$$

where Δm is the added mass and m_{eff} is the effective mass of the device. The spring constant of the QTF was then calculated by loading a small mass onto one of the prongs of the device in the FEM simulations, while the frequency shift produced was obtained. Small cubes of solid material (gold) with known masses were coupled to the end of the right prong of the QTF, as described in [13] and [40]. The frequency shift was obtained in both modes (in-phase and anti-phase) from the FEM simulation output. The sensitivity of the device as a mass sensor was 49.5 ng/Hz and 4.5 ng/Hz for

the QTF-32 and QTF-100 respectively; in good agreement with previous results reported for experimental measurements in [40]. When the added mass became appreciable (with respect to the effective mass of one arm of the QTF) the relationship departed from linearity. From modal simulations, it was possible to extract the results from the in-phase mode; whereas it was not possible to obtain them from the experimental data. Moreover, the mass of the added particles was known perfectly and there was no influence of the glue used to attach them to the QTF arm. Figure 6 shows the expected linear relationship between f^{-2} and the added mass, Δm. Adjusting a linear fit to this data, the effective spring constant and the effective mass of the QTF were extracted from the slope and the interception with the y-axis of the linear regression respectively (see Table 4). Insets in Figure 6 show the nonlinear behavior when the added mass, Δm, becomes large, loading the prong of the QTF in accordance with the coupled oscillators model [13].

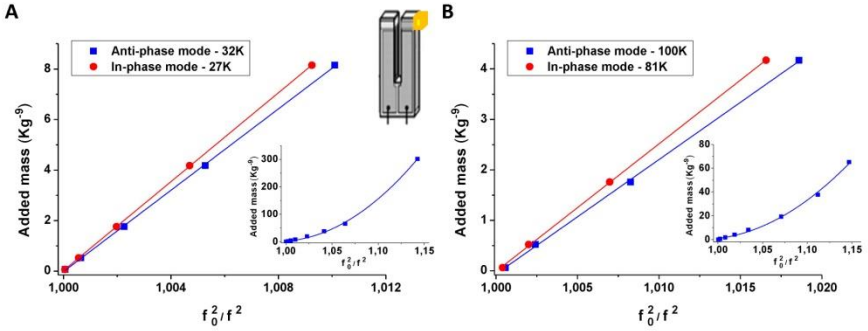

Figure 6. Plots of the mass added at the end of one prong against f^{-2} for (A) QTF-32 and (B) QTF-100, for in-phase (red circles) and anti-phase (blue squares) mode. Both insets show the nonlinear behavior when Δm becomes larger as the coupled oscillator model predicts.

	QTF-32		QTF-100	
	In-Phase	**Anti-Phase**	**In-Phase**	**Anti-Phase**
K_{eff} [N/m]	26 122 ± 49	34 122 ± 251	65 896 ± 551	89 525 ± 1 267
M_{eff} [kg]	$8.79e^{-7}$	$8.05e^{-7}$	$2.53e^{-7}$	$2.27e^{-7}$

Table 4. A simple linear regression is applied to the data from Figure 6 and the effective spring constant (slope) and effective mass (interception) are extracted with a correlation coefficient of 0.999.

3.3 Geometrical Method

If a single harmonic oscillator model is used, each prong of the tuning fork can be considered as a cantilever. Hence, beam theory has been widely applied to estimate the spring constant of one prong of a QTF [8, 10, 41]. Equation X describes the relationship between the stiffness of one prong of the QTF and its physical properties, where *T*, *W* and *L* correspond to the thickness, width, and length of the prong respectively; and *E* (=78.7 GPa for quartz) is the Young's modulus. In addition, the fundamental eigenfrequency is given by equation 6 [28, 42], where *m* is the effective mass of one prong and ρ (=2 644 kg/m^3 for quartz) is the mass density.

$$k = 0.2575\frac{tw^3E}{l^3} \qquad (5)$$

$$f_0 = \frac{1}{2\pi}\sqrt{\frac{k}{m}} = 0.162\sqrt{\frac{E}{\rho}}\frac{t}{l^2} \quad (6)$$

$$k' = 3.83 \cdot w \cdot (E\rho^3)^{1/4} \cdot (tf_0)^{3/2} \quad (7)$$

The elastic constant of one prong (k) for the two QTFs modeled following expression X1 was 21,811 N/m and 58,990 N/m for QTF-32 and QTF-100 respectively. Nevertheless, other expressions for the elastic constant can be used by rearranging the previous ones. The length, l, is isolated in eq. 6 and introduced into eq. 5, leading to equation 7; which is frequency dependent and the variable, l, corresponding to length is eliminated [43].

In Table 5, the three different methods are compared. Note that the Amplitude method devised here and the commonly used Cleveland method agree (0.1% and 4.8% discrepancy). As expected, the geometrical method gives a distinct value, as it treats the QTF as a simple structure consisting of two independent cantilevers. The value is underestimated, but it improves when eq. 7 is used, which is not length dependent (8.7% and 13% discrepancy with the Cleveland method). When eq. 5 is used, the spring constant value is overestimated and it leads to 27.8% and 31.8% deviation for QTF-32 and QTF-100 respectively.

	QTF-32		QTF-100	
	In-Phase	**Anti-Phase**	**In-Phase**	**Anti-Phase**
Amplitude		34 167 ± 476		85 219 ± 1 260
Cleveland	26 122 ± 49	34 122 ± 251	65 896 ± 551	89 525 ± 1 267
Geometry (2*k)		43 622		117 980
Geometry (2*k')		31 163		77 788

Table 5. Comparison of the effective spring constant obtained by adopting three different approaches: the Amplitude method, the Cleveland method and geometrical expressions.

4. Discussion and Conclusions

It is worth mentioning that calculation of the spring constant is very controversial in the research community and the literature is full of discrepancies. Although the cantilever-based model is the most accepted, the coupled oscillators model has also been used [13, 18]. Some studies report that the cantilever model underestimates the spring constant [13, 18]; whereas [19] shows that the calculated value of the spring constant overestimates its true value. Another uncertainty resides in the contribution of the base of the QTF to the spring constant; this is discussed in [44]. [42] indicates that the total stiffness of the QTF is twice the stiffness of one prong: in contrast, [13] estimates it to be more than twice. This discrepancy emerges from the coupling between the two prongs, which is still unclear.

When the QTF is driven electrically, the prongs do not present mechanical coupling; they are connected electrically through the electrodes and when a voltage is applied between them, the QTF prongs are forced into anti-phase oscillation. Moreover, since the movement is somehow governed by the electrode design, the QTF cannot be treated as a pure mechanical oscillator. Indeed, beam theory cannot be applied to tuning fork sensors.

Some previous work reports models of the mechanical and electrical behavior of nanosensors based on QTFs. Nevertheless, oversimplification of the system, in order to arrive at tractable equations,

results in a misunderstanding of the working principles of these novel tools. Having an accurate value for the spring constant of the devices would aid their popularization, due to the benefits they offer with respect to microfabricated cantilevers.

Putting all this together, a method to calculate the spring constant of a QTF from easily measurable parameters is presented in this work. The use of an FEA model which includes the electrical part is the key point, because it gives a value for the mechanical vibration; which in practice is hard to measure experimentally. The validation of the method by comparison with the Cleveland method guarantees that the presented method can be used to calculate the spring constant of a QTF accurately.

Acknowledgments

This work was supported by the Spanish Ministerio de Educación under project TEC2009-10114 and grant BES-2010-031186.

References

[1] P. Guethner, U. Fischer, K. Dransfeld, Scanning near-field acoustic microscopy, Appl. Phys. B. Photophys. Laser Chem., Vol. B 48 (1989)pp. 89-92.

[2] A. Makky, P. Viel, S.W. Chen, T. Berthelot, J. Pellequer, J. Polesel-Maris, Piezoelectric tuning fork probe for atomic force microscopy imaging and specific recognition force spectroscopy of an enzyme and its ligand, J. Mol. Recognit. 26 (2013) 521–531.

[3] F.J. Giessibl, Atomic resolution on Si(111)-7x7 by noncontact atomic force microscopy with a force sensor based on a quartz tuning fork, Appl. Phys. Lett. 76 (2000) 1470.

[4] L. Gross, F. Mohn, N. Moll, P. Liljeroth, G. Meyer, The Chemical Structure of a Molecule Resolved by Atomic Force Microscopy, Science 325 (2009) 1110.

[5] M. Barbic, L. Eliason, J. Ranshaw, Femto-Newton force sensitivity quartz tuning fork sensor, Sens. Actuat. A 136 (2007) 564–566.

[6] T. Ludwing, Casimir force experiments with quartz tuning forks and an atomic force microscope (AFM), J. Phys. A: Math. Theor. 41 (2008) 164025.

[7] J. Polesel-Maris, J. Legrand, T. Berthelot, A. Garcia, P. Viel, A. Makky, S. Palacin, Force spectroscopy by dynamic atomic force microscopy on bovine serum albumin proteins changing the tip hydrophobicity, with piezoelectric tuning fork self-sensing scanning probe, Sens. Actuat. B 161 (2012) 775–783.

[8] K. Karrai, R.D. Grober, Piezoelectric tip-sample distance control for near-field optical microscopes, Appl. Phys. Lett. 66 (1995) 1842–1844.

[9] K. Karrai, I. Tiemann, Interfacial shear force microscopy, Phys. Rev. B, Vol. 62, Num. 19, 2000.

[10] R. Grober, J. Acimovic, J. Schuck, D. Hessman, P. Kindlemann, J. Hespanha, A. Morse, K. Karrai, I. Tiemann, S. Manus, Fundamental limits to force detection using quartz tuning forks, Rev. Sci. Instrum. 71 (2000) 2776.

[11] F.J. Giessibl, Forces and frequency shifts in atomic-resolution dynamic-force microscopy, Phys. Rev. B Vol. 56, Num. 24, 1997.

[12] F.J. Giessibl, Device for contactless scanning of surface, Patent DE-19633546, German Patent and Trademark Office (1996).

[13] A. Castellanos-Gomez, N. Agraït, G. Rubio, Dynamics of quartz tuning fork force sensors used in scanning probe microscopy, Nanotechnology 20 (2009) 5502–5518.

[14] A. Naber, The tuning fork as sensor for dynamic force distance control in scanning near-field optical microscopy, J. Micros. 194 (1999) 307–310.

[15] S.K. Lee, Y.H. Moon, J.H.Yoon, H.S.Chung, Analytical and finite element method design of quartz tuning fork resonators and experimental test of samples manufactured using photolithography I - significant design parameters affecting static capacitance c(0). Vacuum 75 (2004) 57–69.

[16] M. Labardi, Dynamics of probes attached to quartz tuning forks for the detection of surface forces, Nanotechnology 18 (2007) 395505 (9pp).

[17] J. Liu, A. Callegari, M. Stark, M. Chergui, A simple and accurate method for calibrating the oscillation amplitude of tuning-fork based AFM sensors, Ultramicroscopy 109 (2008) 81–84.

[18] B.P. NG, Y. Zhang, S.W. Kok, Y.C. Soh, An improved dynamic model of tuning fork probe for scanning probe microscopy, J. Micros. Oxford 234 (2009) 191–195.

[19] G.H. Simon, M. Heyde, H.P. Rust, Recipes for cantilever parameter determination in dynamic force spectroscopy: spring constant and amplitude, Nanotechnology 18 (2007) 12.

[20] D. van Vörden, M. Lange, M. Schmuck, N. Schmidt, R. Möller, Spring constant of a tuning-fork sensor for dynamic force microscopy, Beilstein J. Nanotechnol. 3 (2012) 809–816.

[21] R. Oria, J. Otero, L. González, L. Botaya, M. Carmona, M. Puig-Vidal, Finite element analysis of electrically excited quartz tuning fork devices, Sensors 2013, 13(6), 7156-7169.

[22] F.J. Giessibl, High-speed force sensor for force microscopy and profilometry utilizing a quartz tuning fork, Appl. Phys. Lett. 73 (1998) 3956–3958.

[23] C.T. Gibson, G.S. Watson, S. Myhra, Determination of the spring constants of probes for force microscopy/spectroscopy, Nanotechnology 7 (1996) 259–262

[24] P.J. Cumpson, J. Hedley, C.A. Clifford, X. Chen, S. Allen, Microelectromechanical system device for calibration of atomic force microscope cantilever spring constants between 0.01 and 4 N/m, J. Vac. Sci. Technol. A 22 (2004) 1444.

[25] N. Morel, M. Ramonda, Ph. Tordjeman, Cantilever calibration for nanofriction experiments with atomic force microscope, Appl. Phys. Lett. 86 (2005) 163103.

[26] J. Cleveland, S. Manne, D. Bocek, P. Hansma, A nondestructive method for determining the spring constant of cantilevers for scanning force microscopy, Rev. Sci. Instrum. 64 (1993) 403.

[27] J. Rychen, T. Ihn, P. Studerus, A. Herrmann, K. Ensslin, H.J. Hug, P.J.A. van Schendel, H.J. Güntherodt, Operation characteristics of piezoelectric quartz tuning forks in high magnetic fields at liquid helium temperatures, Rev. Sci. Instrum., 71 (2000) 4.

[28] Y. Qin, R. Reifenberger, Calibrating a tuning fork for use as a scanning probe microscope force sensor, Rev. Sci. Instrum. 78 (2007) 063704.

[29] P.G. Gucciardi, G. Bachelier, A. Mlayah, M. Allegrini, Interferometric measurement of the tip oscillation amplitude in apertureless near-field optical microscopy, Rev. Sci. Instrum. 76 (2005) 036105.

[30] P. Sandoz, J.M. Friedt, É. Carry, Vibration amplitude of a tip-loaded quartz tuning fork during shear force microscopy scanning, Rev. Sci. Instrum. 79 (2008) 086102.

[31] L. González, J. Otero, G. Cabezas, M. Puig-Vidal, Electronic driver with amplitude and quality factor control to adjust the response of quartz tuning fork sensors in atomic force microscopy applications, Sens. Actuators A Phys., 184 (2012) 112–118.

[32] Y. Seo, W. Jhea, C.S. Hwang, Electrostatic force microscopy using a quartz tuning fork, Appl. Phys. Lett. 80 (2002) 4324.

[33] J.P. Ndobo-Epoya, E. Lesniewskaa, J.P. Guicquero, Shear force microscopy with a nanoscale resolution, Ultramicroscopy 103 (2005) 229–236.

[34] H. Ogi, N. Nakamura, K. Sato, M. Hirao, S. Uda, Elastic, anelastic, and piezoelectric coefficients of alpha-quartz determined by resonance ultrasound spectroscopy, J. Appl. Phys. 100 (2006) 3511–3517.

[35] M. Woszczyna, P. Zawierucha, A. Masalska, G. Jozwiak , E. Staryga, T. Gotszalk, Tunneling/shear force microscopy using piezoelectric tuning forks for characterization of topography and local electric surface properties, Ultramicroscopy 110 (2010) 877–880.

[36] A. Makky, T. Berthelot, C. Feraudet-Tarisse, H. Volland, P. Viel , J. Polesel-Maris, Substructures high resolution imaging of individual IgG and IgM antibodies with piezoelectric tuning fork atomic force microscopy, Sens. Actuat. B 162 (2012) 269– 277.

[37] P. Sandoz, J.M. Friedt, É. Carry, In-plane rigid-body vibration mode characterization with a nanometer resolution by stroboscopic imaging of a microstructured pattern, Rev. Sci. Instrum. 78 (2007) 023706.

[38] Datasheet Tuning Fork Abracon QTF-32. Available online: http://www.abracon.com/Resonators/AB38T.pdf (accessed on July 2014).

[39] Datasheet Tuning Fork Citizen QTF-100. Available online: http://cfm.citizen.co.jp/english /product/pdf/CFS-CFV.pdf (accessed on July 2014).

[40] K. Waszczuk, G. Gula, M. Swiatkowsky, J. Olszewski, W. Herwich, Z. Drulis-Kawa, J. Gutowicz, T. Gotszalk, Evaluation of Pseudomonas aeruginosa biofilm formation using tuning fork mass sensors, Sens. Actuators B Chem. 170 (2012) 7–12.

[41] W. Rensen, N. van Hulst, A. Ruiter, P. West, Atomic steps with tuning-fork-based noncontact atomic force microscopy, Appl. Phys. Lett. 75 (1999) 1640.

[42] F.J. Giessibl, F. Pielmeier, T. Eguchi, T. An, Y. Hasegawa, Comparison of force sensors for atomic force microscopy based on quartz tuning forks and length-extensional resonators, Phys. Rev. B 84 (2011) 125409.

[43] J. Kim, D. Won, B. Sung, S. An, W. Jhe, Effective stiffness of qPlus sensor and quartz tuning fork, Ultramicroscopy 141 (2014) 56–62.

[44] S. Higuchi, H. Kuramochi, O. Kubo, S. Masuda, Y. Shingaya, M. Aono, Angled long tip to tuning fork probes for atomic force microscopy in various environments, Rev. Sci. Instrum. 82 (2011) 3701–3706.

3.2 Force microscopy studies in molecular biology

3.2.1 Associated Publication 3

Micropattern of antibodies imaged by shear force microscopy: Comparison between classical and jumping modes

By

Laura González[a], Jorge Otero[a,b], Juan P. Agusil[b,c], Josep Samitier[a,b,c], Jaume Adan[d], Francesc Mitjans[d] and Manel Puig-Vidal[a]

[a] Department of Electronics, University of Barcelona, C/Marti i Franques 1, 08028 Barcelona, Spain.

[b] IBEC – Institut for Bioengineering of Catalonia, C/Baldiri Reixac, 10-12, 08028 Barcelona, Spain.

[c] Centro de Investigación Biomédica en Red en Bioingeniería Biomateriales y Nanomedicina (CIBER-BBN), C/Poeta Mariano Esquillor s/n, 50018 Zaragoza, Spain

[d] Biomed Division of Leitat Technological Center, Barcelona Science Park, 08028 Barcelona, Spain

Published in

***Ultramicroscopy** 136 (2014) 176– 184.*

Ultramicroscopy 136 (2014) 176–184

Contents lists available at ScienceDirect

Ultramicroscopy

journal homepage: www.elsevier.com/locate/ultramic

Micropattern of antibodies imaged by shear force microscopy: Comparison between classical and jumping modes

L. González [a], J. Otero [a,b], J.P. Agusil [b,c], J. Samitier [a,b,c], J. Adan [d], F. Mitjans [d], M. Puig-Vidal [a,*]

[a] Department of Electronics, University of Barcelona, C/Marti i Franques, 1, 08028 Barcelona, Spain
[b] IBEC – Institute for Bioengineering of Catalonia, C/Baldiri Reixac, 10-12, 08028 Barcelona, Spain
[c] Centro de Investigación Biomédica en Red en Bioingeniería Biomateriales y Nanomedicina (CIBER-BBN), C/Poeta Mariano Esquillor s/n, 50018 Zaragoza, Spain
[d] Biomed Division of Leitat Technological Center, Barcelona Science Park, 08028 Barcelona, Spain

ARTICLE INFO

Article history:
Received 24 April 2013
Received in revised form
10 September 2013
Accepted 16 September 2013
Available online 17 October 2013

Keywords:
Atomic force microscopy
Quartz tuning fork
Self-assembled monolayer
Self-sensing probe
Shear force microscopy

ABSTRACT

Quartz tuning fork devices are increasingly being used as nanosensors in Scanning Probe Microscopy. They offer some benefits with respect to standard microfabricated cantilevers in certain experimental setups including the study of biomolecules under physiological conditions. In this work, we compare three different working modes for imaging micropatterned antibodies with quartz tuning fork sensors: apart from the classical amplitude and frequency modulation strategies, for first time the jumping mode is implemented using tuning forks. Our results show that the molecules suffer less degradation when working in the jumping mode, due to the reduction of the interaction forces.

1. Introduction

Since 1989, when [1] used an atomic force microscope (AFM) to study crystals, polymers, and processes in water, scanning probe microscopy (SPM) techniques have been widely used to image soft samples in a buffer solution. The capacity to study biological samples in their native conditions with nanometric resolution, together with the many aspects that can be studied via accurate measurements (morphology, electrochemical properties, binding forces, surface characteristics, etc.; [2,3,4]) make SPM a valuable tool for experimental research in molecular and cell biology [5]. Lipids [6], proteins [7], DNA [8] and antibodies [9] are just some examples of the wide range of samples that have been studied in molecular biology [10]. Of special interest is the study of these biomolecules when they are microstructured into patterns [11]: printing the molecules with periodic structures on the surfaces has several applications in the development of biosensors [12], the production of molecular switches [13], cell attachment studies [14], and measurement of the interaction forces using chemical force microscopy [15,16]. Moreover, in a buffer, the interaction between substrate and biomolecules is less stable than in air and therefore the strategies adopted to bind the molecules to different substrates are continually being reviewed and improved. Under certain conditions, molecules assemble themselves into self-assembled monolayers (SAMs). SAMs provide a monolayer of immobilized biomolecules, each with the same orientation, which is very useful for ligand–receptor binding studies [17]. For instance, adhesion forces between different protein SAMs on a gold substrate and *Staphylococcus epidermidis* bacteria are measured in [18] to assess coatings for biomaterials. In [19], anti-*Escherichia coli* antibodies immobilized on an indium–tin oxide surface are characterized by AFM to develop an immunosensor. Microcontact printing is one of the most successful techniques [20] for the formation of SAMs on surfaces of different material. Polymeric stamps, usually molded from polydimethylsiloxane (PDMS), are used to transfer the molecular inks onto the surface while reproducing the stamp features. Patterned SAMs are commonly analyzed with SPM due to the high resolution required to measure the thickness and roughness of the biomolecule monolayers accurately [21] and the need to conduct the experiments in a buffer solution.

AFM functions through measurement of the interaction forces between a nanometric tip (usually placed at the end of a microfabricated cantilever) and the sample surface. These small forces are usually detected by means of the reflection of a laser beam from the upper surface of the cantilever, which is measured using a position-sensitive photodiode. The use of nanosensors based on a quartz tuning fork (QTF) is an alternative to the conventional optical detection system and it has been widely used for sample

* Corresponding author. Tel.: +34 934039161.
E-mail address: manel.puig@ub.edu (M. Puig-Vidal).

0304-3991/$ - see front matter © 2013 Elsevier B.V. All rights reserved.
http://dx.doi.org/10.1016/j.ultramic.2013.09.008

imaging [22] and nanocharacterization [23,24]. To form such sensors, a sharpened tip is attached to one of the prongs of a piezoelectric resonator and oscillated parallel to the sample surface in shear force mode [25], or perpendicular to the surface in tapping mode [26]. A change in the oscillation amplitude and resonance frequency of the nanosensor is observed when an interaction force appears between the tip and the sample surface. Thanks to the piezoelectric properties of quartz, QTFs can be driven to resonance acoustically (direct piezoelectric effect) and electrically (inverse piezoelectric effect). If the excitation is mechanical, a dither is used to oscillate the device and the piezoelectric-generated charge is measured [27]; if the excitation is electrical, the sensor is driven with a voltage signal at the resonance frequency, and the current through the device is measured [28].

Unlike standard microfabricated cantilevers, QTF probes present high quality factors (Q) and high static spring constants (K) due to the piezoelectric properties of quartz and the mechanical structure of the resonators. These properties allow stable low oscillation amplitudes to be achieved and thereby make it possible to work in a non-contact regime avoiding the tendency of the tip to jump to contact at small tip-sample distances [29]. The fact that the laser-photodiode detection setup is not needed in QTF-based SPM, makes it easy to work in liquid environments to study biomaterials and biological samples [30]. Other examples of situations in which a non-optical detection method is required are those in which samples are sensitive to light or heat [31] and in AFM studies under cryogenic conditions [32]. Furthermore, it is easier to integrate an optical microscope into the QTF-based system and to implement a multi-probe system [33].

One of the critical points in the study of biomolecules with SPM is that the interaction forces often damage the sample [34]. Different dynamic techniques [35–37] have been implemented to achieve intermittent or non-contact imaging thereby avoiding continuous contact with the sample surface during scanning. The two most commonly used working modes in dynamic AFM are amplitude modulation (AM) and frequency modulation (FM). The AM mode allows high resolution imaging, but is not suitable for working with certain biological samples due to the difficulties in applying low forces [38,39]. FM mode is less destructive because it is often possible to maintain the tip in the non-contact regime. However, the tip is often contaminated, which can cause transitions between the non-contact and contact regimes [40]; fortunately, in liquid media this unstable situation is less likely because long range forces are weaker than in air [41]. To overcome these problems, other techniques such as force volume [42], peak force [43], and jumping mode (JM) [44] are becoming more common. These techniques use a lateral scanning motion with the tip maintained out of contact with the sample. Previous reports demonstrate the success of JM in imaging soft biological samples without damaging them, due to the reduction of lateral and normal forces [45,46].

Only a few studies have reported nanocharacterization of biological samples with QTF probes [24,27,28,47] and there is no comparative study of the different imaging modes in the literature. However, the use of QTFs to image soft matter has great potential as they present a high static spring constant and Q value [48] which allow low oscillation amplitudes to be achieved. The Q values obtained in air (1000–2500) and in liquid (around 300) for QTFs are very high compared to the values obtained with standard silicon cantilevers in air (~400) [49] and liquid (~30). Even when working with a small oscillation amplitude and imaging in the repulsive regime with a cantilever, some sort of sample damage is usually produced [50]. The use of low-amplitude oscillations with QTF probes avoids the undesirable tendency of the tip to jump to contact [51]. The idea of vertical displacement of the sensor for shear force imaging of soft samples was introduced in [52]: the Z position is modulated while scanning to reduce the interaction forces. In this work we go one step further by using the scheme of the Jumping Mode with tuning fork sensors. On this way, the lateral displacement of the probe is always done when there is no interaction between the tip and the sample. We then study three different methods for imaging biomolecules with QTF sensors. We compare the performance of AM, FM and JM AFM when imaging a microcontact-printed pattern of antibodies under physiological conditions.

2. Materials and methods

2.1. Sample preparation

For the surface activation, several $1 \times 1\ cm^2$ pieces of high-grade silicon oxide wafer (NTB, Buchs, Switzerland) were rinsed with absolute ethanol (Panreac, Barcelona, Spain), blown dry with N_2 and activated by sonication in 1 M NaOH solution (Panreac, Barcelona, Spain) for 15 min. Then, the silicon oxide substrates were rinsed with Milli-Q water (Millipore, Billerica, MA, USA) and soaked in 1 M HCl solution (Panreac, Barcelona, Spain) for 15 min. Finally, the substrates were rinsed with Milli-Q water, blown dry with N_2 and stored in a dust-free environment. This process creates SiOH functional groups on the surface for future modification. The activated substrates were immersed in a 2 mM ethanolic solution of 3-Glycidoxypropyldimethoxymethylsilane (3-GOPDTS) (Sigma-Aldrich, St. Louis, MO, USA) for 30 min, rinsed with absolute ethanol, dried under N_2, and baked for 1 h at 80 °C. The modified substrates were rinsed with copious amounts of absolute ethanol, blown dry with N_2 and stored in an inert atmosphere until further use.

A PDMS stamp was produced by pouring a degassed 10:1 (w/w) mixture of PDMS pre-polymer and curing agent (Sylgard 184, Dow Corning, MI, USA) onto a clean silicon master. The master comprised a regular array of square holes measuring $3 \times 3\ \mu m^2$ with a separation of 3 μm between holes. After curing overnight at room temperature and subsequently for 1 h at 65 °C, the PDMS replica was peeled from the master.

To produce a patterned antibody layer on the silicon substrate, the PDMS stamp was inked with a 40 μg/mL solution of mouse monoclonal antibody 5C3 of the IgG class and ~150 kDa (Leitat, Barcelona, Spain) which recognizes the S100A4 protein, in phosphate buffered saline (PBS) (Sigma-Aldrich, St. Louis, MO, USA) for 15 min and then blown dry with N_2. The inked stamp was placed in contact with the modified surface for 5 min.

After printing, the patterned antibody was left to react with the 3-GOPDTS modified substrates for 1 h in a humid atmosphere at room temperature. Afterwards, the patterned substrates were immersed in a 100 mM 2-(2-aminoethoxy)ethanol (AEE) solution (Sigma-Aldrich, St. Louis, MO, USA) in 100 mM sodium hydrogen carbonate buffer (Panreac, Barcelona, Spain) for 30 min, rinsed with carbonate buffer and PBS, and stored in PBS at 4 °C until further use.

To take a fluorescence image of the microcontact patterned antibodies, the entire substrate was incubated with 2 μg/mL of rhu-S100A4 (Leitat, Barcelona, Spain) diluted in PBS for 60 min at room temperature. Afterwards, unbound protein was removed by five washes in PBS containing 0.1% Tween 20 (PBST) and incubated for 30 min with 4 μg/mL of rabbit polyclonal antibody anti-S100A4 (Dako, Glostrup, Denmark, cat:A5114) diluted in PBS. After washing 5 times, the substrate was incubated with Alexa Fluor® 488 goat anti-rabbit IgG (H+L) (Life Technologies, CA, USA, cat: A11088). To characterize the pattern, an upright microscope (E1000, Nikon, Japan) equipped with a CCD camera was used to record the fluorescence of the Alexa Fluor® 488 conjugated goat anti-rabbit. The images obtained were processed with ImageJ (NIH, USA). Fig. 1 shows the sandwich structure obtained with

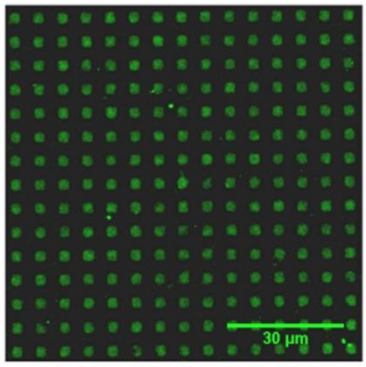

Fig. 1. Fluorescence microscopy images of antibody 5C3 patterned onto the 3-GOPDTS modified silicon surface probed with conjugated Alexa Fluor® 488.

the patterned antibody, antigen and fluorescence-labeled secondary antibody.

2.2. Sensors production and operation

The QTF probes were custom made by attaching a chemically sharpened optical fiber (SiO_2) to one of the prongs of a previously decapsulated commercial *AB38T* (Abracon Corp., CA, USA) QTF with a nominal resonant frequency of 32,768 Hz. To sharpen the probes [53], a 125 μm optical fiber was immersed in a 40% HF solution, with an organic solvent on top to act as a protective layer (C_8H_{18}); then, at the interface between the acid and the solvent, a meniscus formed thereby creating a reaction gradient. The radius of the fiber decreased due to HF etching until the process automatically stopped, resulting in a 150–200 nm tip radius.

The length of the part of the fiber protruding from the fork was between 3 and 4 mm, which was the minimum length necessary to work within the microscope liquid cell, while maintaining the QTF resonating in air. The longer the fiber, the lower of the *Q*-value (due to the extra mass added and the sensor becoming unbalanced). However, the decrease in *Q*-value is more dependent on the depth of immersion of the end of the fiber in the liquid.

The QTFs were operated in shear mode: oscillating parallel to the sample surface. The probes were electrically driven to resonance and the amplitude of oscillation was obtained by measuring the current flowing through the sensor. For the experiments presented in this work, a QTF with a quality factor, *Q*, of 235 and resonance frequency, *f*, of 31780 Hz was used (once the fiber was attached and immersed in the buffer solution). Driving amplitude of 10 mV was selected and the measured current at resonance was 2.3 nA.

2.3. QTF imaging

The QTF sensors were driven electrically by an integrated generator in the *Dulcinea Dynamic Board* of the *Nanotec* commercial AFM (Nanotec Electrónica, Madrid, Spain). A fully-custom-made electronic module was used to drive the QTF and control nanocharacterization [54]. A transimpedance amplifier (TIA) translated the current through the QTF into a voltage, to allow measurement of the oscillation amplitude with a lock-in amplifier. As in all dynamic working modes, we obtained information about the interaction between the tip and the sample by reading the amplitude and the phase of the QTF current signal (see Fig. 2A). Three different imaging modes were employed depending on the main feedback signal:

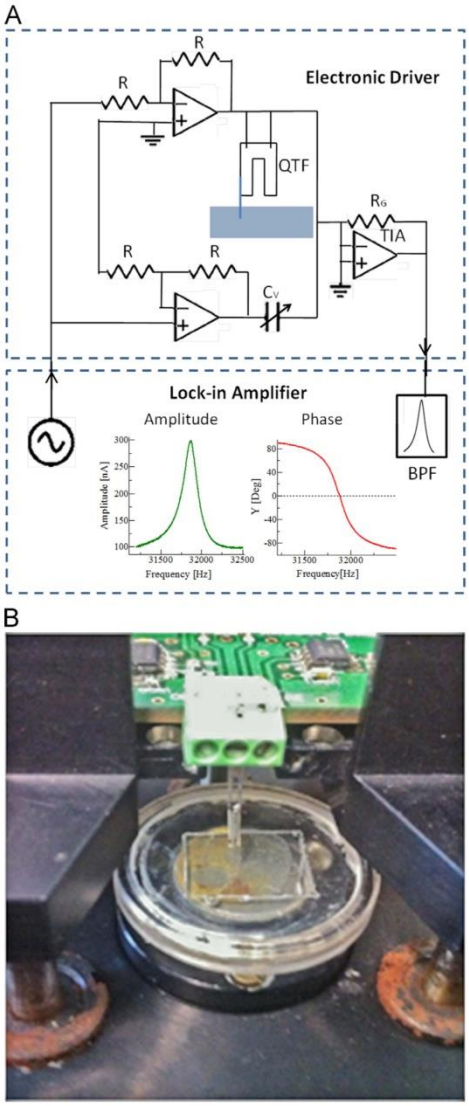

Fig. 2. (A) Scheme of the electronic driver; (B) image of the measurement set-up. The QTF probe is immersed in buffer solution to access the sample using a liquid cell.

amplitude modulation (AM)
frequency modulation (FM)
jumping mode (JM)

In AM mode, an excitation signal with constant amplitude was used to drive the QTF at the resonance frequency and the amplitude of the current was the input of the main feedback. A lower amplitude than the free oscillation amplitude was imposed on the system and the sample was moved in the *Z*-direction to reach the set point value, while the variable phase was also recorded.

In FM mode, the main feedback input signal was the resonant frequency shift of the QTF sensor when a tip–sample interaction

occurred. Another feedback loop was used with a phase-locked loop (PLL) to track the effective resonance frequency of the sensor. The PLL changed the frequency of the excitation signal to maintain a constant 0 phase. A third parallel feedback loop was used to control the amplitude of the driving signal and maintain the amplitude of oscillation, A_0, constant. This method is suitable for working in liquids, as the resonance frequency of the sensor changes with the evaporation of the buffer. This low-frequency drift was followed by the PLL tracking of the resonance frequency.

Jumping mode (JM) operation was originally designed for measuring the deflection of the cantilever at each point of the image [44]. The sensor operates in a closed loop when tip is in contact with the sample, to measure the topography; and in an open loop when the tip is moving away from or approaching the sample, to evaluate the tip–sample interaction as given by the force–distance curves. The sample was moved from one point image to another when it was far from the tip. This system reduces friction forces and damage to the sample, since lateral displacement between the tip and sample only takes place when they are not in contact. In classical AFM, where the sensor is the standard cantilever, the feedback channel is usually the normal force signal. In the present application, it was possible to operate in JM with QTF-based nanosensors working in AM by using the amplitude signal for the topography feedback. A cycle started in closed loop operation and, after a few ms of tip–sample contact, the feedback loop was opened and the jump step began. First, the Z-piezo is withdrawn and the tip could oscillate freely up to the maximum *Z*-distance set in the jump-off parameter. At the furthest *Z*-distance, the lateral position of the sample was changed to that of the next point image. Then the tip was moved close to the sample and the feedback was closed again to begin a new cycle. One cycle was executed at every image point.

3. Results and discussion

The sample was imaged in the three operation modes described above: AM-AFM, FM-AFM, and JM-AFM. All the measurements presented were obtained in buffer solution using a liquid cell (see Fig. 2B). The tip of the QTF probe was immersed in the buffer solution where the sample was also submerged. The measurement buffer was PBS with a pH of 7.4.

3.1. Sensor response as a function of the tip–sample distance

To characterize the dynamic sensor response, amplitude versus tip–sample distance curves were performed by measuring the current, I_{rms}, through the QTF when it was approaching the bare substrate. The QTF was driven at the resonance frequency; I_{rms} was constant when the probe was far from the sample surface and diminished as the QTF approached the sample, as illustrated in Fig. 3A. In AM mode, the set point parameter was adjusted to $I_{set}=1.64$ nA (see blue line in Fig. 3A), this value corresponds to an oscillation amplitude reduction of 78% with respect to the free oscillation amplitude. In FM mode, the set point was chosen to be 3.04 Hz, corresponding to the frequency shift with respect to the free resonance frequency (f–f_0) (see Fig. 3B).

3.2. Imaging results

The results obtained in AM mode are shown in Fig. 4. Micron-sized images show the pattern of antibodies anchored on the surface without well-defined edges. It is known that AM-AFM images of biomolecules are highly dependent on operational parameters. The set point A_{set} was tuned to 78% of the free oscillation amplitude: $A_{set}/A_{free}=0.78$, the minimum value for

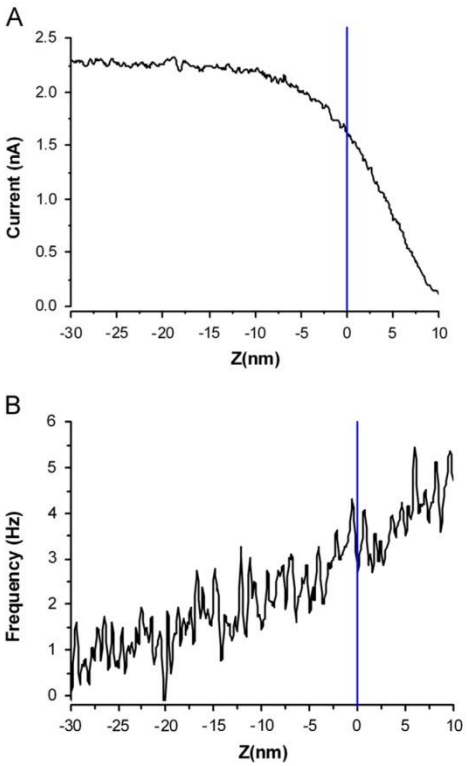

Fig. 3. Sensor dynamic response as a function of tip–sample distance. (A) Current, I_{rms}, against distance relationship; and (B) excitation frequency against distance when the QTF is approaching the substrate, driven at a constant voltage of 10 mV. Blue lines on the two graphs show the set point for each mode. (For interpretation of the references to color in this figure legend, the reader is referred to the web version of this article.)

stable operation, in an attempt to apply the minimum force needed to keep the tip in range of the sample surface. In order to minimize the tip–sample interaction, we employed small voltage-driven amplitude: 10 mV. Even so, lateral oscillation of the QTF and the scanning motion produced irreversible damage to the sample; part of the sample was removed. The sample was progressively degraded with successive scans. Two consecutive images were taken, while maintaining the same working parameters. The second image is of worse quality and lower contrast than the first, resulting from the high shear forces applied. The boundaries of the features are undefined and the height is highly uneven and different from the real size (see the profile in Fig. 4C). The height histogram shows a peak at 3.90 ± 1.78 nm in the lower region of the sample, which corresponds to the functionalized substrate. It was not possible to fit a Gaussian function to the upper values of the histogram corresponding to the antibody height, due to the broad spread of values. The histogram presents a tail towards higher values, corresponding to antibody features reaching values up to 17 nm without any characteristic peak. The value obtained for the height of the antibodies is far from the theoretical value, which is approximately 4 nm, as all the IgG molecules adopt the classic Y-shape [55].

The FM results are summarized in Fig. 5. In general terms, image quality was slightly better than in AM although the FM mode was noisier because of the added parallel feedback loops.

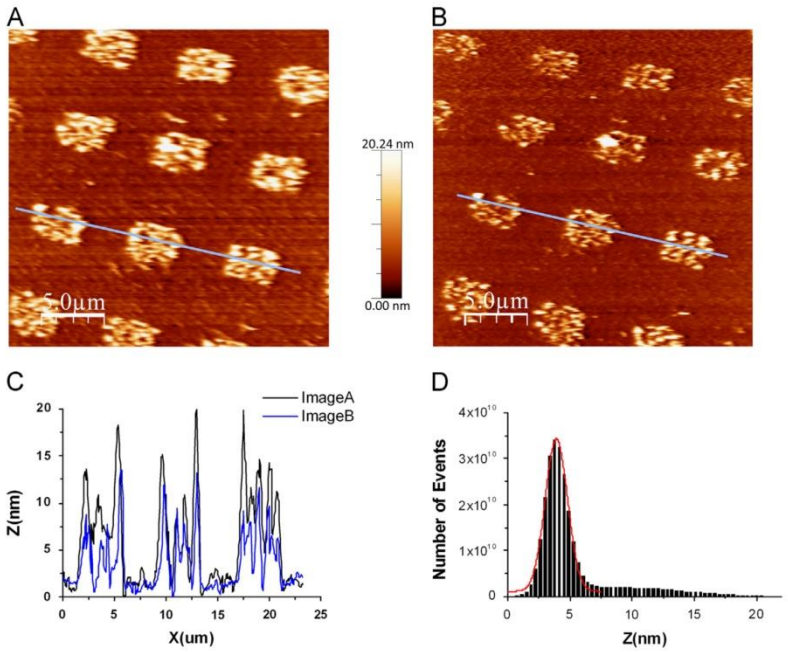

Fig. 4. (A) and (B): Two consecutive images of SAM of 5C3 antibody patterns obtained with QTF probes in the AM mode. The quality and contrast of both images are poor and sample degradation is evident while scanning. The topographic profiles and histogram of the first image are shown in (C) and (D) respectively.

It was not so evident that sample suffered irreversible damage as in the previous case during the scanning process. The distribution of the antibodies showed patterns with better defined edges, but the two consecutive images were still blurred. Sample degradation is less than in the case of the AM mode, so lateral forces were smaller in the FM than in the AM mode, as expected. The set point f_{set} was tuned to 3.04 Hz, the minimum frequency shift value for produce the image. The FM feedback maintained the frequency shift, which is highly dependent to the force gradient, to reconstruct the topography of the sample. Having a high Q value in FM mode is advantageous, especially in liquid conditions [56] and hence control over the interaction was greater than in AM mode. A profile of the topography image can be seen in Fig. 5C, which illustrates the irregular heights of the antibody features. The histogram of the same image is shown in Fig. 5D and it is possible to distinguish two different peaks corresponding to the two different regions of the sample; a Gaussian function was fitted to both. The highest peak is at 3.53 ± 1.9 nm and the lowest at 8.87 ± 7.17 nm, corresponding to non-patterned and antibody-patterned regions respectively. In comparison with AM, better contrast is obtained in the images but the height of the features is still far from the theoretical value.

The results obtained in JM are shown in Fig. 6. In contrast to the other two methods, the images present well-defined edges of the antibody features, and the results are both reproducible and repeatable after consecutive images. The amplitude set point A_{set} was fixed to 91.5% of the free oscillation amplitude: $A_{set}/A_{free}=0.91$. The set-up parameters were adjusted to produce minimum tip–sample interactions. Time excursion along the Z-direction of the tip from the sample between one point and the following was: $Jump_{off}=40$ nm (the tip jump needed to be large enough to overcome adhesion forces, even though in a liquid environment). The contact time was set to 4.8 ms (10 cycles). JM-AFM consecutive images of the same region of the sample did not show any visible damage to the sample. The height histogram presents two very clear distinct peaks, so the image contrast was substantially increased with respect to the other two methods. The topography height of the area outside the antibody pattern was 1.41 ± 0.67 nm and the height of the antibody features was 4.41 ± 1.55 nm, which is in good agreement with the theoretical height of the antibody monolayer (see profile in Fig. 6C).

3.3. Comparison between AM, FM and JM AFM

The results show that lateral forces in AM and FM modes are higher than in JM and tip–sample contact causes irreversible damage on the sample. This is mainly because the lateral and vertical displacements of the tip are not synchronized in either the AM or the FM mode. In JM, tip–sample interaction time is reduced with respect to the other two dynamic techniques, thereby minimizing the induced lateral tip–sample interaction. Moreover, when the tip and the sample are immersed in liquid, there are no capillary forces and Van der Waals forces are highly reduced. Therefore, the set point is difficult to maintain due to the inhomogeneity of the antibody features. It could be that some antibodies adopt a Y-shaped distribution and others a T-shape, and moreover the molecules might not be equally distributed across the features. Fig. 3A shows that the current versus distance curve decreases monotonically as the tip approaches the sample. The reduction of the current through the fork corresponds to the reduction in the oscillation amplitude; the parameter used for primary feedback control in AM. In contrast, Fig. 3B shows that the resonance frequency increases while tip–sample distance decreases. Although it is noisier, it is known that frequency shift is fairly sensitive, particularly when the tip is close to the sample [57,58]; there is greater variation in frequency than in amplitude. Hence, the use of FM allows better control of the set point and the feedback conditions. However, the lack of significant Van der

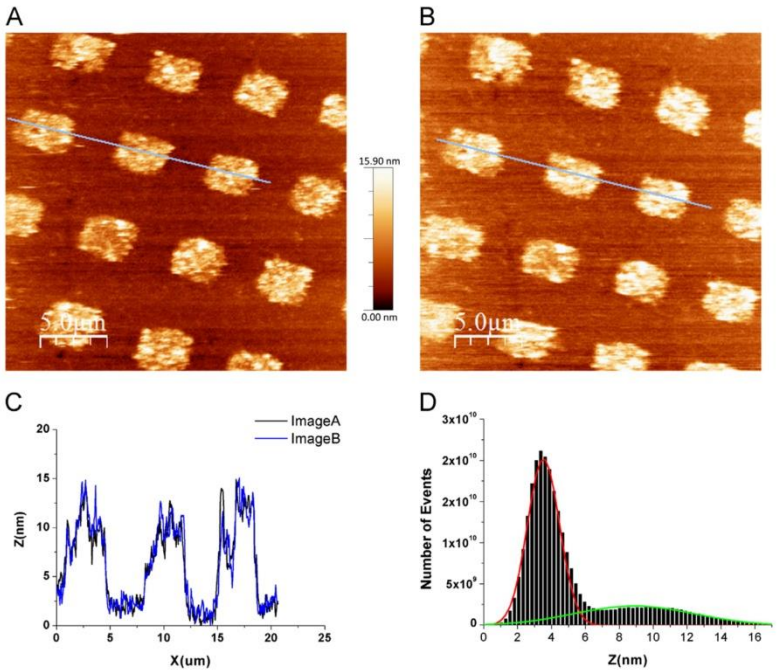

Fig. 5. (A) and (B): Two consecutive images of SAM of 5C3 antibody patterns obtained with QTF probes in the FM mode. The quality and contrast of both images are slightly better than those taken in the AM mode. The topographic profiles and histogram of the first image are shown in (C) and (D) respectively.

Waals forces in liquids means that feedback control is more stable in both AM and FM modes under liquid conditions and indeed is similar in the two modes. In addition, working with biological samples, the tip easily becomes contaminated thereby changing the attractive/repulsive regimes and leading to instabilities in control, especially when the adhesion surface changes significantly; as in our case, where the sample has two different regions with different adhesion properties of the surface.

In AM, the amplitude and phase variations in the current through the QTF, with respect to the signal driving the voltage, are used as the feedback control. The system responds with a step-like change in amplitude, on a time scale of Q/f_0 [59]. The higher is the quality factor, the lower the system response and therefore the image acquisition time. In FM, the frequency shift with respect to the resonance frequency without interaction is measured via the PLL and this value is used as the feedback signal in the closed-loop system. The system responds with a step-like change in frequency, on a time scale of $1/f_0$ [59]. Scan rates can thus be higher in FM than in AM, even taking into account that the QTF quality factor is substantially higher than that of standard cantilevers, even in liquid environments. However, when the QTF probe is immersed in a buffer solution, Q is greatly reduced due to the viscosity of the liquid inducing overdamped hydrodynamics due to friction forces and making it difficult to apply the low forces required in AM.

We have shown that JM-AFM is a suitable technique for imaging a self-assembled monolayer of patterned antibodies with QTF nanosensors under liquid conditions. JM-AFM images are well-defined and reproducible. Using this technique we measured the height of the antibodies to be 4.41 ± 1.55 nm, which is in good agreement with the theoretical height of 4 nm and other recent studies in liquid with standard AFM [55]. Fig. 7 exhibits a direct comparison of the histograms of the images taken with the three studied imaging modes and their topographical profiles showing the clear performance improvement in results going from AM to JM. These results demonstrate the effectiveness of QTF probes working in JM which minimizes the shear and friction forces exerted on the sample. One drawback of using the JM is the low scan rate. All the images in this study were of 512×512 points and taken at a scan rate of 1 Hz with the three different imaging modes. Acquisition time for the AM and FM images was about 10 min, whereas the total acquisition time for one image in the JM was about 55 min. Acquisition time depends on the control parameters, but the measurement cycle in the JM is longer due to the time-consuming process of approach to and withdrawal from the sample of the tip at each image point. This slow scan rate makes it difficult to study dynamic processes of biomolecules, but the images obtained are of significantly better quality than those obtained with other dynamic scanning methods. Table 1 summarizes the performance of the three different imaging modes implemented in this study.

4. Conclusions

In this work, we have compared the performances of three different imaging modes applied to micropatterned antibodies characterization using QTF-based nanosensors. We have observed that micropatterned biomolecules can be imaged with QTF without damaging the sample when working in the JM of AFM. The other modes tested, AM-AFM and FM-AFM, produce serious alterations that are irreversible. Tip–sample forces are lower in JM since the lateral scanning and QTF oscillation are desynchronized, thereby minimizing the lateral forces during interaction. Although the modulation of the vertical displacement has shown

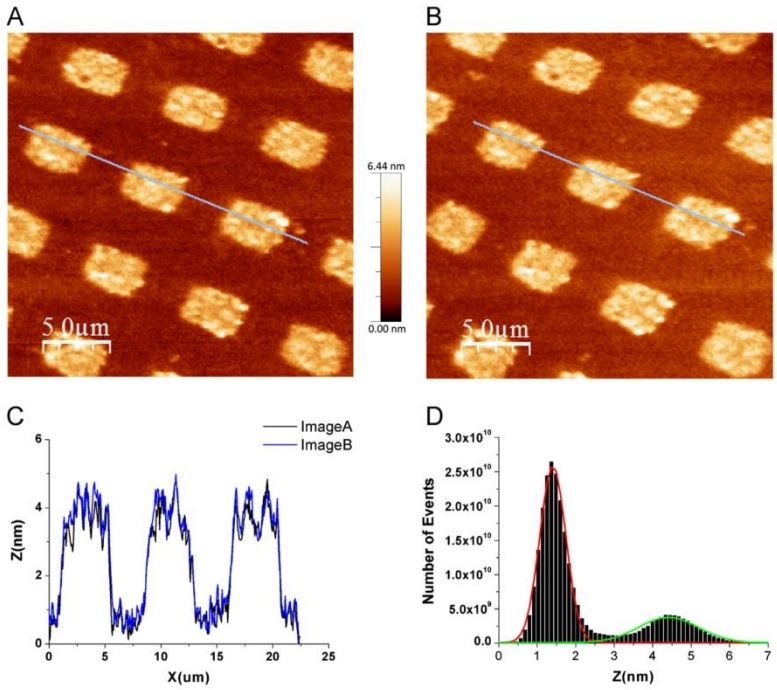

Fig. 6. (A) and (B): Two consecutive images of SAM of 5C3 antibodies obtained with QTF probes in JM. The quality and contrast of both images were clearly better than those taken in the AM and FM modes. The topographic profiles and histogram of the first image are shown in (C) and (D) respectively.

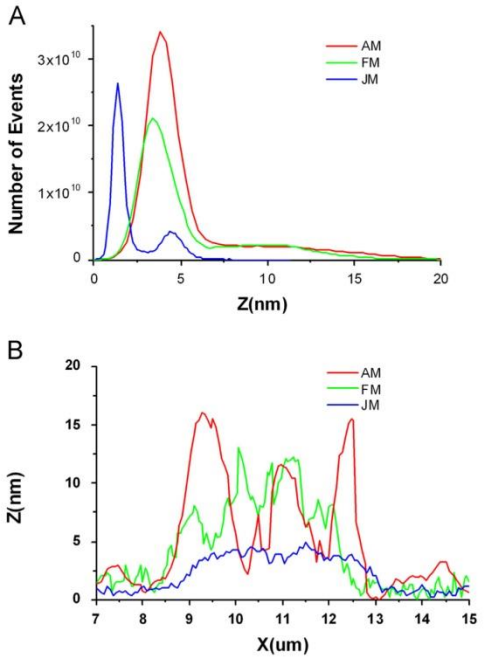

Fig. 7. Direct comparison of the histograms of the images taken with the three studied imaging modes and their topographical profiles.

Table 1
Summary of the performance of the three working modes implemented.

Mode	Time (s) for 512 × 512 image	Contrast	Real height	Sample damage
AM	512	Very low	NO	YES
FM	512	Low	NO	SOME
JM	3000	High	YES	NO

to be useful in shear force imaging of soft samples, this improvement alone shows a reduction of the resolution by a factor of 4 [52]. In contrast, if using a more complex setup for the control system (Jumping Mode, where the tip is always moved laterally when no interaction occurs) and Quartz Tuning Fork sensors for the detection of the shear force, our results show that there is no loss in the resolution of the images. Besides, there is a good correspondence between the experimental height of the sample and the theoretical value. We can therefore conclude that QTFs are good nanoprobes for imaging soft biological samples because the applied forces are very low due to the weak interactions present in the liquid when working in JM. Nevertheless, one of the drawbacks of JM is the low scanning rate, which makes it difficult to monitor fast processes.

Some studies in the literature report SPM measurements with QTF for different samples, but there is no standard procedure to perform such measurements. Here, we have compared three different techniques for measuring the same sample as an important step forward in the use of QTF nanosensors. This work therefore contributes to the standardization of QTF probes as a tool for dynamic SPM to image soft biological samples as patterned molecules in liquid.

Acknowledgments

This work was supported in part by the Spanish *Ministerio de Economía y Competitividad* through Project TEC2009-10114 and Grant BES-2010-031186 and also by the regional Catalan authorities under project VALTEC09-2-0058. CIBER-BBN is an initiative funded by the VI National R&D&I Plan 2008–2011, *Iniciativa Ingenio 2010*, the Consolider program, CIBER Actions and financed by the *Instituto de Salud Carlos III* with assistance from the European Regional Development Fund. The Nanobioengineering group has support from the Commission for Universities and Research of the Department of Innovation, Universities, and Enterprise of the regional Catalan authorities (2009 SGR 505). This study was also supported by the "Fundación M. Botín", Santander, Spain. This work was partially funded by CIBER-BBN under the project MICROPLEX.

References

[1] B. Drake, C.B. Prater, A.L. Weisenhorn, S.A. Gould, T.R. Albrecht, C.F. Quate, D. S. Cannel, H.G. Hansma, P.K. Hansma, Imaging crystals, polymers, and processes in water with the atomic force microscope, Science 243 (1989) 1586–1589.
[2] D.J. Müller, Y.F. Dufrêne, Atomic force microscopy: a nanoscopic window on the cell surface, Trends Cell Biol. 21 (2011) 461–469.
[3] I. Casuso, F. Rico, S. Scheuring, Biological AFM: where we come from – where we are – where we may go, J. Mol. Recognit. 24 (2011) 406–413.
[4] Y. Zhang, et al., High-resolution imaging and nano-manipulation of biological structures on surface, Microsc. Res. Tech. 74 (2011) 614–626.
[5] K.-A.D. Walker, S.H. Doak, P.R. Dunstan, Mechanisms of cell–cell adhesion identified by immunofluorescent labelling with quantum dots: a scanning near-field optical microscopy approach, Ultramicroscopy 111 (2011) 1200–1205.
[6] S. Garcia-Manyes, F. Sanz, Nanomechanics of lipid bilayers by force spectroscopy with AFM: a perspective, Biochim. Biophys. Acta 1798 (2010) 741–749.
[7] D.J. Muller, A. Engel, Strategies to prepare and characterize native membrane proteins and protein membranes by AFM, Curr. Opin. Colloid Interface Sci. 13 (2008) 338–350.
[8] Y.L. Lyubchenko, L.S. Shlyakhtenko, AFM for analysis of structure and dynamics of DNA and protein–DNA complexes, Methods 47 (2009) 206–213.
[9] H. Torun, O. Finkler, F.L. Degertekin, Atomic force microscope based biomolecular force-clamp measurements using a micromachined electrostatic actuator, Ultramicroscopy 122 (2012) 26–31.
[10] D. Fotiadis, S. Scheuring, S.A. Müller, A. Engel, D.J. Müller, Imaging and manipulation of biological structures with the AFM, Micron 33 (2002) 385–397.
[11] S.A. Ruiz, C.S. Chen, Microcontact printing: a tool to pattern, Soft Matter 3 (2007) 168–177.
[12] N.K. Chaki, K. Vijayamohanan, Self-assembled monolayers as a tunable platform for biosensor applications, Biosensors Bioelectronics 17 (1–2) (2002) 1–12.
[13] S.J. van der Molen, P. Liljeroth, Charge transport through molecular switches, J. Phys.: Condens. Matter 22 (2010) 133001.
[14] N. Cheng, X. Cao, Photoactive SAM surface for control of cell attachment, J. Colloid Interface Sci. 348 (2010) 71–79.
[15] H. Kim, et al., Characterization of mixed self-assembled monolayers for immobilization of streptavidin using chemical force microscopy, Ultramicroscopy 108 (2008) 1140–1143.
[16] R.D. Rodriguez, A. Anne, E. Cambril, C. Demaille, Optimized hand fabricated AFM probes for simultaneous topographical and electrochemical tapping mode imaging, Ultramicroscopy 111 (2011) 973–981.
[17] M.-J. Chang, et al., High spatial resolution label-free detection of antigen–antibody binding on patterned surface by imaging ellipsometry, J. Colloid Interface Sci. 360 (2011) 826–833.
[18] Y. Liu, J. Strauss, T.A. Camesano, Adhesion forces between Staphylococcus epidermidis and surfaces bearing self-assembled monolayers in the presence of model proteins, Biomaterials 29 (33) (2008) 4374–4382.
[19] L. Yang, Y. Li, AFM and impedance spectroscopy characterization of the immobilization of antibodies on indium–tin oxide electrode through self-assembled monolayer of epoxysilane and their capture of Escherichia coli O157:H7, Biosensors Bioelectronics 20 (2005) 1407–1416.
[20] S.A. Claridge, et al., From the bottom up: dimensional control and characterization in molecular monolayers, Chem. Soc. Rev. 42 (2013) 2725–2745.
[21] J. Chalmeau, et al., Patterned domains of supported phospholipid bilayer using microcontact printing of Pll-g-PEG molecules, Colloids Surfaces B: Biointerfaces 89 (2012) 188–195.
[22] W.H.J. Rensen, N.F. van Hulst, S.B. Kämmer, Imaging soft samples in liquid with tuning fork based shear force Microscopy, Appl. Phys. Lett. 77 (2000) 1557.
[23] J. Polesel-Maris, et al., Force spectroscopy by dynamic atomic force microscopy on bovine serum albumin proteins changing the tip hydrophobicity, with piezoelectric tuning fork self-sensing scanning probe, Sensors Actuators B 161 (2012) 775–783.
[24] J. Otero, R. Baños, L. Gonzalez, E. Torrents, A. Juarez, M. Puig-Vidal, Quartz tuning fork studies on the surface properties of Pseudomonas aeruginosa during early stages of biofilm formation, Colloids Surfaces B: Biointerfaces 102 (2013) 117–123.
[25] A.G.T. Ruiter, J.A. Veerman, K.O. van der Werf, N.F. van Hulst, Dynamic behavior of tuning fork shear-force feedback, Appl. Phys. Lett. 71 (1) (1997).
[26] N.B. Matsko, Self-sensing and –actuating probes for tapping mode AFM measurements of soft polymers at a wide range of temperatures, J. Mod. Phys. 2 (2011) 72–78.
[27] M. Hofer, et al., Molecular recognition imaging using tuning fork-based transverse dynamic force microscopy, Ultramicroscopy 110 (2010) 605.
[28] A. Makky, et al., Substructures high resolution imaging of individual IgG and IgM antibodies with piezoelectric tuning fork atomic force microscopy, Sensors Actuators B 162 (2012) 269–277.
[29] B. Cappella, G. Dietler, Force–distance curves by atomic force microscopy, Surface Sci. Rep. 34 (1999) 1–104.
[30] J. Otero, L. González, M. Puig-Vidal, Nanocharacterization of soft biological samples in shear mode with quartz tuning fork probes, Sensors 12 (4) (2012) 4803–4819.
[31] J. Rychen, T. Ihn, P. Studerus, A. Herrmann, K. Ensslin, A low-temperature dynamic mode scanning force microscope operating in high magnetic fields, Rev. Sci. Instrum. 70 (1999) 2765–2770.
[32] C.H. Yang, T.H. Chang, M.J. Yang, W.J.A. Moore, Low noise transimpedance amplifier for cryogenically cooled quartz tuning fork force sensors, Rev. Sci. Instrum. 73 (2002) 2713–2716.
[33] J. Otero, L. González, G. Cabezas, M. Puig-Vidal, Multitool platform for morphology and nanomechanical characterization of biological samples with coordinated self-sensing probes, IEEE/ASME Trans. Mechatronics 18 (3) (2013) 1152–1160.
[34] E. Thormann, et al., Probing material properties of polymeric surface layers with tapping mode AFM: which cantilever spring constant, tapping amplitude and amplitude set point gives good image contrast and minimal surface damage? Ultramicroscopy 110 (2010) 313–319.
[35] G. Guanglu, et al., MAC mode atomic force microscopy studies of living samples, ranging from cells to fresh tissue, Ultramicroscopy 107 (2007) 299–307.
[36] Z. Parlak, et al., Controlling tip–sample interaction forces during a single tap for improved topography and mechanical property imaging of soft materials by AFM, Ultramicroscopy 109 (2009) 1121–1125.
[37] D. Martínez, et al., Noninvasive protein structural flexibility mapping by bimodal dynamic force microscopy, Phys. Rev. Lett. 106 (2011) 198101.
[38] S.D. Solares, Eliminating bistability and reducing sample damage through frequency and amplitude modulation in tapping-mode atomic force microscopy, Meas. Sci. Technol. 18 (2007) 592–600.
[39] R. García, R. Pérez, Dynamic atomic force microscopy methods, Surface Sci. Rep. 47 (2002) 197–301.
[40] M. Gauthier, et al., Interplay between nonlinearity, scan speed, damping, and electronics in frequency modulation atomic-force microscopy, Phys. Rev. Lett. 89 (2002) 146104.
[41] A.L. Weisenhorn, et al., Forces in atomic force microscopy in air and water, Appl. Phys. Lett. 54 (1989) 2651.
[42] H. An, et al., Material properties of lipid microdomains: force–volume imaging study of the effect of cholesterol on lipid microdomain rigidity, Biophys. J. 99 (2010) 834–844.
[43] D. Alsteens, et al., High-resolution imaging of chemical and biological sites on living cells using peak force tapping atomic force microscopy, Langmuir 28 (2012) 16738–16744.
[44] P.J. de Pablo, J. Colchero, J. Gómez-Herrero, A.M. Baró, Jumping mode scanning force microscopy, Appl. Phys. Lett. 73 (1998) 3300.
[45] F. Moreno-Herrero, P.J. de Pablo, M. Álvarez, J. Colchero, J. Gómez-Herrero, A.M. Baró, Jumping mode scanning force microscopy: a suitable technique for imaging DNA in liquids, Appl. Surf. Sci. 210 (2003) 22–26.
[46] F. Moreno-Herrero, J. Colchero, J. Gómez-Herrero, A.M. Baró, Atomic force microscopy contact, tapping, and jumping modes for imaging biological samples in liquids, Phys. Rev. E 69 (2004) 031915.
[47] G.Y. Shang, W.H. Qiao, F.H. Lei, J.F. Angiboust, M. Troyon, M. Manfait, Development of a shear force scanning near-field fluorescence microscope for biological applications, Ultramicroscopy 105 (2005) 324.
[48] E. Wutscher, F.J. Giessibl, Atomic force microscopy at ambient and liquid conditions with stiff sensors and small amplitudes, Rev. Sci. Instrum. 82 (2011) 093703.
[49] T. Fukuma, K. Kobayashi, K. Matsushige, H. Yamada, True atomic resolution in liquid by frequency-modulation atomic force microscopy, Appl. Phys. Lett. 87 (2005) 034101.
[50] A. San Paulo, R. García, High-resolution imaging of antibodies by tapping-mode atomic force microscopy: attractive and repulsive tip–sample interaction regimes, Biophys. J. 78 (3) (2000) 1599–1605.
[51] M. Labardi, Dynamics of probes attached to quartz tuning forks for the detection of surface forces, Nanotechnology 18 (2007) 395505.
[52] R. Brunner, A. Simon, T. Stifter, O. Marti, Modulated shear-force distance control in near-field scanning optical microscopy, Rev. Sci. Instrum. 71 (2000) 1466–1471.
[53] P. Hoffmann, B. Dutoit, R. Salathé, Comparison of mechanically drawn and protection layer chemically etched optical fiber tips, Ultramicroscopy 61 (1995) 165.
[54] L. González, J. Otero, G. Cabezas, M. Puig-Vidal, Electronic driver with amplitude and quality factor control to adjust the response of quartz tuning

fork sensors in atomic force microscopy applications, Sensors Actuators A 184 (2012) 112–118.
[55] J.N. Ngunjiri, et al., Immobilization of proteins on carboxylic acid functionalized nanopatterns, Anal. Bioanal. Chem. 405 (2013) 1985–1993.
[56] D. Ebeling, H. Hölscher, B. Anczykowski, Increasing the Q factor in the constant-excitation mode of frequency-modulation atomic force microscopy in liquid, Appl. Phys. Lett. 89 (2006) 203511.
[57] A. Castellanos-Gomez, N. Agraït, G. Rubio-Bollinger, Dynamics of quartz tuning fork force sensors used in scanning probe microscopy, Nanotechnology 20 (2009) 215502.
[58] Y. Qin, R. Reifenberger, Calibrating a tuning fork for use as a scanning probe microscope force sensor, Rev. Sci. Instrum. 78 (2007) 063704.
[59] F.J. Giessibl, Advances in atomic force microscopy, Rev. Mod. Phys. 75 (2003) 949–983.

3.2.2 Associated Manuscript 3

Piezoelectric tuning fork biosensors for the quantitative measurement of biomolecular interactions

By

Laura González[a], Mafalda Rodrigues[b], Angel M. Benito[a], Lluïsa Pérez-García[b], Manel Puig-Vidal[a] and Jorge Otero[a]

[a] Department of Electronics, University of Barcelona, C/Marti i Franques 1, 08028 Barcelona, Spain.

[b] Department of Pharmacology and Therapeutic Chemistry, University de Barcelona, Av. Joan XXIII s/n, 08028 Barcelona, Spain.

submitted for peer-review to

Biosensors and Bioelectronics.

Piezoelectric tuning fork biosensors for the quantitative measurement of biomolecular interactions

Laura González[1], Mafalda Rodrigues[2], Angel Maria Benito[1], Lluïsa Pérez-García[2], Manel Puig-Vidal[1], Jorge Otero[1]

[1]Department of Electronics, University of Barcelona, C/Marti i Franques, 1, 08028 Barcelona, Spain.

[2]Department of Pharmacology and Therapeutic Chemistry, University de Barcelona, Av. Joan XXIII s/n, 08028 Barcelona, Spain.

Abstract

The quantitative measurement of biomolecular interactions is of high interest in molecular biology. Atomic Force Microscopy (AFM) acting as a biosensor has proof its ability to determine the affinity between biomolecules of interest. Nevertheless, the detection scheme presents certain limitations to develop a compact biosensor. Recently, piezoelectric Quartz Tuning Forks are being used as laser-free detection sensors for AFM. However, only a few studies have been done in soft biological samples, especially in quantified molecular recognition experiments. In this work, we show the ability of the QTF probes to perform specific interaction measurements between biotin-streptavidin complex in buffer solution. For the first time, a variant of dynamic force spectroscopy based on adhesion energies *E* (aJ) representation versus pulling rates *v* (nm/s) is presented. Results are compared with conventional atomic force microscopy (AFM) measurements and show the great potential of these sensors to realize molecular interaction studies.

Keywords

Atomic force microscopy; Quartz tuning fork; Self-sensing probe; Force Spectroscopy; Protein-protein interactions; Molecular recognition

1. Introduction

The quantitative measurement of the interactions between biomolecules is currently a hot topic in molecular biology research [1[4]. About 60% of all pharmaceuticals have membrane proteins as main target [5[7], so of special interest is the measurement of protein-protein interactions: results can give a crucial insight on how receptors in the cell membrane react to different molecules. Several techniques are being successfully used to measure protein-protein interactions (see [8[9] for further details); among them, Atomic Force Microscopy (AFM) is of special interest because it can be employed to obtain high resolution molecular images and directly measure the unbinding force of individual ligand-receptor complexes [10]. For instance, glucagon/anti-glucagon pairs are studied in [11] under different pH values demonstrating that the pH dependence of antigen-antibody bond forces can be measured with an AFM sensor. In [12], the spatial organization of the peptidoglycan on the cell walls of living bacteria is investigated and in [13] antigen-antibody binding forces on lymphoma patient cancer cells are measured to find potential effective targets for cancer. AFM functions through the measurement of the interaction forces between a nanometric tip, placed at the end of a micro-fabricated cantilever, and the sample surface. The forces are detected by means of the

reflection of a laser beam on the rear side of the cantilever which is measured using a position-sensitive photodiode. Beyond its use as an imaging tool, AFM can measure the interaction forces between the tip and the sample, in the so-called force spectroscopy mode. The streptavidin-biotin system was one of the first to be studied at the single molecule level using force spectroscopy due to its high affinity and specificity of interaction [14[16]. The basics of these measurements is certainly straightforward: one of the biomolecules is linked on the tip, the other one is immobilized on the surface, and the interaction force vs. the tip-sample distance is recorded in a series of experiments. After data analysis, some parameters of the interaction can be quantified. The dissociation rate k_0 can be determined after a dynamic study over different pulling speeds between the ligand-receptor pair and parameters related to binding potential can be obtained which are related to energy landscape of the studied bond [17[18].

One of the main applications of the measurement of protein interactions is the molecular recognition: the AFM is used as a biosensor to determine the degree of affinity between the biomolecules [19[20]. In recent years, efforts have been made to incorporate the AFM's force detection scheme into compact biosensors. The reported solution have been focused on developing chips compatible with the optical readout [21[22] or in the integration of laser-free sensors, mainly cantilevers with piezoresistive readout [23]. Nevertheless, the development of these cantilever-based biosensors requires specific microfabrication facilities, usually involving non-standard fabrications steps, which is a huge drawback for the growth of this research, being limited to a few research groups around the world [24[25]. On the other hand, the use of nanosensors based on a quartz tuning fork (QTF) is a promising alternative to the conventional silicon cantilevers [26[29] and it has been widely used for sample imaging and nanocharacterization [30[32]. Instead the optical detection system used in conventional AFM, the mechanical oscillation of the QTF is transduced to a piezoelectric current and detected by a transimpedance amplifier. Moreover, tuning forks show additional advantages as low stable amplitude *A*, high quality factor *Q* and high spring constant *K* which permits the forces in the pico-range [33]. Also, QTFs do not present one of the main problems of cantilevers: thermal drift (due to the heat dissipation of the laser diode or due to the intrinsic properties of piezoresistive materials). To build QTF-based sensors, a sharpened tip is attached to one of the prongs of a piezoelectric resonator and oscillated parallel to the sample surface in shear force mode [34], or perpendicular to the surface in perpendicular mode [35]. When a force acts on the tip, there is a change in the resonant frequency of the sensors (which can be measured as a change in the vibration amplitude if working at constant excitation frequency) [36].

QTF-based nanosensors have been used to image cells [30], bacteria [37] and biomolecules [38]. Sub-molecular resolution in air has also been obtained in [39] and qualitative recognition has been performed between avidin and lysozyme antibody in [40] in shear mode. Nevertheless, there are few works on quantitative molecular interaction forces with such a probe in solution. In [41], the specific interaction between a ligand and its receptor in aqueous media is studied with the QTF sensors quantifying the withdrawal forces. The latter employs the piezoelectric oscillating perpendicular to the sample surface. Small non-linear jumps in the phase curve are observed when an unbinding event between ligand-receptor is produced. After a series of assumptions, the phase variations are translated to a force gradient curve, but

the measurements are not quantified in energy terms, so they cannot be compared with results obtained with alternative methods.

Herein, we present the application of quartz tuning fork probes for molecular interaction analysis between the biotin-streptavidin complex. We have applied a variant of the dynamic force spectroscopy (DFS) technique commonly used for AFM systems to QTF working in shear force detection. DFS consists on measurements of the needed force to unbind individual receptor-ligand systems. Nevertheless, we have measured the adhesion energies between the biotin-streptavidin system at different pulling velocities and results have been compared with those obtained with AFM measurements under the same experimental conditions. Adhesion energy [42[43] was the parameter that it was possible to measure directly from the amplitude-distance curves obtained with QTF sensors. In this work, it is demonstrated the effectiveness of the piezoelectric quartz tuning fork sensors in shear mode to perform specific interaction measurements between a ligand and its receptor in liquid media.

2. Materials and Methods

2.1 Sensors production and operation

In our experiments we used QTFs with a resonance frequency of 32,768 Hz (model *AB38T*, Abracon Corp., USA). The nanosensors were custom made by attaching the functionalized probe to one of the prongs of the QTF decapsulated. The quality factor (*Q*) of these devices arrives up to 100,000 when packaged in vacuum. The device is then decapsulated and the probe is glued to one tine. The Q factor falls because the quartz structure is resonating in air instead of vacuum and due to the added mass of the fiber. Around 3-4 mm probe length is enough to work with the fiber tip inside the liquid cell but the fork resonating in the air.

As a previous step to the functionalization, the optical fiber (SiO_2) was chemically sharpened [44]. In brief, a 125 µm optical fiber was immersed in a 40% HF solution, with an organic solvent (iso-octane C_8H_{18}) on top to protect against the acid vapors; then, a meniscus is formed creating a reaction gradient at the interface between the acid and the solvent, being a self-terminating process after 90 minutes. After the etching stops, the fibers are rinsed with ethanol and water, functionalized with biotin and mounted to the resonator with cyanoacrylate glue (see figure 1A).

The sensor was mounted on an adapted STM head integrated in a commercial AFM microscope (Nanotec Electrónica, Spain). A fully custom-made electronic module was used to drive the nanosensor electrically [45] to its resonance frequency. A transimpedance amplifier (TIA) (model OPA656, Texas Instruments, USA) converts the current flowing through the QTF into voltage with a 10^6 V/A gain. The QTFs were operated in shear mode and in amplitude modulation: oscillating parallel to the sample surface at constant frequency excitation and reading the ampltiude and phase variations when an interaction between the tip and the sample is produced (*see fig. 1B*). When there is a tip-sample interaction force, the frequency response is shifted and a lower amplitude than the free oscillation amplitude is measured (*see fig. 1C*).

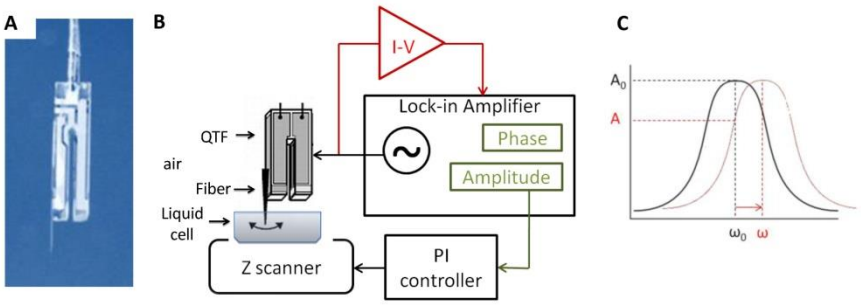

Figure 1. (A) QTF sensor decapsulated with a fiber probe attached to one of the prongs. (B) Scheme of the QTF measurement setup. The QTF probe is excited electrically with an AC signal by setting the resonance frequency. The current through the device is measured by a lock-in amplifier (C) Principle of operation in amplitude mode.

For the experiments presented in this work, a QTF with a quality factor, *Q*, of 1500 and resonance frequency, *f*, of 34,830 Hz was used (once the fiber was attached and immersed in the buffer solution). Driving amplitude of 20 mV was selected and the measured current at resonance was 5.2 nA corresponding to a free oscillation amplitude of 3.88 nm (*see eq. 2*). Spring constant value has been determined by finite element simulations using a model developed in our group resulting in k≈34.000 [46[47].

2.2 Functionalization of the biosensors and the test samples

For the surface activation, several 1×1 cm pieces of glass coverslips and optical fibers (SiO_2) previously sharpened were immersed in a piranha solution (3:1 concentrated H_2SO_4 and 30% H_2O_2 solution) for 1 hour, rinsed with MilliQ water and dried under nitrogen. After that, the substrates and fibers were placed in a mixture of $NH_4/H_2O_2/H_2O$ (1:1:5) for 30 min. Then, they were rinsed with Milli-Q water, blown dry with N_2 and stored in a dust-free environment. This process created SiOH functional hydroxyl groups on the surface for future modification.

For the functionalization of the fibers with biotin, the aminosilanization process was done by immersing the activated fibers overnight in a solution of 3-aminopropyltriethoxysilane (APTES) (Sigma-Aldrich, St. Louis, MO, USA) 2% in acetone. Then, the fibers were rinsed with acetone three times, dried under N_2 and baked for 20 min. at 90°C. Then, fibers were incubated in a solution of 20 µg/mL biotin N-hydroxysuccinimide ester in DMSO 1% (Sigma-Aldrich, St. Louis, MO, USA) in PBS (100 mM, pH 7.4) for 6 h. After that, the functionalized probes were rinsed twice in a PBS solution with EDTA 0.1% and triton x-100 1% for 15 min., twice in PBS for another 15 min. and stored in PBS at 4°C until further use. The same procedure was followed to functionalize the AFM tips.

For the functionalization of the substrates with estreptavidin (Sigma-Aldrich, St. Louis, MO, USA), the activated substrates were immersed overnight in a 2 % solution in ethanol of Triethoxysilylundecanal (TESUD) (ABCR, Germany) and (6-{2-[2-(2-Methoxy-ethoxy)-ethoxy]-ethoxy}-hexyl)trimethoxysilane (MTMS) (Sikemia, France) corresponding to TESUD/MTMS (1:100). Then, the samples were washed three times with ethanol, dried under N_2 and baked for 20 min. at 90°C. After that, substrates were incubated in a solution of 20 µg/mL

streptavidin (Sigma-Aldrich, St. Louis, MO, USA) in PBS (100 mM, pH 7.4) with 5mM of sodium cianoborohydride for 6 h. Finally, the functionalized probes were rinsed twice in a PBS solution with EDTA 0.1% and triton x-100 1% for 15 min., twice in PBS for another 15 min. and stored in PBS at 4°C until further use.

To take a fluorescence image of the functionalized fibers with biotin, they were immersed for 30 min. in a solution (20 µg/mL) of avidin labeled with Texas Red. After that, the functionalized probes were rinsed twice in a PBS solution with EDTA 0.1% and triton x-100 1% for 15 min. Fig. 2 shows the optical images of the QTF probe functionalized with biotin and conjugated with Avidin – TR (DMIRB wide-field transmitted light and fluorescence microscope, Leica Microsystems, Germany).

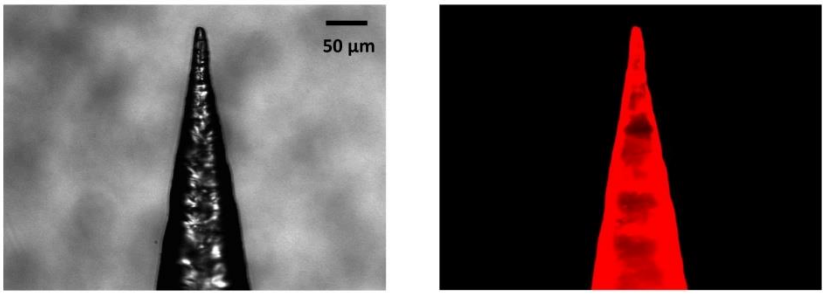

Figure 2. Tuning Fork tip functionalized with biotin and conjugated with Avidin - Texas Red. Optical microscopy images with normal light (left) and fluorescence filters (right).

2.3 Data acquisition and analysis

Experiments with standard AFM tips were performed using an AFM microscope (MFP-3D, Asylum Research, USA). Cantilevers used were made of silicon nitride with a nominal spring constant K=0.06 N/m (PNP-DB type cant.B, NanoAndMore GmbH, Germany). Independently, we calibrated the spring constant using the thermal fluctuation analysis according to [48] obtaining a value of K=0.025 N/m.

Force measurements were acquired bringing the biotin-coated AFM tip or QTF probe into contact with the substrate functionalized with immobilized estreptavidin in phosphate-buffered saline (PBS) at room temperature. The retraction speed was varied from 200 to 1000 nm/s whereas the approaching velocity was kept constant. The respective molecular loading rates were calculated by multiplying the experimental velocities by the measured molecular elasticities that were determined from the force curve graphs [49]. All data were consecutively analyzed according to the stochastic Bell-Evans model of a forced dissociation under an external load [50[51].

The maximum indentation was controlled in both cases to minimize the contact area. Force-distance curves were acquired under identical conditions and individually analyzed with custom-made MATLAB-based analysis software (The MathWorks, Natick, MA) to calculate molecular adhesion forces and adhesion energies.

For AFM measurements, the adhesion energy was computed as the area under the force-distance retraction curve with the baseline taken at zero force. For QTF measurements, the first step is to translate the amplitude-distance curves into force-distance curves by eq. 1 [52].

$$F = \left(1 - \frac{I}{I_0}\right)\frac{k_s A_0}{\sqrt{3}Q} \quad (1)$$

$$A_0 = \sqrt{\frac{V I_0 Q}{k_s w_0}} \quad (2)$$

The force curves are obtained following eq. 1 where I is the measured through the QTF, I_0 is the current when the probe is far from the sample, k_s is the spring constant, Q is the quality factor and A_0 is the free oscillation amplitude. The mechanical vibration amplitude was calculated using the expression given by eq. 2 [53], where V is the excitation voltage, I_0 is the measured current through the QTF, and f_0 is the free resonance frequency. Then, the area confined between approach and withdrawal lines is calculated to obtain the adhesion energy. In general, force and energy are correlated such as [54]:

$$E = -\int_{h_1}^{h_2} F\, dh \quad (3)$$

Where E is the adhesion energy, F is the pull-off force, and h is the separation distance. To calculate the adhesion energy, the integral in eq. 3 was evaluated using the Trapezoidal rule [54].

3. Results

Amplitude versus tip–sample distance curves were performed by measuring the current, I_{rms}, through the QTF when the functionalized biotin QTF probe was approaching onto the immobilized avidin on the sample surface at different retraction speeds. The QTF was driven at the resonance frequency; I_{rms} was constant when the probe was far from the sample surface and diminished as the QTF approached the sample. Fig. 3 b and c, show two representative graphs of an amplitude-displacement curve for the biotin-streptavidin system for two retraction speeds: 300 and 440 nm/s, respectively. We checked the specificity of the interaction adding free biotin which cancels the adhesion forces. The approach and withdrawal curves are almost identical without showing any distinct nonlinear jump. Interestingly, however, we observed hysteresis between the approach and the retraction curves, indicating there is an interaction between the biotin-streptavidin system. The area confined between approach and withdrawal curves is related to bond energy and it is increased with retraction speed. Control curves over a non-functionalized bare glass surface were performed to confirm that the measured hysteresis was due to the specific interaction between biotin-streptavidin system and no hysteresis is observed in this case (see Fig. 3).

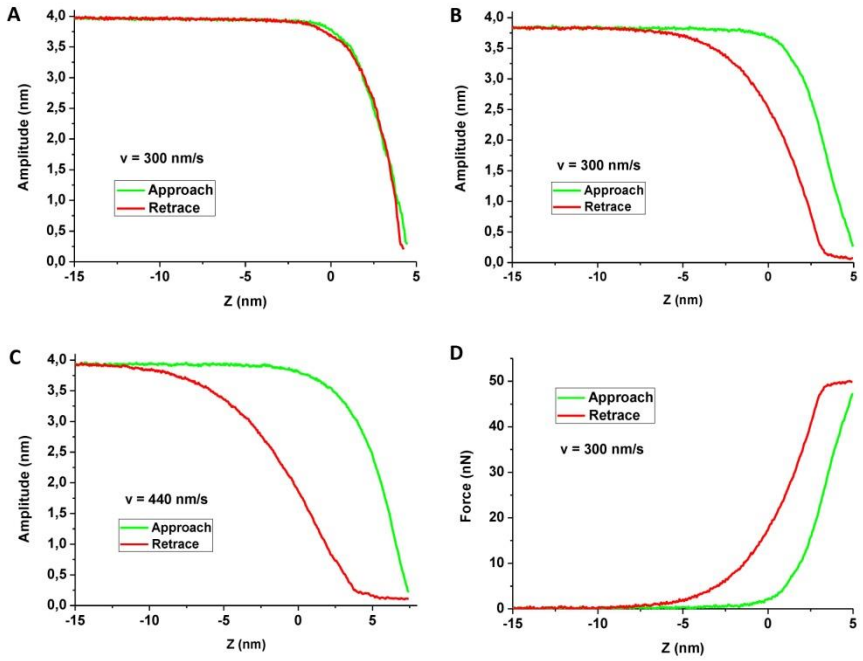

Figure 3. (A) Amplitude versus tip–sample distance control curve over a non-functionalized bare glass surface. (B)(C) Representative amplitude-distance curves of the interaction between biotin functionalyzed QTF probe over streptavidin immovilized on the sample surface at retraction speeds of 300 and 400 nm/s respectively (D) Amplitude-distance curve at 300 nm/s translated into force-distance curve by using eq. 1 and 2.

The amplitude-distance curves which presented hysteresis (~65% of trials) are translated to force-curves for each retraction speed using eq. 1 as illustrated in fig. 3D. The area confined between approach and retraction curves is calculated to obtain the energy. Histograms of adhesion energies from about 100 interactions for each speed are presented in fig. 4 where a Gaussian function is fitted in each one to extract the mean adhesion energy for each retraction velocity (see table in fig. 4). Adhesion energy values can be represented versus the pulling velocity in logarithmic scale as illustrated in fig. 5.

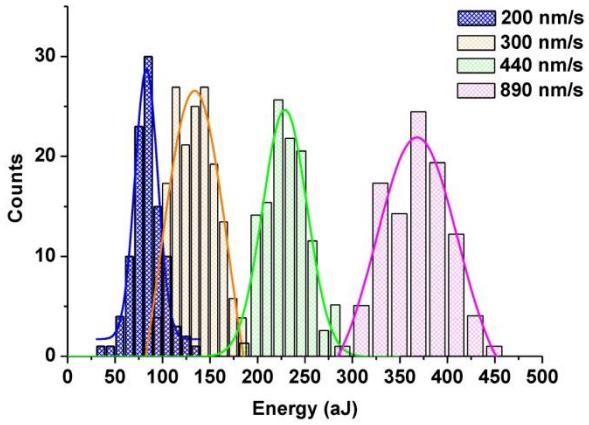

Figure 4. (A) Histograms Histograms of the adhesion energy between a biotin QTF probe and avidin surface at retraction speeds of (A) 200 nm/s (B) 300 nm/s (C) 440 nm/s and (D) 890 nm/s. All histograms were fitted to a Gaussian function. The centers of the energy distribution were (A) 83±12 aJ (B) 135±36 aJ (C) 228±23 aJ and (D) 369±43 aJ, respectively.

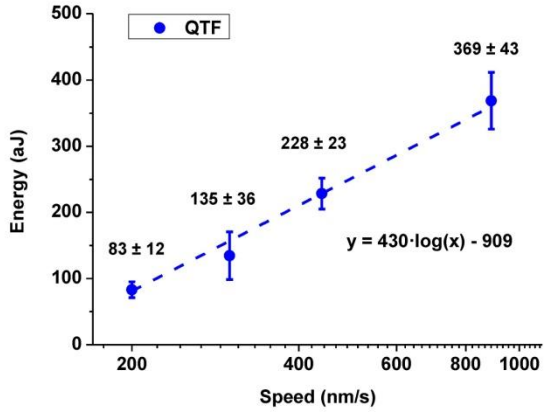

Figure 5. (A) Summary results of adhesion energy between a biotin QTF probe and avidin surface for different retraction speeds obtained by applying a gaussian fit on the histograms. (B) Representation of the adhesion energy versus retraction speed within logarithmic scale.

Same measurements were performed with a standard AFM tip and several force-distance curves were acquired at same conditions. Figure 6 show a representative force-curve of the interaction of the biotin-avidin system at pulling speed of 500 nm/s, corresponding to a loading rate of 5200 pN/s. The adhesion energy *E* was determined by integrating the area under a single-molecule force-versus-distance curve. We found typical single-molecule adhesion energies of E = 1.2 - 4 aJ at a binding probability of > 60%. These energies are about two orders of magnitude smaller than those observed by QTF force spectroscopy and reflect

the fact that fewer molecules are probed in AFM experiments. In this case, it was possible to obtain the unbinding forces *F* of each single event. Mean rupture forces *F* for each pulling velocity are summarized in fig. 6. Adhesion energy values can be represented versus the pulling velocity in logarithmic scale as illustrated in fig. 7.

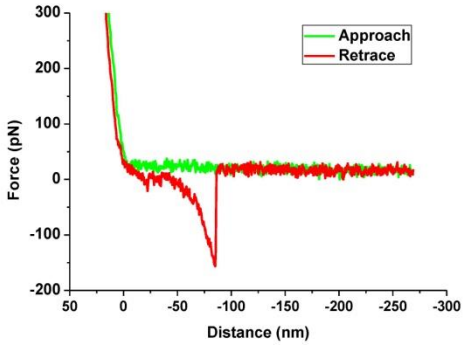

AFM	
Speed (nm/s)	***F (pN)***
300	137 ± 49
500	193 ± 67
700	212 ± 64
1000	218 ± 49

Figure 6. Representative force-distance curve of the interaction between biotin functionalyzed AFM tip over avidin immovilized on the sample surface at retraction speed of 500 nm/s.

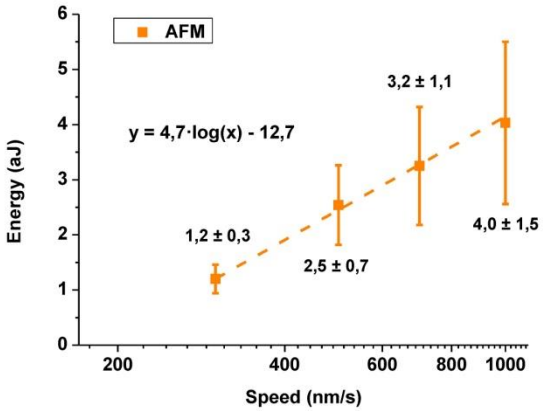

Figure 7. (A) Summary results of adhesion energy and unbinding forces between a biotin functionalized AFM tip and streptavidin surface for different pull-off speeds. (B) Representation of the adhesion energy versus retraction speed within logarithmic scale.

4. Discussion

As another technology, QTF based nanosensors for nanocharacterization is constantly improving through different advances in instrumentation level and the emergence of new applications. In spite of the great potential of the technique to detect specific interactions between ligand and receptor, the capacity to measure discrete interaction is compromised. Because the binding force of an individual molecular pair is not known, the number of interacting molecules cannot be exactly determined. The total number of streptavidin-biotin bonds formed in an experiment depends on receptor density, the duration of contact, and the area of contact. Moreover, it is difficult to quantify the unbinding force because there is not a complete mechanical model of the QTF sensor to obtain the magnitude of the measured forces when working in shear mode. However, following the same procedure than [55], it is possible to arrive to an approximation of the number of bonds presented in a given measurement. From the adhesion energy value from measurements of the QTF at speed of 300 nm/s, the binding force can be approximated as adhesion energy divided by the binding length, about 0.8 nm [56], resulting in 175 nN. We can also consider the estimated binding force per estreptavidin-biotin pair measured with the standard AFM tip, being 137 pN at the same pulling speed of 300 nm/s. Under this assumption, the adhesion between the biotin tip and the estreptavidin surface in our experiments with QTF corresponds to a contribution from about 1275 molecular pairs. Furthermore, if we assume a dense coverage of the surface with estreptavidin (30 nm^2 per molecule of estreptavidin) then, the interaction area is equivalent to half the area of a sphere with a radius of 78 nm. This value is close to the obtained probe radius of the etched fibers which is around 100 nm. This would mean that in our experiment, 80% of the entire curvature of the tip contributes to the adhesion. Taking account this assumption, we can estimate that the difference between the adhesion energies obtained with the QTF probe and the AFM tip is basically due to the contact area since the tip radius in the QTF probe is approximately 10 times higher than the AFM tip radius (nominal radius considered as ~10nm). This means a relation of 100 times in terms of contact area. Figure 8 show the results obtained of adhesion energies measured with both QTF and AFM sensors and can be compared. Interestingly, however, the magnitude of the measured energies are different in 2 orders of magnitude, the tendency of both results is equivalent showing a great proportionality between them in a factor of 100. We think that this proportionality constant could be related with the difference in the contact area between both sensors due to the different tip radius.

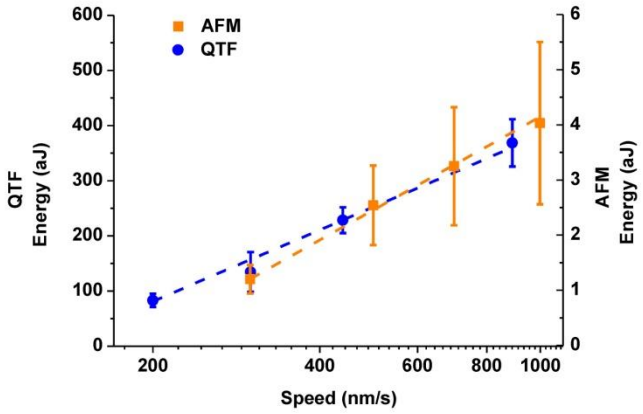

Figure 8. Representation of the adhesion energy of biotin-streptavidin complex versus retraction speed within logarithmic scale measured with conventional AFM tips and QTF probes.

5. Conclusions

The main purpose of this work is to proof that the QTF biosensors are able to quantitatively measure the interaction between proteins. On this way, we have been able to quantify the results and compare them with the ones obtained with a conventional AFM microscope. We have presented a new procedure based on AFM dynamic force spectroscopy applied to QTF-based nanosensors for molecular interaction studies. By using this procedure, the adhesion energy of the biotin-streptavidin complex has been analyzed obtaining comparable results to those measured with conventional AFM tip. Nevertheless, tapered glass fibers apexes should be improved for the purpose of achieving single-molecule measurements. The obtained results show good agreement between QTF and AFM experiments, so they open the door to the use of QTF as biosensors in biomolecular measurements in liquid conditions, in compact solutions where a laser-free detection scheme is needed.

Appendix: consistency of the results by the calculation of the dissociation rate constant

In standard AFM measurements, it is possible to obtain the common dynamic spectrum from unbinding forces and loading rates to extract the dissociation kinetics of the streptavidin-biotin complex. The rupture force of these linkages was determined from the magnitude of the measured force peaks and was measured at different force loading rates. Variation in the loading rate *Lr* of the AFM measurements was achieved with different cantilever retraction rates *v*. *Lr* is the product of the system spring constant, *k*s and *v: Lr = Ks x v*. The system spring constant depends on the elastic properties of both the cantilever and the substrate to which estreptavidin is attached. The measured system spring constants were in the range of 8.6-12 mN/m and were obtained from the slope of the force vs displacement relationship of each

single event. Consequently, the loading rate of the force measurements was varied from 2600 to 12000 pN/s to cover only one energy barrier. According to Bell-Evans theory [50,[57], the dependence of the unbinding force *F* on the force loading rate *Lr* follows the relationship of eq. 4. Here, k_B is Boltzmann's constant, k_0 is the dissociation rate constant in the absence of applied force and x_β is the reaction length.

$$F = \frac{k_B T}{x_\beta} ln\left(\frac{L_r x_\beta}{k_0 k_B T}\right) \qquad (4)$$

Plotting the rupture force *F vs*. ln(*Lr*) it is possible to estimate the reaction length, x_β, for a given regime of applied external forces from the slope of the fitted line to experimental data in the force spectrum plot. The dissociation rate constant, k_0, can be deduced by linearly extrapolating the data to zero external force (*F*=0). The obtained results were k_0= 3.74 s^{-1} and x_β = 0.08 nm which were in agreement with the values founded in the literature. For instance, a value of k_0=2.98±2.61 s^{-1} and x_β = 0.024 nm for *Lr* between 1700 and 9600 pN/s and k_0= 2.09 s^{-1} and x_β = 0.05 nm for *Lr* of 1000-5000 pN/s were reported respectively in [58] and [59].

Acknowledgments

The authors thank F. Rico for fruitful discussions. This work was supported in part by the Spanish Ministerio de Economía y Competitividad through Project TEC2009-10114 and Grant BES-2010-031186.

References

[1] Y.F. Dufrêne, Atomic force microscopy: A powerful molecular toolkit in nanoproteomics, Proteomics 9 (2009) 5400–5405.

[2] Y.F. Dufrêne, E. Evans, A. Engel, J. Helenius, H. Gaub, D. Müller, Five challenges to bringing single-molecule force spectroscopy into living cells, nature methods, Vol. 8 Num. 8, 2011.

[3] A.A. Ivanov, F.R. Khuri, H. Fu, Targeting protein–protein interactions as an anticancer strategy, Trends in Pharmacological Sciences, Vol. 34, No. 7, 2013.

[4] Q. Wang, W.E. Moerner, Single-molecule motions enable direct visualization of biomolecular interactions in solution, Nature Methods 11 (2014) 555–558.

[5] M.A. Yildirim, K.I. Goh, M.E. Cusick, A.L. Barabasi, M. Vidal, Drug-target network, Nat. Biotechnol. 25 (2007) 1119-1126.

[6] T.M. Bakheet, J.D. Andrew, Properties and identification of human protein drug targets, Bioinformatics 25 (4) (2009) 451-457.

[7] K.M. Giacomini, Membrane transporters in drug development, Nature Reviews Drug Discovery 9 (2010) 215-236.

[8] F. Ritort, Single-molecule experiments in biological physics: methods and applications, J. Phys.: Condens. Matter 18 (2006) R531–R583.

[9] K.C. Neuman, A. Nagy, Single-molecule force spectroscopy: optical tweezers, magnetic tweezers and atomic force microscopy, Nature Methods Vol. 5, Num. 6, 2008.

[10] C.A. Bippes, D.J. Muller, High-resolution atomic force microscopy and spectroscopy of native membrane proteins, Rep. Prog. Phys. 74 (2011) 086601.

[11] S. Lin, Y. Wang, L. Huang, C. Lin, S. Hsu, C. Lee, Dynamic response of glucagon/anti-glucagon pairs to pulling velocity and pH studied by atomic force microscopy, Biosensors and Bioelectronics 22 (2007) 1013–1019.

[12] G. Andre, S. Kulakauskas, M.P. C., B. Navet, M. Deghorain, E. Bernard, P. Hols, Y.F. Dufrêne,Imaging the nanoscale organization of peptidoglycan in living Lactococcus lactis cells, Nature Communications 1 (2010) 27.

[13] M. Li, X. Xiao, L. Liu, N. Xia, Y. Wanga, Z. Donga, W. Zhang, Atomic force microscopy study of the antigen antibody binding force on patient cancer cells based on ROR1 fluorescence recognition, J. Mol. Recognit. 26 (2013) 26 432–438.

[14] E.L. Florin, V.T. Moy, H.E. Gaub, Adhesion forces between individual ligand-receptor pairs, Science 264 (1994) 5157: 415–417.

[15] G.U. Lee, D.A. Kidwell, R.J. Colton, Sensing discrete streptavidin biotin interactions with atomic-force microscopy, Langmuir 10 (1994) 2: 354–357.

[16] V.T. Moy, E.L. Florin, H.E. Gaub, Intermolecular forces and energies between ligands and receptors, Science 266 (1994) 5183: 257–259.

[17] C. Lee, Y. Wang, L. Huang, S. Lin, Atomic force microscopy: Determination of unbinding force, off rate and energy barrier for protein–ligand interaction, Micron 38 (2007) 446–461.

[18] A. Fuhrmann, R. Ros, Single-molecule force spectroscopy: a method for quantitative analysis of ligand–receptor interactions, Nanomedicine 5(4), (2010) 657–666.

[19] U. Dammer, M. Hegner, D. Anselmetti et Al. 1996. Specific antigen/antibody interactions measured by force microscopy. Biophys. J. 70(5) (1996) 2437–2441.

[20] A. Fuhrmann, J. Schoning, D. Anselmetti, D. Staiger, R. Ros, Quantitative analysis of single-molecule RNA-Protein interaction, Biophys. J. 96(12) (2009) 5030-5039.

[21] S.R. Nettikadan, J.C. Johnson, S.G. Vengasandra, J. Muys, E. Henderson, ViriChip: a solid phase assay for detection and identification of viruses by atomic force microscopy, Nanotechnology 15 (2004) 383–389.

[22] K. Schoenwald, Z. C. Peng, D. Noga, S. R. Qiu, T. Sulchek, Integration of atomic force microscopy and a microfluidic liquid cell for aqueous imaging and force spectroscopy, Rev. Sci. Instrum. 81 (2010) 053704.

[23] A. Quist, A. Chand, S. Ramachandran, D. Cohena, R. Lal, Piezoresistive cantilever based nanoflow and viscosity sensor for microchannels, Lab Chip 6 (2006) 1450–1454.

[24] N. Moldovan, K. Kim, H.D. Espinosa, Design and fabrication of a novel microfluidic nanoprobe, Journal of Microelectromechanical Systems 15 (2006) 1.

[25] T. Yin, Y. Zhao, Josef Horak et Al., A micro-cantilever sensor chip based on contact angle analysis for a label-free troponin I immunoassay, Lab Chip 13 (2013) 834.

[26] F.J. Giessibl, Advances in atomic force microscopy, Reviews of Modern Physics 75 (2003) 949–983.

[27] J.Polesel-Maris, C. Lubin, F. Thoyer, J. Cousty, Combined dynamic scanning tunneling microscopy and frequency modulation atomic force microscopy investigations on polythiophene chains on graphite with a tuning fork sensor, Journal of Applied Physics 109 (2011) 074320 .

[28] M. Lange, D. van Vörden, R. Möller, A measurement of the hysteresis loop in force-spectroscopy curves using a tuning-fork atomic force microscope, Beilstein J. Nanotechnol., 3 (2012) 207–212.

[29] J. Welker, F.J. Giessibl, Revealing the angular symmetry of chemical bonds by atomic force microscopy, Science 336 (2012) 6080: 444–9.

[30] W.H.J. Rensen, N.F. van Hulst, and S.B. Kämmer, Imaging soft samples in liquid with tuning fork based shear force microscopy, Appl. Phys. Lett. 77 (2000) 1557.

[31] J. Otero, L. González, M. Puig-Vidal, Nanocharacterization of soft biological samples in shear mode with quartz tuning fork probes, Sensors 12(4) (2012) 4803-4819.

[32] A. Makky, P. Viel, S.W. Chen, T. Berthelot, J. Pellequer, J. Polesel-Maris, Piezoelectric tuning fork probe for atomic force microscopy imaging and specific recognition force spectroscopy of an enzyme and its ligand, J. Mol. Recognit. 26 (2013) 521–531.

[33] E. Wutscher, F.J. Giessibl, Atomic force microscopy at ambient and liquid conditions with stiff sensors and small amplitudes, Rev. Sci. Instrum. 82 (2011) 093703.

[34] A.G.T. Ruiter, J.A. Veerman, K.O. van der Werf, N.F. van Hulst, Dynamic behavior of tuning fork shear-force feedback, Appl. Phys. Lett. Vol. 71, No. 1, 1997.

[35] N.B. Matsko, Self-sensing and actuating probes for tapping mode AFM measurements of soft polymers at a wide range of temperatures, Journal of Modern Physics 2 (2011) 72-78.

[36] K. Karrai, I. Tiemann, Interfacial shear force microscopy, Physical Review B Vol. 62 Num. 19 (2000).

[37] J. Otero, R. Baños, L. Gonzalez, E. Torrents, A. Juarez, M. Puig-Vidal, Quartz tuning fork studies on the surface properties of Pseudomonas aeruginosa during early stages of biofilm formation, Colloids and Surfaces B: Biointerfaces 102 (2013) 117– 123.

[38] L. González, J. Otero, J.P. Agusil, J. Samitier, J. Adan, F. Mitjans, M. Puig-Vidal, Micropattern of Antibodies Imaged by Shear Force Microscopy: Comparison between Classical and Jumping Modes, Ultramicroscopy 136 (2014) 176-184.

[39] A. Makky et Al., Substructures high resolution imaging of individual IgG and IgM antibodies with piezoelectric tuning fork atomic force microscopy, Sensors and Actuators B 162 (2012) 269– 277.

[40] M. Hofer *et al.*, Molecular recognition imaging using tuning fork-based transverse dynamic force microscopy, Ultramicroscopy 110 (2010) 605.

[41] J. Polesel-Maris et Al., Force spectroscopy by dynamic atomic force microscopy on bovine serum albumin proteins changing the tip hydrophobicity, with piezoelectric tuning fork self-sensing scanning probe, Sensors and Actuators B 161 (2012) 775–783.

[42] A. Harder, V. Walhorn, T. Dierks, X. Fernàndez-Busquets, D. Anselmetti, Single-molecule force spectroscopy of cartilage aggrecan self-adhesion, Biophysical Journal 99 (2010) 3498–3504.

[43] F.P. Gordesli, N.I. Abu-Lail, The role of growth Temperature in the adhesion and mechanics of pathogenic L. monocytogenes: An AFM study, Langmuir 28 (2012) 1360–1373.

[44] S. Mononobe, Near-field optical fiber probes and the imaging applications: Progress in Nano-Electro-Optics III, Springer, Berlin, 2005.

[45] L. González, J. Otero, G. Cabezas, M. Puig-Vidal, Electronic driver with amplitude and quality factor control to adjust the response of quartz tuning fork sensors in atomic force microscopy applications , Sensors and Actuators A 184 (2012) 112– 118.

[46] R. Oria, J. Otero, L. González, L. Botaya, M. Carmona, M. Puig-Vidal, Finite element analysis of electrically excited quartz tuning fork devices, Sensors, 13 (2013) pp. 7156 - 7169.

[47] L. González, R. Oria, L. Botaya, M. Puig-Vidal, J. Otero, Determination of the static spring constant of electrically-driven quartz tuning forks with two freely oscillating prongs, Nanotechnology, *submitted*.

[48] J.L. Hutter and J. Bechhoefer, Calibration of atomic-force microscope tips, Rev. Sci. Instrum., Vol. 64, No. 7, 1993.

[49] A. Fuhrmann, D. Anselmetti, P. Reimann, Refined procedure of evaluating experimental single-molecule force spectroscopy data, Phys. Rev. E. 68 (2008) 045103.

[50] E. Evans and K. Ritchie, Dynamic strength of molecular adhesion bonds, Biophys. J. 72 (1997) 1541–1555.

[51] R. Merkel, P. Nassoy, E. Evans, Energy landscapes of receptor-ligand bonds explored with dynamic force spectroscopy, Nature 397 (1999) 50–53.

[52] K. Karraï, R.D. Grober, Piezo-electric tuning fork tip-sample distance control for near field optical microscopes, Ultramiscorscopy 61 (1995) p.197-205.

[53] J. Liu, A. Callegari, M. Stark, M. Chergui, A simple and accurate method for calibrating the oscillation amplitude of tuning-fork based AFM sensors, Ultramicroscopy 109 (2008) 81–84.

[54] M.G. Cox, The area under a curve specified by measured values, Metrologia 44 (2007) 365–378.

[55] V.T. Moy, E.L. Florin, H.E. Gaub, Adhesive forces between ligand and receptor measured by AFM, Colloids Surfaces A: Physicochem. Eng. Aspects 93 (1994) 343-348.

[56] 0. Livnah, E.A. Bayer, M. Wilchck, J.L. Sussman, Three-dimensional structures of the avidin and the avidin-biotin complex, Proc. Natl. Acad. Sci. USA, 90 (11) (1993) 5076.

[57] G.I. Bell, Models for specific adhesion of cells to cells, Science 200 (1978) 4342: 618–627.

[58] M.O. Piramowicz, P. Czuba, M. Targosz, K. Burda, M. Szymoński, Dynamic force measurements of avidin–biotin and streptavdin–biotin interactions using AFM, Acta Biochim. Pol. 53 (2006) (1):93-100.

[59] C. Yuan, A. Chen, P. Kolb, V.T. Moy, Energy landscape of streptavidin-biotin complexes measured by atomic force microscopy, Biochemistry 39 (2000) (33):10219–10223.

3.2.3 Associated Publication 4

High-Speed Force Spectroscopy Unfolds Titin at the Velocity of Molecular Dynamics Simulations

By

Felix Rico[a], Laura González[b], Ignacio Casuso[a], Manel Puig-Vidal[b] and Simon Scheuring[a]

[a]U1006 INSERM, Aix-Marseille Université, Parc Scientifique et Technologique de Luminy, 163 avenue de Luminy, 13009Marseille, France.

[b] Bioelectronics Group, Department of Electronics, University of Barcelona, C/Marti i Franques 1, 08028 Barcelona, Spain.

Published in

***Science** 342 (2013) 741.*

High-Speed Force Spectroscopy Unfolds Titin at the Velocity of Molecular Dynamics Simulations

Felix Rico,[1] Laura Gonzalez,[2] Ignacio Casuso,[1] Manel Puig-Vidal,[2] Simon Scheuring[1]*

The mechanical unfolding of the muscle protein titin by atomic force microscopy was a landmark in our understanding of single-biomolecule mechanics. Molecular dynamics simulations offered atomic-level descriptions of the forced unfolding. However, experiment and simulation could not be directly compared because they differed in pulling velocity by orders of magnitude. We have developed high-speed force spectroscopy to unfold titin at velocities reached by simulation (~4 millimeters per second). We found that a small β-strand pair of an immunoglobulin domain dynamically unfolds and refolds, buffering pulling forces up to ~100 piconewtons. The distance to the unfolding transition barrier is larger than previously estimated but is in better agreement with atomistic predictions. The ability to directly compare experiment and simulation is likely to be important in studies of biomechanical processes.

Titin, a molecular spring in muscle sarcomeres, is important in striated muscle function and has been implicated in diseases such as heart failure (*1*). Titin consists of ~300 modules including immunoglobulin (Ig)–type, fibronectin III–type, and Pro-Glu-Val-Lys (PEVK) domains (*2*). Force spectroscopy (FS) unfolding of individual titin molecules, using optical tweezers (*3*, *4*) and atomic force microscopy (AFM) (*5*), opened a new research field relating protein mechanics, structure, and folding. AFM force-extension curves revealed sawtooth-like patterns (periodicity 25 to 28 nm) that indicated unfolding of individual Ig-like domains (*5*). Combinations of AFM experiments with steered molecular dynamics (SMD) simulations enriched atomic-level descriptions (*6*–*8*) of receptor-ligand binding (*9*, *10*) and forced protein unfolding (*5*). Forced unfolding (pulling speed 0.3 to 0.5 μm/s) of titin I91 concatemers (*8*, *11*, *12*) resulted in extension of each domain by ~0.7 nm, which correlated with the separation of antiparallel β strands A and B observed in SMD simulations (*8*, *11*). Subsequent rupture of the A′-G β-strand pair led to complete domain unfolding (*11*, *13*, *14*). However, a velocity difference of about six orders of magnitude prevented direct comparison of SMD with FS. Indeed, simulations resulted in unfolding forces of ~1 nN, nearly an order of magnitude greater than experimental values (*11*, *12*). Improved computational abilities have allowed simulations that unfolded I91 at 2800 μm/s (still faster than experiment by ~2.5 orders of magnitude), reporting forces of ~500 pN (*15*).

High-speed AFM [HS-AFM (*16*)] allows imaging biomolecules at video rate (*17*–*19*) through miniaturization of piezoelectric elements and the cantilever (*20*). We developed an analogous technique, high-speed FS (HS-FS), with short cantilevers (*21*) that allowed titin molecules to be pulled at speeds up to ~4000 μm/s. This is faster than conventional AFM by ~2.5 orders of magnitude and reaches current limits for SMD simulations.

Our HS-FS setup consists of a miniature piezoelectric actuator and a short cantilever with small viscous damping (0.035 pN μm^{-1} s^{-1}) (Fig. 1A and figs. S1 and S2). Titin I91 concatemers were unfolded by HS-FS at pulling velocities ranging over six orders of magnitude, from 0.0097 to 3870 μm/s. Only force curves with at least three sawtooth-like unfolding peaks were analyzed (*22*) (Fig. 1B and fig. S3). As reported in (*5*, *23*), unfolding forces increased with pulling velocity (Fig. 2A). At slow velocities, HS-FS unfolding forces were in excellent agreement with conventional FS (Fig. 2B). At pulling velocities higher than previously (>100 μm/s), unfolding forces followed a steeper slope that reached values greater than 500 pN and overlapped those obtained by simulations (Fig. 2B). Variations in the slope of the plot of mean rupture forces versus the logarithm of the velocity (force spectrum) have been observed for receptor-ligand interactions (*24*–*26*) but have rarely been documented for protein unfolding (*27*), probably because of the limited range of accessible pulling rates.

The microscopic model developed by Hummer and Szabo (*26*, *28*) allowed us to fit the wide range of pulling velocities and describes well the nonlinear upturn in the dynamic force spectrum (*26*, *28*) (Fig. 2B and supplementary materials). According to this theory, at moderate velocities, unfolding is dominated by the pulling rate and stochastic fluctuations (i.e., spontaneous unfolding of the domain under a given force). At high velocities, stochastic fluctuations of the protein along the unfolding pathway become irrelevant and the unfolding process becomes deterministic (*28*), because the protein is pulled so fast that it has no time to explore its energy landscape.

The slope in the dynamic force spectrum is related to the position of the energy barrier;

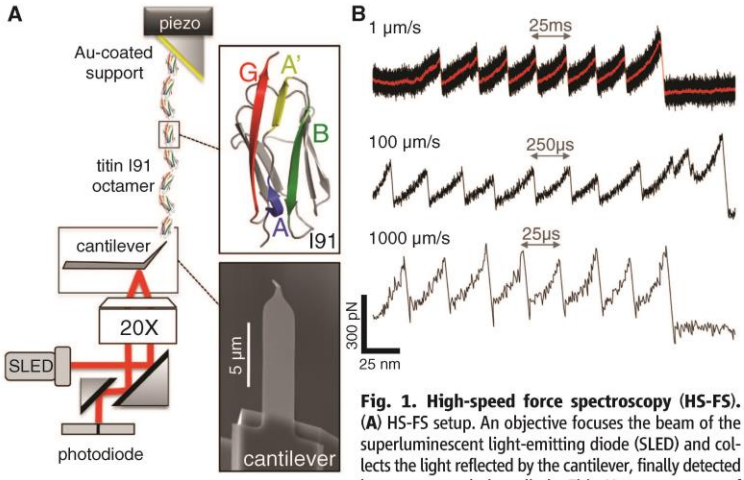

Fig. 1. High-speed force spectroscopy (HS-FS). (**A**) HS-FS setup. An objective focuses the beam of the superluminescent light-emitting diode (SLED) and collects the light reflected by the cantilever, finally detected by a segmented photodiode. Titin I91 concatemers of eight domains are immobilized on a tilted gold-coated surface via C-terminal cysteines. They are pulled by their N-terminal histidine tag with a nickel-coated tip at the end of a short cantilever. Tilting the sample surface further reduces hydrodynamic forces. Top inset shows a titin I91 domain (PDB ID: 1TIT) with relevant β strands colored in blue (A), yellow (A′), green (B), and red (G). Bottom inset shows a scanning electron micrograph of a short cantilever. (**B**) Force-extension curves acquired at three different retraction velocities: 1, 100, and 1000 μm/s. The 1 μm/s curve is moving average–filtered (red trace, 65-μs time window). Times to unfold a single I91 domain are indicated by arrows.

[1]U1006 INSERM, Aix-Marseille Université, Parc Scientifique et Technologique de Luminy, 163 avenue de Luminy, 13009 Marseille, France. [2]Bioelectronics Group, Department of Electronics, Universitat de Barcelona, c/ Marti Franques 1, 08028 Barcelona, Spain.

*Corresponding author. E-mail: simon.scheuring@inserm.fr

therefore, the slope upturn at high velocities corresponds to a shift of the barrier closer to the native state. From our data, the regime transition occurs at experimental velocities of ~1000 μm/s and a critical force of ~350 pN (supplementary materials). Our fastest experiment at 3870 μm/s is situated at the beginning of the deterministic regime, whereas most of the HS-FS data points characterize the transition from the stochastic regime to the deterministic regime (Fig. 2B). SMD simulations at much higher velocities (>>1000 μm/s) have generally been carried out in this deterministic regime. Although SMD simulation–derived forces are in agreement with our fastest pulling data, the theoretically predicted trend deviates from simulations at velocities of $>10^4$ μm/s. These deviations may be explained by slight differences in the simulated conditions (e.g., temperature) or by the simple cusp shape of the potential in the theory. More refined theories may be necessary to describe the unfolding at very high velocities. The model fit results in an energy landscape where the unfolding transition barrier (x_β) is located at 0.89 nm and the molecular elasticity (k_m) is 376 pN/nm, leading to an unfolding barrier height (ΔG) of $36 k_B T$ and a spontaneous unfolding rate k_0 of 2×10^{-10} s^{-1} (fig. S4). Similar values were obtained by fitting a unified model valid for different potential shapes (*28*) to the unfolding forces at velocities of ≤100 μm/s; this suggested that the reported parameters are independent of the potential shape (fig. S6). Our barrier position (0.89 nm) is larger than previous experimental estimates [0.25 nm (*23*); 0.30 nm (*5*)] but is in better agreement with the distance (1.1 to 1.4 nm) at which the secondary structure of I91 breaks in simulations (*8*, *15*). The relatively narrow range of experimental velocities in former FS experiments did not show an upturn in the force spectra and hence justified the Bell-Evans assumption of a fixed distance to the transition barrier under force. Our experiments at higher velocities show that this assumption is not valid. Furthermore, the data allowed us to estimate a diffusion coefficient of the protein along the reaction coordinate of the free energy landscape $D \approx 4 \times 10^3$ nm^2/s (supplementary materials). This is orders of magnitude slower than diffusion coefficients of proteins in solution (~10^8 nm^2/s) (*29*).

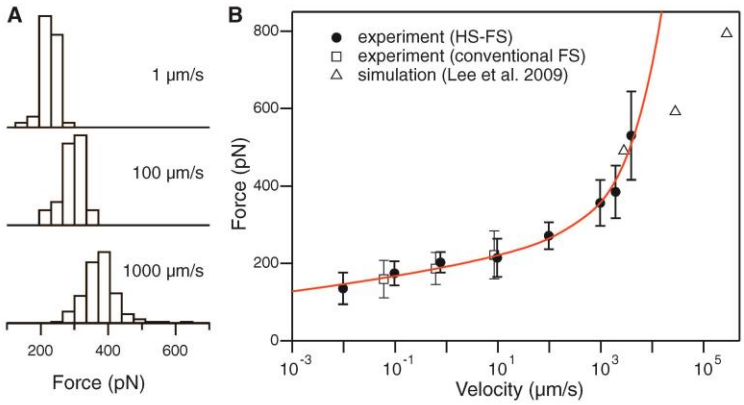

Fig. 2. High-speed dynamic force spectrum of titin I91. (**A**) Unfolding force histograms of the 1, 100, and 1000 μm/s retraction velocity experiments. (**B**) Average unfolding forces versus retraction velocity obtained using HS-FS, conventional FS (error bars denote SD), and steered molecular dynamics simulations [data from Lee *et al.* (*15*)]. Solid red line is the fit to the entire dynamic range of HS-FS with the full microscopic model (*26*) with fitting parameters (±SD) of $x_\beta = 0.89 \pm 0.05$ nm, $D = 3925 \pm 183$ nm^2/s, and $k_m = 376 \pm 28$ pN/nm.

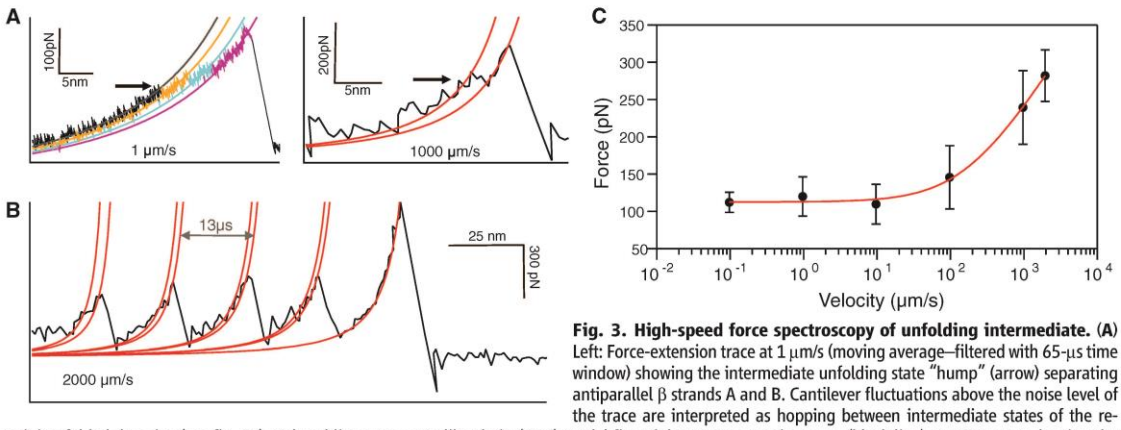

Fig. 3. High-speed force spectroscopy of unfolding intermediate. (**A**) Left: Force-extension trace at 1 μm/s (moving average–filtered with 65-μs time window) showing the intermediate unfolding state "hump" (arrow) separating antiparallel β strands A and B. Cantilever fluctuations above the noise level of the trace are interpreted as hopping between intermediate states of the remaining folded domains (see fig. S5). Colored lines are worm-like chain (WLC) model fits. Right: Force-extension trace (black line) at 1000 μm/s showing the intermediate unfolding state "hump" (arrow). Red lines are the best fits of the WLC model to the hump and complete unfolding peaks. The difference between the contour lengths is consistent with a separation of $n \times 0.7$ nm of each A-B β-strand pair of the remaining folded domains (*11*). (**B**) Force-extension curve at 2000 μm/s showing unfolding of four I91 domains. Red lines are WLC fits to the "hump" and complete unfolding peaks. The contour length distance difference between the "hump" and the complete unfolding decreases with the decreasing number of remaining folded domains. (**C**) Dynamic force spectrum of the intermediate unfolding state. Solid red line is the best fit of the model developed by Friddle *et al.* (*33*) to the experimental data with fitting parameters (±SD) $x_t = 0.060 \pm 0.004$ nm, $f_{eq} = 113 \pm 1$ pN, and $k_{NI} = 6959^{+1398}_{-990}$ s^{-1}.

Slow diffusion has been interpreted as a result of cantilever viscous damping (*30*) or by local minima along the unfolding pathway (*31*). Given the much smaller damping coefficient of the cantilevers used here, our data support the hypothesis that roughness in the free energy landscape slows unfolding. Although our estimated barrier height ($36.4k_BT$) is similar to that measured from chemical unfolding ($37k_BT$), the intrinsic unfolding rate (2×10^{-10} s^{-1}) is much slower than estimates from FS at slow pulling velocity (3.3×10^{-4} s^{-1}) and chemical unfolding (4.9×10^{-4} s^{-1}) (*23*). The fast intrinsic dissociation rate from slow FS and Bell-Evans analysis suggests an oversimplified view of forced unfolding, whereas chemical unfolding explores unrestricted unfolding pathways different from the physiologically relevant directional unfolding during muscle relaxation. Indeed, our slow k_0 suggests that the titin I91 domains unfold only very rarely at the estimated physiological forces (~5 pN) acting on distal titin Ig domains (*32*).

The use of short cantilevers with fast response (response time $\tau_c \approx 0.7$ μs; Fig. 1) allowed us not only to pull fast but also at conventional velocities (10 to 1000 nm/s) with microsecond time resolution. This response time is almost three orders of magnitude shorter than that of conventional cantilevers and allowed estimation of a lower limit for the relaxation time of the unfolded polypeptide chain (<2 μs; fig. S3). Before complete domain unfolding, an intermediate state has previously been documented by the so-called "hump" in force curves (Fig. 3A, arrows). This intermediate state is characterized by a force drop in the stretching regime (Fig. 3A, arrows), caused by the separation of the A-B β-strand pair as revealed by simulations (*11*, *12*). HS-FS measurements show separation of the A-B β-strand pair in several domains within 1 μs (Fig. 3B, first peak). Additionally, at high retraction speeds (>1 mm/s), the first domain as well as consecutive domains presented a "hump" before unfolding. The percentage of domains displaying intermediate unfolding decreased from ~95% at the lowest velocities to ~40% at the highest velocities. At 2 mm/s, the time between domain unfolding was ~10 μs (Fig. 3B). Thus, this short time lapse after the unfolding of the preceding domain is sufficient for domains to refold into their native state. This result allows us to set the lower limit for the refolding rate from the intermediate to the native state to at least ~10^5 s^{-1}, much faster than previous estimates (25 s^{-1}) (*11*).

We analyzed the intermediate unfolding state up to 2000 μm/s; beyond this velocity, it is difficult to assess an accurate measurement (Fig. 3 and fig. S3). At conventional pulling velocities, the average unfolding forces to the intermediate state are independent of pulling rate. At velocities faster than ~100 μm/s, average "hump" forces increase drastically, reaching values up to ~300 pN (Fig. 3C), consistent with "hump" forces observed in simulations (*15*). The slow pulling regime (<100 μm/s) is dominated by near-equilibrium unfolding and refolding of the A-B β-strand pair and defines the equilibrium force (Fig. 3A). At higher velocities, refolding of the A-B β-strand pair is negligible and the structure unfolds stochastically at forces that increase with the logarithm of the pulling rate (*33*) (Fig. 3C and supplementary materials). The model fitted our results with an unfolding rate at zero force from native to intermediate (k_{NI}^0) of 7×10^3 s^{-1}, an even faster folding rate at zero force from intermediate to native (k_{IN}^0) of 4×10^5 s^{-1}, a distance x_t to the transition barrier of only 0.06 nm, and an equilibrium force f_{eq} of 113 pN where $k_{NI}^0 = k_{IN}^0 = 2.8 \times 10^4$ s^{-1}. This results in an equilibrium free energy difference between the native and intermediate states of $\sim 4.1k_BT$, in agreement with the expected energy of three hydrogen bonds.

Although the absolute values of the calculated rates should be interpreted with care, the refolding rate of 4×10^5 s^{-1} is in excellent agreement with the lower limit (~10^5 s^{-1}) determined directly through observation of reformed A-B β-strand pairs in high-velocity unfolding traces (fig. S3). This suggests fast dynamic equilibrium of unfolding and refolding of β strand pair A and B at pulling forces up to ~100 pN, probably maintained by the antiparallel structure. This behavior has been observed in SMD runs (*12*, *15*). Furthermore, a recent computational small protein folding study reported that an antiparallel three–β-strand domain required an average of 21 μs to fold (*34*). This suggests a novel insight into the A-B β-strand pair and perhaps into short β folds in general: unfolding at fast rates, and refolding at even faster rates, as a feature of their structural equilibrium.

The combination of SMD with experimental FS has been important in understanding protein unfolding and mechanical stability. Our HS-FS methodology provides pulling velocities over six orders of magnitude and provides microsecond time resolution, achieving rates comparable to SMD simulations and thus allowing direct comparison of experimental and simulated unfolding forces. We expect that the now accessible dynamic range of HS-FS will stimulate the development of novel theories. Our results imply detailed mechanisms of the various steps during titin I91 unfolding: At zero and moderate forces, the protein fluctuates between the native and intermediate states. Under increasing force, only the intermediate state is populated. Thus, the tethered molecule reveals slow diffusion along the unfolding pathway, which, in combination with a high energy barrier, results in high mechanical stability. Direct comparison of FS and SMD simulations will likely provide new insights into other important biological processes such as lipid membrane dynamics (*35*) and receptor-ligand unbinding (*7*, *9*).

References and Notes

1. D. S. Herman *et al.*, *N. Engl. J. Med.* **366**, 619–628 (2012).
2. K. Maruyama, S. Matsubara, R. Natori, Y. Nonomura, S. Kimura, *J. Biochem.* **82**, 317–337 (1977).
3. M. S. Z. Kellermayer, S. B. Smith, H. L. Granzier, C. Bustamante, *Science* **276**, 1112–1116 (1997).
4. L. Tskhovrebova, J. Trinick, J. A. Sleep, R. M. Simmons, *Nature* **387**, 308–312 (1997).
5. M. Rief, M. Gautel, F. Oesterhelt, J. M. Fernandez, H. E. Gaub, *Science* **276**, 1109–1112 (1997).
6. H. Grubmüller, B. Heymann, P. Tavan, *Science* **271**, 997 (1996).
7. S. Izrailev, S. Stepaniants, M. Balsera, Y. Oono, K. Schulten, *Biophys. J.* **72**, 1568–1581 (1997).
8. H. Lu, B. Isralewitz, A. Krammer, V. Vogel, K. Schulten, *Biophys. J.* **75**, 662–671 (1998).
9. E. L. Florin, V. T. Moy, H. E. Gaub, *Science* **264**, 415–417 (1994).
10. G. U. Lee, L. A. Chrisey, R. J. Colton, *Science* **266**, 771–773 (1994).
11. P. E. Marszalek *et al.*, *Nature* **402**, 100–103 (1999).
12. H. Lu, K. Schulten, *Biophys. J.* **79**, 51–65 (2000).
13. S. B. Fowler *et al.*, *J. Mol. Biol.* **322**, 841–849 (2002).
14. R. B. Best *et al.*, *J. Mol. Biol.* **330**, 867–877 (2003).
15. E. H. Lee, J. Hsin, M. Sotomayor, G. Comellas, K. Schulten, *Structure* **17**, 1295–1306 (2009).
16. T. Ando *et al.*, *Proc. Natl. Acad. Sci. U.S.A.* **98**, 12468–12472 (2001).
17. T. Uchihashi, R. Iino, T. Ando, H. Noji, *Science* **333**, 755–758 (2011).
18. N. Kodera, D. Yamamoto, R. Ishikawa, T. Ando, *Nature* **468**, 72–76 (2010).
19. I. Casuso *et al.*, *Nat. Nanotechnol.* **7**, 525–529 (2012).
20. T. Ando, T. Uchihashi, T. Fukuma, *Prog. Surf. Sci.* **83**, 337–437 (2008).
21. M. B. Viani *et al.*, *J. Appl. Phys.* **86**, 2258 (1999).
22. R. B. Best *et al.*, *Anal. Chim. Acta* **479**, 87–105 (2003).
23. M. Carrion-Vazquez *et al.*, *Proc. Natl. Acad. Sci. U.S.A.* **96**, 3694–3699 (1999).
24. R. Merkel, P. Nassoy, A. Leung, K. Ritchie, E. Evans, *Nature* **397**, 50–53 (1999).
25. X. H. Zhang, E. Wojcikiewicz, V. T. Moy, *Biophys. J.* **83**, 2270–2279 (2002).
26. G. Hummer, A. Szabo, *Biophys. J.* **85**, 5–15 (2003).
27. Z. T. Yew, M. Schlierf, M. Rief, E. Paci, *Phys. Rev. E* **81**, 031923 (2010).
28. O. K. Dudko, G. Hummer, A. Szabo, *Phys. Rev. Lett.* **96**, 108101 (2006).
29. L. J. Lapidus, W. A. Eaton, J. Hofrichter, *Proc. Natl. Acad. Sci. U.S.A.* **97**, 7220–7225 (2000).
30. R. Berkovich *et al.*, *Proc. Natl. Acad. Sci. U.S.A.* **109**, 14416–14421 (2012).
31. H. Lannon, J. S. Haghpanah, J. K. Montclare, E. Vanden-Eijnden, J. Brujic, *Phys. Rev. Lett.* **110**, 128301 (2013).
32. H. Li *et al.*, *Nature* **418**, 998–1002 (2002).
33. R. W. Friddle, A. Noy, J. J. De Yoreo, *Proc. Natl. Acad. Sci. U.S.A.* **109**, 13573–13578 (2012).
34. K. Lindorff-Larsen, S. Piana, R. O. Dror, D. E. Shaw, *Science* **334**, 517–520 (2011).
35. L. Redondo-Morata, M. I. Giannotti, F. Sanz, *Langmuir* **28**, 6403–6410 (2012).

Acknowledgments: We thank A. Sastre and J. Otero for helpful discussions. Supported by European Research Council starting grant 310080 and Agence National de la Recherche grant ANR-12-BS10-009-01. L.G. was a recipient of travel grants (FPI grant BES-2010-031186 from the Spanish Ministerio de Economía y Competitividad and STSM COST Action TD1002-10006).

Supplementary Materials

www.sciencemag.org/content/342/6159/741/suppl/DC1
Materials and Methods
Supplementary Text
Figs. S1 to S6
References (*36*–*39*)

29 April 2013; accepted 30 September 2013
10.1126/science.1239764

4 Summary of results

Results are englobed in two sections, technology development and then its validation with experimental measurements on biomolecules.

Technology development

- To overcome the differences between QTF sensors, a module to control the quality factor (Q) and vibration amplitude (A) was developed. The quality factor is controlled analogically and the amplitude vibration digitally (with an algorithm). The control module is integrated with the QTF and drives the interface circuitry, which was designed to be transparent to commercial atomic force microscopes. As the sensor is electrically excited, current losses appears produced by the parasitic capacitance related to contacts, cables, etc. Also, we added a module to compensate this effect. Direct measurements on a commercial interferometer showed that the effective Q factor can be adjusted to experimental requirements while maintaining the mechanical amplitude of oscillation constant. Experimental amplitude vs. distance curves confirmed that the developed driver achieves an equivalent dynamic response from distinct handmade sensors (with varying mechanical characteristics) by means of electronic adjustment.
- A feasible technique to improve the lateral resolution of a QTF was developed. The technique is effective for measurements in shear mode in a liquid medium, for studies of biological samples. The method is based on attaching a standard AFM tip to the end of a fiber that has previously been sharpened chemically achieving the same performance as that of a commercial AFM tip. A comparable topographic image of a specific patterned structure and a soft sample were successfully obtained in a buffer solution.
- To study the sensor dynamics a 3D finite-element model of the QTF was developed in ANSYS. Model includes the coupling between the mechanical and the electrical behavior of the device by implementing the electric part, composed of a: voltage source, electrodes, and compensation circuit. Experimental measurements obtained with 2 different models of QTF validate the finite element model with a good agreement. From finite element simulations, it is possible to obtain parameters that are difficult to measure, such as the amplitude of oscillation or sensitivity. Also, we determined the spring constant value by means of two methods based on the simulations: the Amplitude and Cleveland methods. The results obtained using these methods were compared to those using the geometrical method, and showed that the latter overestimates the spring constant of the device.

- A technique to perform high-speed force spectroscopy (HS-FS) was developed. Homewritten software based on Labview programming was implemented to control the HS-FS setup. A multichannel analog to digital converter was used with maximum acquisition rate of 2 megasamples per second and channel, to drive piezo displacement and acquire cantilever deflection.

Technology validation in real molecular studies

- Three different working modes have been compared for biomolecules imaging with quartz tuning fork sensors working in shear mode. The studied sample was a self-assembled monolayer (SAM) of micropatterned antibodies. Apart from the classical amplitude and frequency modulation strategies, for first time the jumping mode was implemented using tuning forks. Results show that the molecules suffer less degradation when working in the jumping mode, due to the reduction of the interaction forces.
- The ability of quartz tuning fork probes for molecular interaction analysis was validated by experimental measurements between the biotin-streptavidin complex. We have applied a variant of the dynamic force spectroscopy (DFS) technique commonly used for AFM systems to QTF working in shear force detection. We have measured the adhesion energies between the biotin-streptavidin system at different pulling velocities and results have been compared with those obtained with AFM measurements under the same experimental conditions showing a good agreement between them.
- Titin unfolding measurements were performed with the developed technology at velocities reached by simulation (∼4 millimeters per second). We found that a small β-strand pair of an immunoglobulin domain dynamically unfolds and refolds, buffering pulling forces up to ∼100 piconewtons. The distance to the unfolding transition barrier is larger than previously estimated but is in better agreement with atomistic predictions.

5 *Discussion and conclusions*

The main objective accomplished in this work of thesis is the development of sensors technologies applied to force spectroscopy measurements and the demonstration of its possibilities in real molecular studies. Scanning probe microscopy (SPM) is a fast growing technology that has been the source for the development of an immense variety of applications to investigate nanoscale structures and molecules. As another technology, SPM is constantly improving through different advances in instrumentation level and the emergence of new applications. In the introductory chapter of this document there is a revision on the different aspects involved with biomolecular forces characterization, with specific detail in the Scanning Probe Microscopy. From the analysis of the main limitations of quartz tuning fork based nanosensors on one side and the conventional force spectroscopy with AFM tips on the other side, the main considerations for the technological developments were determined.

Nanocharacterization based on self-sensing probes in AFM systems is a growing research field and there is the need for new technological developments. Some works have been reported on soft matter but a standard procedure to perform molecular studies is missing. The developed instrumentation and the dynamics analysis of quartz tuning fork based sensors show the potential to measure the morphology and mechanical properties of biological samples.

As mentioned before, QTF sensors present some advantages in front of the cantilevers in certain applications since QTF based probes do not need a laser-photodiode. But probably the main drawback is that tuning fork probes are usually hand-made. A $Si0_2$ fiber tip is sharpened (etching it with HF) and attached to one of the tines of the quartz resonator. The nanotool is driven to its resonance frequency electrically and the amplitude of oscillation is determined by measuring the current through the device by the use of an I-V converter and a lock-in amplifier. Even when an accurate micrometric setup was used for QTF sensor production, the frequency response obtained for each sensor differed.

In this work, an electronic driver is developed to simultaneously control the two main parameters to adjust sensor dynamic response: Q (quality factor) and A (oscillation amplitude). Therefore, adjusting these two parameters electronically, the response of different sensors can be adjusted to counteract the effect of the imbalance due to the loaded prong and maintain identical sensor characteristics while performing the same experiment. Since the tip mass loads were very similar between the sensors, we succeeded in standardizing their dynamic response. Moreover, the electronic module can be easily integrated into commercial microscopes and reliably used in AFM systems.

Another consequence of the custom-made probes is that the lateral resolution is low compared with the commercial AFM tips. Some other methods to achieve a lateral resolution comparable with the one obtained with standard cantilevered probes have been reported, but they are limited to experiments conducted in air or vacuum. A new method is proposed in this thesis based on attaching a standard AFM tip to the end of the fiber probe which has been previously sharpened. Only the end of the probe is immersed in the buffer solution during measuring. Competitive topographic images of a specific patterned structure obtained and a soft sample in liquid environment are presented showing that with the improved sensors it is possible to acquire images with high resolution in liquid media, necessary to study biomaterials or biological samples under physiological conditions. The achieved lateral resolution is about 6 times higher than this of the naked micro etched fiber and it is equivalent to that achieved with a commercial AFM tip. The technique overcomes the problems reported in previous works where the AFM tips were directly attached to the end of one of the prongs of the tuning fork. Therefore, to use the QTF sensor to take measurements in liquid environments at least part of the prong needed to be immersed in the buffer solution (damping the oscillation of the QTF and therefore reducing its quality factor). Moreover, if the liquid is conductive, the electrodes of the nanosensors might be short-circuited.

A key parameter to obtain a quantitative value for the interaction forces is the effective spring constant (K_{eff}) of the QTF. It is worth mentioning that calculation of the spring constant is very controversial in the research community and the literature is full of discrepancies. Although the cantilever-based model is the most accepted, the coupled oscillators model has also been used. When the QTF is driven electrically, the prongs do not present mechanical coupling; they are connected electrically through the electrodes and when a voltage is applied between them, the QTF prongs are forced into anti-phase oscillation. Moreover, since the movement is somehow governed by the electrode design, the QTF cannot be treated as a pure mechanical oscillator. Indeed, beam theory cannot be applied to tuning fork sensors.

Some previous work reports models of the mechanical and electrical behavior of nanosensors based on QTFs. Nevertheless, oversimplification of the system, in order to arrive at tractable equations, results in a misunderstanding of the working principles of these novel tools. Having an accurate value for the spring constant of the devices would aid their popularization, due to the benefits they offer with respect to microfabricated cantilevers. A method to calculate the spring constant of a QTF from easily measurable parameters is presented in this thesis. The use of a finite element analysis (FEA) model which includes the electrical part is the key point, because it gives a value for the mechanical vibration; which in practice is hard to measure experimentally. The validation of the method by comparison with the Cleveland method guarantees that the presented method can be used to calculate the spring constant of a QTF accurately.

Results obtained in real biological experiments are promising and show the possibilities of the shear force microscopy improvements developed in this work of thesis. In a first experiment, a self-assembled monolayer (SAM) of micropatterned antibodies was imaged with three different techniques and in a second experiment, a molecular interaction analysis was done between biotin-streptavidin and results were compared with those obtained with AFM tip.

In the first experiment, a comparison between three different working modes to image micropatterned antibodies with quartz tuning fork sensors is performed. Apart from the classical amplitude (AM) and frequency modulation (FM) strategies, jumping mode (JM) is for first time implemented using these nanosensors. The self-assembled monolayer (SAM) of biomolecules can be imaged without damaging the sample when working in the JM. The other modes tested, AM and FM, produce serious alterations that are irreversible. Tip–sample forces are lower in JM since the lateral scanning and QTF oscillation are desynchronized, thereby minimizing the lateral forces during interaction. A good correspondence between the experimental height of the sample and the theoretical value is found. Nevertheless, one of the drawbacks of JM is the low scanning rate, which makes it difficult to monitor fast processes.

In the second experiment with quartz tuning fork sensors, a new procedure based on AFM dynamic force spectroscopy applied to QTF-based nanosensors for molecular interaction studies is carried out. Adhesion energy of the biotin-streptavidin complex has been analyzed obtaining comparable results to those measured with conventional AFM tip. Some studies in the literature report SPM measurements with QTF for different samples, but there is no standard procedure to perform such measurements. These results open the door to the exciting feasibility of the employment of self-sensing probes in a single measurement in liquid conditions.

With the high speed force spectroscopy development, it is possible to overcome one of the current limitations of the technique increasing temporal resolution (~1μs) and reaching pulling velocities over mm/s. This allows studying protein unfolding at μs-timescale and results can be compared with SMD simulations. The validation of the technique was performed with titin unfolding measurements allowing the direct observation of the molecule dynamics between transition and native states. Importantly, the unfolding forces measured by HS-FS in the mm/s velocity range agreed in magnitude to those obtained by molecular dynamics simulations. Also, intermediate unfolding states were observed and analyzed showing consistence with simulation results.

With respect to future investigations, a few routes are particularly promising and build upon the work presented in this thesis:

- Further work in finite element analysis (FEA) would lead to reproduce the whole sensor incorporating the glue, the fiber and surrounding media. In order to complete the whole model used in AFM measurements, part of the fiber needs to be immersed in a liquid medium. This could be done by dividing the fluid volume in two, having one part of air fluid and the other part of buffer solution. This approach will proportionate the value of key parameters as oscillation amplitude or spring constant in a more realistic scenario. Moreover, the response of the QTF to elastic and frictional forces could be studied by applying forces at the end of the probe and taking advantage of the pre-stress simulation features of ANSYS.
- Molecular recognition studies it would be desirable to perform using the new QTF probes with an integrated AFM tip at the fiber end to ensure single-molecule measurements. It would be interesting to repeat biotin-streptavidin interaction measurements with the developed probes to compare results with those obtained with the naked fiber. As well as further studies on another ligand-receptor pairs as antibody-antigen.
- The potential of HS-FS has not been fully exploited, since, to our knowledge, attempts to perform HS-FS for elasticity or receptor-ligand binding experiments have yet to be reported. First experiments on biotin-streptavidin system has been successfully carried out to showing that it is also compatible with the single molecule measurements of receptor-ligand interactions with a dynamic range of 6 decades. We expect that HS-FS will establish itself as a powerful technique to systematically contrast experiments with molecular predictions from MD simulations. Also, force-clamp mode was also implemented in the developed software and although it needs some improvement, interesting tests could be performed to obtain more information about the molecular fingerprint of the proteins.

6 Appendix

6.1 Acronyms

Abbreviation	Description
AC	alternating current
AFM	atomic force microscopy / microscope
BFP	biomembrane force probe
DC	continuous current
FS	force spectroscopy
HS-AFM	high speed atomic force microscopy
KPM	kelvin probe microscopy
MFM	magnetic force microscopy
MT	magnetic tweezers
OT	optical tweezers
QTF	quartz tuning fork
SAM	self-assembled monolayer
SFA	surface force apparatus
SFM	shear force microscopy
SNAM	scanning near acoustic microscopy
SNOM	scanning near-field optical microscopy
SMFS	single-molecule force spectroscopy
SPM	scanning probe microscopy
STM	scanning tunneling microscopy
SMD	steered molecular dynamics

6.2 Publications

- González, L.; Otero, J.; Algusil, J.P.; Samitier, J.; Adan, J.; Mitjans, F.; Puig-Vidal, M. (2014) Micropattern of antibodies imaged by shear force microscopy: Comparison between classical and jumping modes. **Ultramicroscopy**. 136, 176 – 184
- Rico, F.; Gonzalez, L.; Casuso, I.; Puig-Vidal, M.; Scheuring, S. (2013) High-speed force spectroscopy unfolds titin at the velocity of molecular dynamics simulations. **Science**. 342, 741 - 743.
- Otero, J.; Gonzalez, L.; Cabezas, G.; Puig-Vidal, M. (2013) Multitool platform for morphology and nanomechanical characterization of biological samples with coordinated selfsensing probes. **IEEE/ASME Transactions on Mechatronics**. 18 – 3, 1152 - 1160.
- Oria, R.; Otero, J.; González, L.; Botaya, L.; Carmona, M.; Puig-Vidal, M. (2013) Finite element analysis of electrically excited quartz tuning fork devices. **Sensors**. 13, 7156 - 7169.
- Otero, J.; Baños, R.; González, L.; Torrents, E.; Juárez, A.; Puig-Vidal, M. (2013) Quartz tuning fork studies on the surface properties of Pseudomonas Aeruginosa during early stages of biofilm formation. **Colloids and Surfaces B-Biointerfaces**. 102, 117 - 123.
- Gonzalez, L.; Otero, J.; Cabezas, G.; Puig-Vidal, M. (2012) Electronic driver with amplitude and quality factor control to adjust quartz tuning fork sensors response for atomic force microscopy. **Sensors and Actuators A-Physical**. 184, 112 - 118.
- Otero, J.; Gonzalez, L.; Puig-Vidal, M. Nanocharacterization of soft biological samples in shear mode with quartz tuning fork probes. **Sensors**. 12 (2012) pp. 4803 - 4819.
- Otero, J.; Guerrero, H.; Gonzalez, L.; Puig-Vidal, M. A Feedfordward adaptive controller to reduce the imaging time of large-sized biological samples with a SPM-based multiprobe station. **Sensors**. 12 (2012), pp. 686 - 703.
- González, L.; Oria, R.; Botaya, L.; Puig-Vidal, M.; Otero, J.; Determination of the static spring constant of electrically-Driven quartz tuning forks with two freely oscillating prongs, **Nanotechnology**, *submitted*.
- González, L.; Martínez-Martín, D.; Otero, J.; de Pablo, P.J.; Puig-Vidal, M.; Gómez-Herrero, J.; Improving the lateral resolution of quartz tuning fork-based sensors in liquid by integrating commercial AFM tips into the fiber end, **Sensors and Actuators A-Physical**, *submitted.*
- González, L.; Rodrigues, M.; Benito, A.M.; Pérez-García, Ll.; Puig-Vidal, M.; Otero, J.; Piezoelectric tuning fork biosensors for the quantitative measurement of biomolecular interactions, **Biosensors and Bioelectronics**, *submitted.*
- J. Otero, M. Puig-Vidal, G., Cabezas, L. González, Microscopy device with a resonant fork and a control unit for a nanosensor based on a resonant fork, **Patent ES 201031135**, 23 July 2010.

6.3 Acknowledgements

At the end of my thesis, it is a pleasant task to express my thanks to all those who contributed in many ways to the success of this study and made it an unforgettable experience for me.

First I would like to express my deepest thanks to my two supervisors. Dr. Manel Puig, thank you for trusting me and for giving me the opportunity to accomplish my Ph.D. thesis in this interesting and challenging topic and for your support all this time. Special thanks to Dr. Jorge Otero, for being my AFM teacher, for your countless ideas and your steady motivation, giving me the scientific and personal support to manage my work and helping me to successfully move my thesis forward.

I am very grateful to all the labmates (and friends) I have had during these four years with whom I have shared so many pleasant moments both inside and outside the laboratory. Antonio, Josep, Edgar, Camilo, Gonzalo, Roger, Angel, Victor, Luis, Xavi, without you, it would not have been possible to carry out this thesis. Thank you for providing such a nice atmosphere and an inspiring working environment! I also would thank to the entire Electronics Department, all the professors and staff, for your help whenever I have needed it.

My acknowledgment to Nanobioengineering group from Institute for Bioengineering of Catalonia (IBEC) leaded by Prof. Josep Samitier for the collaboration during these years. Thanks to Juan Pablo for preparing the samples with micropatterns of antibodies by micro-contact printing. Also thanks to Dr Francesc Mitjans and Dr Jaume Adan from Biomed Division of Leitat Technological Center for providing the antibodies.

I am very thankful to Dra Lluïsa Pérez and Mafalda Rodrigues from the Department of Pharmacology and Therapeutic Chemistry of Pharmacy Faculty for the fruitful collaboration that we have formed. Thank you Mafalda, for preparing the functionalization of the biotin-streptavidin samples, for your concerning about providing proper sample, discussing results, and your help in general.

Many other people from University of Barcelona have helped me in this thesis, so many thanks to: Dr. Gerard Oncins from Scientific-technical Services, for his help in the biotin-streptavidin measurements with Asylum microscope, Dr Nasser Darwish for his help in the dangerous task of fibers sharpening in the cleanroom, Dr Gabriel Gomila for helpful discussions, Dr Manuel Carmona for his help about ANSYS modeling, Dr Christophe Serre for his help with interferometer equipment,…

I want to express my sincere gratitude to Dr Simon Scheuring and his group from INSERM (Institut national de la santé et de la recherche médicale). First in Paris and then in Marseille, it has been a pleasure to spent several months in different occasions in your lab. Many thanks for giving me this opportunity, for making me

feel as a member of your group, for your help and financial support. Special thanks to Dr Ignacio Casuso and Dr Felix Rico, I really admire you. I cannot describe how many things I have learnt working with you two. Thank you for your professionalism, your enthusiasm, your patience and your friendship. I cannot forget the rest of the group, past and present members, for our scientific and non-scientific discussions, for suggesting experiments, for your kindles and help. I am especially indebted to Adai, Lorena, Laura, Mohammed, Niko, Anna, Martina, Ludo (and more…) who made my research experience in France truly enjoyable.

I am very grateful to Prof. Julio Gómez and Dr Pedro de Pablo and his group from the Physics of Condensed Matter Department of Universidad Autónoma de Madrid (UAM) for accepting me in his laboratory and his support. Special thanks to Dr. David Martínez. You have been my other AFM teacher and I learned so much from our discussions. Thanks to Aida for preparing the samples, Santi for his technical help and Miriam, Merche, Alvaro (and more...) for your encouragement. I also want to thank Cristina, Alex and the rest of the chemists group for creating good atmosphere in the lab.

I would like to acknowledge the financial support from the Spanish Government for the FPI Grant (BES-2010-031186) and the NANOBIOROB project funding (TEC2009-10114).

And finally, I wish to express my thanks to all my friends and family that encouraged and helped me in one or another way and they make me better as a person. Especially to my father, for his unconditional support in whatever I do.

6.4 References

[1] Leake, M. C. (2013) The physics of life: one molecule at a time, Phil. Trans. R. Soc. B 368 20120248.

[2] Ritort, F. (2006) Single-molecule experiments in biological physics: methods and applications, J. Phys. Condens. Matter 18 R531

[3] Roy, R.; Hohng S.; Ha, T. (2008) A practical guide to single-molecule FRET, Nature Methods 5, 507–516.

[4] Mashanov, G. (2003) Visualizing single molecules inside living cells using total internal reflection fluorescence microscopy, Methods 29, 142–52.

[5] Yildiz, A.; Forkey, J.; McKinney, S.; Ha, T.; Goldman, T.; Selvin, P. (2003) Myosin V walks hand-over-hand: single fluorophore imaging with 1.5 nm localization, Science 300, 2061–5.

[6] Nölting, B. (2009) Methods in modern biophysics, 2nd edn. Berlin, Germany: Springer.

[7] Harriman O. L. J.; Leake M. C. (2011) Single molecule experimentation in biological physics: exploring the living component of soft condensed matter one molecule at a time. J. Phys. Condens. Matter. 23, 503101.

[8] Hinterdorfer P.; Baumgartner, W.; Gruber, H. J.; Schilcher, K.; Schindler, H. (1996) Detection and localization of individual antibody-antigen recognition events by atomic force microscopy. Proc. Natl. Acad. Sci. USA 93, 3477-3481.

[9] Ebner A.; Wildling, L.; Zhu, R.; Rankl, C.; Haselgrübler, T.; Hinterdorfer, P.; Gruber, H. J. (2008) Functionalization of probe tips and supports for single-molecule recognition force microscopy, Top Curr Chem. 285, 29-76.

[10] Claridge, S. A.; et al. (2013) From the bottom up: dimensional control and characterization in molecular monolayers, Chem. Soc. Rev. 42, 2725–2745.

[11] Piner, R.D.; Zhu, J.; Xu, F.; Hong, S.; Mirkin, C. A. (1999) "Dip-pen" nanolithography, Science 283, 661.

[12] Benoit, M.; Gabriel, D.; Gerisch, G.; Gaub, H. E. (2000). Discrete interactions in cell adhesion measured by single-molecule force spectroscopy. Nat. Cell. Biol. 2, 313-317.

[13] Florin, E.; Moy, V.; Gaub, H. E. (1994). Adhesion forces between individual ligand-receptor pairs. Science 264, 415-417.

[14] Bustamante, C.; Bryant, Z.; Smith, S. B. (2003). Ten years of tension: Single-molecule DNA mechanics. Nature 421, 423-427.

[15] Moffitt, J. R.; Chemla, Y. R.; Smith, S. B.; Bustamante, C. (2008). Recent advances in optical tweezers. Annu. Rev. Biochem. 77, 205-228.

[16] Oesterhelt, F.; Oesterhelt, D.; Pfeiffer, M.; Engel, A.; Gaub, H. E.; Muller, D. J. (2000). Unfolding pathways of individual bacteriorhodopsins. Science 288, 143-146.

[17] Cisneros, D. A.; Oesterhelt, D.; Muller, D. J. (2005). Probing origins of molecular interactions stabilizing the membrane proteins halorhodopsin and bacteriorhodopsin. Structure 13, 235-242.

[18] Rief, M.; Gautel, M.; Oesterhelt, F.; Fernandez, J. M.; Gaub, H. E. (1997). Reversible unfolding of individual titin immunoglobulin domains by AFM. Science 276, 1109-1112.

[19] Oberhauser, A. F.; Marszalek, P. E.; Erickson, H. P.; Fernandez, J. M. (1998). The molecular elasticity of the extracellular matrix protein tenascin. Nature 393, 181-185.

[20] Howard, J. (2001). Mechanics of motor proteins and the cytoskeleton, Sinauer Associates, Sunderland, MA, USA.

[21] Merkel, R.; Nassoy, P.; Leung, A.; Ritchie, K.; Evans, E. (1999). Energy landscapes of receptor-ligand bonds explored with dynamic force spectroscopy. Nature 397, 50-53.

[22] Rief, M.; Oesterhelt, F.; Heymann, B.; Gaub, H. E. (1997). Single molecule force spectroscopy on polysaccharides by atomic force microscopy. Science 275, 1295-1297.

[23] Bustamante, C.; Marko, J. F.; Siggia, E. D.; Smith, S. (1994). Entropic elasticity of lambdaphage DNA. Science 265, 1599-1600.

[24] Clausen-Schaumann, H.; Seitz, M.; Krautbauer, R.; Gaub, H. E. (2000). Force spectroscopy with single bio-molecules. Curr. Opin. Chem. Biol. 4, 524-530.

[25] Cui, Y.; Bustamante, C. (2000). Pulling a single chromatin fiber reveals the forces that maintain its higher-order structure. Proc. Natl. Acad. Sci. USA 97, 127-132.

[26] Oesterhelt, F.; Rief, M.; Gaub, H. E. (1999). Single molecule force spectroscopy by AFM indicates helical structure of poly(ethylene-glycol) in water. New Journal of Physics 1, 6.1-6.11.

[27] Merkel, R.; Nassoy, P.; Leung, A.; Ritchie, K.; Evans, E. (1999) Energy landscapes of receptor-ligand bonds explored with dynamic force spectroscopy, Nature, 397-6714.

[28] Evans, E.; Ritchie, K.; Merkel, R. (1995). Sensitive force technique to probe molecular adhesion and structural linkages at biological interfaces. Biophys J. 68, 2580-2587.

[29] Ashkin, A. (1970). Acceleration and trapping of particles by radiation pressure. Phys. Rev. Lett. 24, 156.

[30] Ashkin, A.; Dziedzic, J. M.; Bjorkholm, J. E.; Chu, S. (1986). Observation of a single-beam gradient force optical trap for dielectric particles. Opt. Lett. 11, 288.

[31] Gosse, C.; Croquette, V. (2002). Magnetic tweezers: Micromanipulation and force measurement at the molecular level. Biophys J. 82, 3314-3329.

[32] Israelachvili, J. N.; Adams, G. E. (1978). Measurement of forces between two mica surfaces in aqueous electrolyte solutions in the range 0–100 nm. J. Chem. Soc., Faraday Trans. 74, 975-1001.

[33] Leckband, D.; Israelachvili, J. (2001). Intermolecular forces in biology. Q. Rev. Biophys. 34, 105-267.

[34] Leckband, D. (2000). Measuring the forces that control protein interactions. Annu. Rev. Biophys. Biomol. Struct. 29, 1-26.

[35] Lu, H.; Isralewitz, B.; Krammer, A.; Vogel, V.; Schulten, K. (1998). Unfolding of titin immunoglobulin domains by steered molecular dynamics. Biophys. J. 75, 662–671.

[36] Heymann, B.; Grubmüller, H.; (2001) Molecular dynamics force probe simulations of antibody/antigen unbinding: entropic control and nonadditivity of unbinding forces, Biophys J. 81(3), 1295–1313.

[37] Binnig, G.; Quate, C. F.; Gerber, C. (1986). Atomic force microscope. Phys. Rev. Lett. 56, 930.

[38] Binnig, G.; Rohrer, H.; Gerber, C.; Weibel, E. (1982). Tunneling through a controllable vacuum gap. Appl. Phys. Lett. 40, 178-180.

[39] Nonnenmacher, M.; O'boyle, M. P.; Wickramasinghe, H. K. (1991). Kelvin probe force microscopy. Appl. Phys. Lett. 58, 2921-2923.

[40] Martin, Y.; Wickramasinghe, H. K. (1987). Magnetic imaging by ``force microscopy'' with 1000 Å resolution. Appl. Phys. Lett. 50, 1455-1457.

[41] Lewis, A.; Isaacson, M.; Harootunian, A.; Muray, A. (1984). Development of a 500 Å spatial resolution light microscope: I. Light is efficiently transmitted through lambda/16 diameter apertures. Ultramicroscopy 13, 227-231.

[42] Weissenhorn, A.; Hansma, P.; Albrecht, T.; Quate, C. (1989). Forces in atomic force microscopy in air and water Appl. Phys. Lett. 54, 2651-2660.

[43] Withers, J.; Aston, D. (2006). Nanomechanical measurements with AFM in the elastic limit. Advances in Colloid and Interface Science 120(1-3), 57-67.

[44] Vadillo-Rodriguez, V.; [and others]. (2007). Surface Viscoelasticity of Individual Gram-Negative Bacterial Cells Measured Using Atomic Force Microscopy. J. Bacteriol 190 (12), 4225-4232.

[45] Leonenko, Z.; Finot, E.; Amrein, M. (2007). Adhesive interaction measured between AFM probe and lung epithelial type II cells. Ultramicroscopy 107, 948-953.

[46] Marszalek, P.E.; Dufrêne, Y. F. (2012). Stretching single polysaccharides and proteins using atomic force microscopy. Chem. Soc. Rev. 41, 3523–3534.

[47] Scheuring, S.; Sturgis, J.N. (2005). Chromatic adaptation of photosynthetic membranes. Science 309, 484–487

[48] Hoh, H.; Lal, R.; John, S.; Revel, J.; Arnsdorf, M. (1991). Atomic force microscopy and dissection of gap junctions. Science 253, 1405–1408.

[49] Alessandrini, A.; Gerunda, M.; Facci, P.; Schnyder, B.; Koetz, R. (2003). Tuning molecular orientation in protein films. Surf. Sci. 542, 64–71.

[50] Guthold, M.; Zhu, X.; Rivetti, C.; Yang, G.; Thomson, N.; Kasas, S.; Hansma, H.; Smith, B.; Hansma, P.; Bustamante, C. (1999). Direct observation of one-dimensional diffusion and transcription by Escherichia coli RNA polymerase. Biophys. J. 77, 2284–2294.

[51] Ando, T.; Kodera, N.; Takai, E.; Maruyama, D.; Saito, K.; Toda, A. (2001). A high-speed atomic force microscope for studying biological macromolecules. Proc. Natl. Acad. Sci. U.S.A. 98, 12468–12472.

[52] Viani, M.; Pietrasanta, L.; Thompson, J.; Chand, A.; Gebeshuber, I.; Kindt, J.; Richter, M.; Hansma, H.; Hanjma, P. (2000). Probing protein–protein interactions in real time. Nat. Struct. Biol. 7, 644–647.

[53] Fisher, T.; Oberhauser, A.; Carrion-Vasquez, M.; Marszalek, P.; Fernandez, J. (1999). The study of protein mechanics with the atomic force microscope. Trends Biochem. Sci. 24, 379–84.

[54] Wu, J. (2010). The Jump-to-Contact Distance in Atomic Force Microscopy Measurement. Journal of Adhesion 86 (11), 1071 – 1085.

[55] Burnham, N.; Colton, R.; Pollock, H. (1993). Interpretation of force curves in force microscopy. Nanotechnology 4, 64-80.

[56] Fernandez, J. M.; Li, H. (2004). Force-clamp spectroscopy monitors the folding trajectory of a single protein. Science 303, 1674-1678.

[57] Oberhauser, A. F.; Hansma, P. K.; Carrion-Vazquez, M.; Fernandez, J. M. (2001). Stepwise unfolding of titin under force-clamp atomic force microscopy. Proc. Natl. Acad. Sci. USA 98, 468-472.

[58] Schlierf, M.; Li, H.; Fernandez, J. M. (2004). The unfolding kinetics of ubiquitin captured with single-molecule force-clamp techniques. Proc. Natl. Acad. Sci. USA 101, 7299-7304.

[59] Lee, G. U.; Chrisey L. A.; Colton R. J. (1994). Direct measurements of the forces between complementary strands of DNA. Science 266, 771–773.

[60] Dammer, U.; Hegner, M.; Anselmetti, D.; Wagner, P.; Dreier, M.; Huber, W.; Güntherodt, H. J. (1996). Specific antigen/antibody interactions measured by force microscopy. Biophys. J. 70(5), 2437–2441.

[61] Grubmüller, H.; Heymann, B.; Tavan, P. (1996). Ligand binding: molecular mechanics calculation of the streptavidin-biotin rupture force. Science 271, 997.

[62] Izrailev, S.; Stepaniants, S.; Balsera, M.; Oono, Y.; Schulten, K. (1997). Molecular dynamics study of unbinding of the avidin-biotin complex. Biophys. J. 72, 1568–1581.

[63] Lee, G. U.; Chrisey L. A.; Colton R. J. (1994). Sensing discrete streptavidin-biotin interactions with atomic force microscopy. Science 266, 771–773.

[64] Marszalek, P. E.; Lu, H.; Li, H.; Carrion-Vazquez, M.; Oberhauser, A. F.; Schulten, K.; Fernandez, J.M. (1999). Mechanical unfolding intermediates in titin modules. Nature 402, 100–103.

[65] Lu, H.; Schulten, K. (2000). The key event in force-induced unfolding of Titin's immunoglobulin domains. Biophys. J. 79, 51–65.

[66] Lee, E. H.; Hsin, J.; Sotomayor, M.; Comellas, G.; Schulten, K. (2009). Discovery Through the Computational Microscope. Structure 17, 1295–1306.

[67] Meng, Q.; Yi, C. (2011). Single Molecule Force Spectroscopy on Biomacromolecules. Progress in Physics 31 No.3.

[68] Ando, T.; Kodera, N.; Takai, E.; Maruyama, D.; Saito, K; Toda, A. (2001). A high-speed atomic force microscope for studying biological macromolecules. Proc. Natl. Acad. Sci. USA 98, 12468–12472.

[69] Ando, T.; Uchihashi, T.; Fukuma, T. (2008) High-speed atomic force microscopy for nano-visualization of dynamic biomolecular processes, Prog. Surf. Sci. 83, 337-437.

[70] Kodera, N.; Sakashita, M.; Ando, T. (2006). Dynamic proportional-integral differential controller for high-speed atomic force microscopy. Rev. Sci. Instrum. 77 (8):083704

[71] Kodera, N.; Yamashita, H.; Ando, T. (2005). Active damping of the scanner for high-speed atomic force microscopy. Rev. Sci. Instrum. 76: 053708.

[72] Ando, T.; Uchihashi, T.; Scheuring, S. (2014) Filming biomolecular processes by high-Speed atomic force microscopy, Chem. Rev., 114, 3120–3188.

[73] Kodera, N.; Yamamoto, D.; Ishikawa, R.; Ando, T. (2010). Video imaging of walking myosin V by high-speed atomic force microscopy. Nature 468, 72–76.

[74] Casuso, I.; Khao, J.; Chami, M.; Paul-Gilloteaux, P.; Husain, M.; Duneau, J.-P.; Stahlberg, H.; Sturgis, J.N.; Scheuring, S. (2012). Characterization of the motion of membrane proteins using high-speed atomic force microscopy. Nat. Nanotechnol. 7, 525–529.

[75] Colom, A.; Casuso, I.; Boudier, T.; Scheuring, S. (2012). High-speed atomic force microscopy: cooperative adhesion and dynamic equilibrium of junctional microdomain membrane proteins. J. Mol. Biol. 423, 249–256.

[76] Colom, A.; Casuso, I.; Rico, F.; Scheuring, S. (2013) A hybrid high-speed atomic force-optical microscope for visualizing single membrane proteins on eukaryotic cells. Nat. Commun. 4, 2155.

[77] Giessibl, F. J.; Hembacher, S.; [and others]. (2000). Subatomic features on the silicon (111)-(7x7) surface observed by atomic force microscopy. Science 289, 422-425.

[78] Albers, B.; Liebmann, M.; [and others]. (2008). Combined low-temperature scanning tunneling/atomic force microscope for atomic resolution imaging and site-specific force spectroscopy. Rev. Sci. Instrum. 79, 033704.

[79] Barbic, M.; Eliason, L.; Ranshaw, J. (1997). Femto-Newton force sensitivity quartz tuning fork sensor. Sensors and Actuators A 136, 564.

[80] Ludwig, T. (2008). Casimir force experiments with quartz tuning forks and an atomic force microscope (AFM), J. Phys. A: Math. Theor. 41, 164025.

[81] Günther, P.; Fischer, U. Ch.; Dransfeld, K. (1988). Scanning near-field acoustic microscopy, Appl. Phys. B: Laser and Optics 48, 89.

[82] Karrai, K.; Grober, R. D. (1995). Piezoelectric tip-sample distance control for near-field optical microscopes. Appl. Phys. Lett. 66, 1842-1844.

[83] Kageshima, M.; Jensenius, H.; [and others]. (2002). Noncontact atomic force microscopy in liquid environment with quartz tuning fork and carbon nanotube probe. Appl. Surf. Sci. 188, 440-444.

[84] Polesel-Maris, J.; Lubin, C.; Thoyer, F.; Cousty, J. (2011). Combined dynamic scanning tunneling microscopy and frequency modulation atomic force microscopy investigations on polythiophene chains on graphite with a tuning fork sensor. Journal of Applied Physics 109, 074320.

[85] Giessibl, F. J. (1998). High-speed force sensor for force microscopy and profilometry utilizing a quartz tuning fork. Appl. Phys. Lett. 73, 3956-3958.

[86] Castellanos-Gomez, A.; Agraït, N.; Rubio-Bollinger, G. (2011). Force-gradient-induced mechanical dissipation of quartz tuning fork force sensors used in atomic force microscopy. Ultramicroscopy 111, 186–190.

[87] Giessibl, F. (2001). A direct method to calculate tip–sample forces from frequency shifts in frequency-modulation atomic force microscopy. Appl. Phys. Lett. 78, 123.

[88] Wutscher, E.; Giessibl, F. J. (2011). Atomic force microscopy at ambient and liquid conditions with stiff sensors and small amplitudes. Rev. Sci. Instrum. 82, 093703.

[89] Liu, J.; Callegari, A.; Stark, M.; Chergui, M. (2008). A simple and accurate method for calibrating the oscillation amplitude of tuning-fork based AFM sensors. Ultramicroscopy 109, 81–84.

[90] Ichii, T.; Fujimura, M.; Negami, M.; Murase, K.; Sugimura H. (2012). Frequency modulation atomic force microscopy in ionic liquid using quartz tuning fork sensors, Jpn. J. Appl. Phys. 51, 08KB08.

[91] Schoenwald K.; Peng, Z. C.; Noga, D.; Qiu, S. R.; Sulchek, T. (2010). Integration of atomic force microscopy and a microfluidic liquid cell for aqueous imaging and force spectroscopy. Rev. Sci. Instrum. 81, 053704.

[92] Otero, J.; Gonzalez, L.; Cabezas, G.; Puig-Vidal, M. (2013). Multitool platform for morphology and nanomechanical characterization of biological samples with coordinated self-sensing probes. IEEE/ASME Trans. On Mec., 18, No. 3.

[93] Waszczuk, K.; Gula, G.; Swiatkowski, M.; Olszewski, J.; Herwich, W.; Drulis-Kawa, Z.; Gutowicz, J.; Gotszalk, T. (2012). Evaluation of Pseudomonas aeruginosa biofilm formation using piezoelectric tuning fork mass sensors. Sensors and Actuators B 170, 7– 12.

[94] Otero, J.; Baños, R.; Gonzalez, L.; Torrents, E.; Juarez, A.; Puig-Vidal, M. (2013). Quartz tuning fork studies on the surface properties of Pseudomonas aeruginosa during early stages of biofilm formation. Colloids and Surfaces B: Biointerfaces 102, 117– 123.

[95] Polesel, J.; Legrand, J.; Berthelot, T.; Garcia, A.; Viel, P.; Makky, A.; Palacin, S. (2012). Force Spectroscopy by Dynamic Atomic Force Microscopy on Bovine Serum Albumin proteins changing the tip hydrophobicity, with piezoelectric tuning fork self-sensing scanning probe. Sensors and Actuators B 161, 775– 783.

[96] Hofer, M.; Adamsmaier, S.; et al. (2010). Molecular recognition imaging using tuning fork-based transverse dynamic force microscopy. Ultramicroscopy 110, 605-611.

[97] Edwards, H.; Taylor, L.; et al. (1997). Fast, high-resolution atomic force microscopy using a quartz tuning fork as actuator and sensor. J. Appl. Phys. 82, 980.

[98] Hembacher, S.; Giessibl, F.; Mannhart, J. (2004). Force Microscopy with Light-Atom Probes. Science 305, 380.

[99] Mononobe, S. (2005). Near-field optical fiber probes and the imaging applications: Progress in Nano-Electro-Optics III. Springer, Berlin.

[100] Rensen, W.H.; van Hulst, N.F.; Kämmer, S.B. (2000). Imaging soft samples in liquid with tuning fork based shear force microscopy. Appl. Phys. Lett. 77, 1557–1559.

[101] Kwon, J.; Jeong, S.; Kang, Y. (2011) Topography and near-field image measurement of soft biological samples in liquid by using a tuning fork based bent optical-fiber sensor. Rev. Sci. Instrum. 82, 043707.

[102] Makky, A.; Berthelo, T.; Feraudet-Tarisse, C.; Volland, H.; Viel, P.; Polesel-Maris, J. (2012) Substructures high resolution imaging of individual IgG and IgM antibodies

with piezoelectric tuning fork atomic force microscopy. Sens. Actuat. B 162, 269–277.

[103] Grzegorz, G. et al. (2012) Piezoelectric tuning fork based mass measurement method as a novel tool for determination of antibiotic activity on bacterial biofilm, Sensors and Actuators B 170, 7– 12.